This is to certify that the
dissertation entitled

Dynamic Solvation of Zn(II)-Cytochrome *c* in the Native Fold and the Unfolding Transition State

presented by

Sanela Lampa-Pastirk

has been accepted towards fulfillment
of the requirements for the

Ph.D. degree in Chemistry

Warren F. Beck

Major Professor's Signature

08/19/2005

Date

Dynamic Solvation of Zn(II)-Cytochrome *c* in the Native Fold and the Unfolding Transition State

by

Sanela Lampa-Pastirk

A DISSERTATION

Submitted to
Michigan State University
in partial fulfillment of the requirements
for the degree of
DOCTOR OF PHILOSOPHY
Department of Chemistry

2005

ABSTRACT

Dynamic Solvation of Zn(II)-Cytochrome *c* in the Native State and at the Unfolding Transition State

by

Sanela Lampa-Pastirk

This dissertation introduces a new approach for the study of protein motions at the native structure and near the transition state for protein unfolding or misfolding reactions. An embedded intrinsic electronic chromophore is used as a solvatochromic probe of the motions on the energy landscape of the surrounding protein and associated solvent and as a trigger for the unfolding reaction. This approach is demonstrated with Zn(II)-cytochrome *c*, a small globular protein containing a porphyrin macrocycle as an intrinsic chromophore.

Picosecond time-resolved measurements of the dynamic Stokes shift of the fluorescence from Zn(II)-cytochrome *c* with Q-band excitation show that the fastest protein motions occur in the hydrophobic core; much slower motions occur in the solvent-contact layer. The two classes of motion are apparently not strongly coupled. The nonpolar response that accompanies the excited-state photodissociation of the Zn(II) ion's protein derived axial ligands occurs on a different timescale.

With Soret-band excitation, the fluorescence spectrum from Zn(II)-cytochrome *c* exhibits a prompt red shift that reports an entry of water molecules into the hydrophobic core. The initial red shift is followed by an unusual blue shift that reports an extrusion of water from the hydrophobic core. These results suggest a new approach for optically triggering protein unfolding reactions from the native state with complete control over the surrounding solution conditions and temperature. We call this method *the optical G jump* because it provides an effectively instantaneous transition from the equilibrated native state to an excited Gibbs-free energy level. The protein system is then allowed to propagate on the energy landscape using whatever trajectories are available under the solution conditions and temperature. This method opens exciting new perspectives for studying disease related protein misfolding reactions.

Igoru

Acknowledgments

I thank Professor Jane Vanderkooi and Wayne Wright from the School of Medicine, University of Pennsylvania for the generous gift of the Zn(II)-substituted cytochrome c sample that was used in this work. I am also grateful for the indispensable assistance of Professor Gary Blanchard during the picosecond TCSPC fluorescence measurements. I would like to thank past and present members of the research group, Elizabeth Carson, Katherine Shelly and Kevin Dillman.

I would particularly like to thank my advisor Warren Beck, for help, guidance and invaluable discussions through my graduate studies and supporting me both professionally and personally.

TABLE OF CONTENTS

LIST OF TABLES

LIST OF FIGURES[⊗]

[⊗] Images in this dissertation are presented in color.

Introduction

Knowledge of the protein folding process has developed remarkably in recent years from an understanding that proteins fold in a linear multi-state kinetic pathway to the idea of a multidimensional energy landscape that involves many possible folding trajectories. An important concept in studying the mechanism of protein folding was that protein structures can exist in a large number of conformations and actively switch between them. Some of these conformations are crucial for the function of the protein; however, some appear to be misfolded and toxic species appear that can be responsible for a significant number of diseases. The work presented in this dissertation is mainly motivated by the wish to gain an understanding of the molecular mechanism that produces misfolded proteins from their native folded structures. The difficulty in determining the role played by misfolded proteins in the molecular mechanism of the diseases is that no methods have been available that permit synchronous triggering of the unfolding reactions under physiological conditions that do not involve the manipulation of the bulk solution composition or temperature. This work will propose a new experimental approach to address this problem.

The dissertation is organized as follows:

The role of protein folding and misfolding in disease is discussed in chapter 1. We review the main concepts of protein folding, the energetics, the models and the methods of investigation of folding reactions.

Chapter 2 describes preparation of the ZnCytc and its spectroscopic characteristics. Information about the time-correlated single-photon counting method is included with the detailed description of the experimental set up used in this work and the method of data analysis.

In Chapter 3 we examine nonpolar solvation dynamics of the native Zn(II)-substituted cytochrome *c* with *Q*-band excitation. We show that Zn(II) porphyrin exhibits excited-state photodissociation of the protein-derived axial ligands. We discuss the protein-matrix response to the axial-ligand photodissociation reaction in ZnCytc in terms of nonpolar solvation dynamics, a reorganization of the protein in response to a change in size of an imbedded structure.

The main focus of Chapter 4 is polar solvation dynamics of the native Zn(II)-substituted cytochrome *c* with *Q*-band excitation of Zn(II) porphyrin in cytochrome *c*. The solvent-response function obtained from the dynamic Stokes shift measurements of the time-resolved fluorescence spectrum exhibits biexponential decay with two distinct time constants. We discuss these two components in terms of the motions of the hydrophobic core and the motions in the solvent-contact layer. We show that the polar solvation dynamics is not strongly coupled to the nonpolar dynamics discussed in Chapter 3.

In chapter 5 we present the solvation dynamics of Zn(II)-substituted cytochrome *c* with Soret-band excitation. We introduce the *optical G jump* as a new method for optical triggering of the protein unfolding reaction. When irradiated with light in a blue region of

the spectrum, the Zn(II) porphyrin as an internal chromophore can serve as a trigger for unfolding the protein and as a sensor for the subsequent motions of the protein and water molecules. We show the direct experimental observation of the fast dynamics of entrance and exit of water molecules from the hydrophobic core.

Chapter 6 concludes the dissertation by proposing future investigations of the protein unfolding and misfolding reactions based on the methods developed in the work presented here.

1. Polypeptide and Solvent Dynamics in Native and Misfolded States of Proteins

For a long time the main motivation for understanding the protein folding mechanism was the remarkable efficiency and accuracy with which these large structures fold into highly specific and biologically active structures that are essential for the function of living organisms. However, the motivation for studying protein folding changed in the 1990s with the discovery that proteins on their own can be disease-causing species.

Today, it is well established that the inability of proteins to fold properly or to maintain the folded state is a direct cause for a number of diseases. Markedly associated with protein misfolding are the transmissible spongiform encephalopathies that include Creutzfeldt–Jakob disease in humans, scrapie in sheep, and bovine spongiform encephalopathy ("mad cow disease"). Also involving misfolding are the amyloidoses, the most famous of which are Alzheimer's disease and Parkinson's disease.[1-3] All of these diseases are thought to be associated with the accumulation of amyloid fibrils, but the critical step seems to be the decay of the native folded form of the protein in question.[4]

Native proteins are soluble molecules with distinct structures that perform a variety of functions in living organisms through their selective interaction with other molecules in the surrounding solvent. The protection of the hydrophobic core of the protein from the surrounding solvent is critical to the stability of the native fold.[5] Unlike

the native forms, the amyloid fibrils derived from them are insoluble generic forms of protein.[6] The first step that leads to the formation of amyloid fibrils is the failure of the protein to assume the proper native fold. Misfolded or partially unfolded proteins form small soluble aggregates, which associate into protofibrils and then finally into insoluble mature fibrils. The aggregation always occurs from a misfolded or partially unfolded state of the protein.[1,7] The fully formed fibrils exhibit nearly identical structures regardless of the protein of origin; they all have a characteristic cross-beta-sheet configuration[1,7] despite having essentially identical structures. The rates at which the misfolded proteins aggregate depend strongly on the physicochemical properties of the proteins, such as the spatial organization of charges, a preference for certain secondary structural features, and hydrophobicity.[8]

While it is known that amyloidic polyneuropathy arises directly from a single-point mutation of the protein transthyretin that results in the formation of amyloid structures,[9-11] the ability to form amyloid fibrils is apparently a general property of polypeptides and is not necessarily dependent on specific amino-acid sequences or native-fold topologies.[12] This idea is supported by the finding that proteins not related to the amyloid diseases can unfold and aggregate *in vitro* and create amyloid fibers of almost identical structure to those found in amyloidoses.[13] Dobson and co-workers showed that even myoglobin and cytochrome *c* can form amyloid fibrils under the conditions that favor unfolding of the native structures.[14,15] Further, the SH3 domain from bovine phosphatidyl-inositol-3'-kinase and the N-terminal domain of *E. coli* HypF protein can form fibers *in vitro*.[16,17] It is notable that the native structure of these globular

proteins mostly contains alpha helices as the secondary structural element; in order to form amyloid fibrils, some of these alpha helices have to unfold and refold to form b-sheet-rich structures.[14,15]

The role of misfolded or aggregated protein structures in the progress of disease is the subject of current vigorous debate. The key questions under consideration are which of the various forms of a misfolded or aggregated protein is the species that initiates the disease, and how this species takes part in the molecular mechanism for the disease.[13,18,19]

The current trend in this discussion seems to indicate that small aggregate structures formed from the misfolded proteins are the disease-causing species. It was found that structurally disorganized pre-fibrilar aggregates are highly cytotoxic while structurally well-defined mature fibrilar forms of the same protein are generally harmless.[20-23] The prefibrilar forms are thought to be toxic because they expose hydrophobic regions of the protein to the surrounding solvent.[21] An important example of this principle is the protein alpha-synuclein, mutant forms of which are associated with Parkinson's disease. This protein can be present in several different aggregation states: the unfolded monomer, an oligomeric form that is rich in beta-sheet-containing structures, a protofibrilar form, and the mature amyloid fibril. The protofibrilar form is likely to be the toxic agent, but the possibility that the unfolded monomeric form also is toxic cannot be excluded.[24]

The long-term goal of understanding the molecular mechanism behind diseases associated with protein misfolding and aggregation will require a combination of

computational and experimental approaches. In this chapter we will provide background for protein folding mechanisms and possible approaches for studying mechanisms of folding and misfolding.

1.1. Protein Folding

1.1.1. Energetics

Folding of the protein is a process during which a one-dimensional, almost linear structure of polypeptide with a certain amino acid sequence forms a characteristic three-dimensional structure of a biologically functional native protein. The characteristic features of this structure are stability, compact and unique internal organization and presence of the nonpolar core. The stability of native protein can be expressed in terms of Gibbs free energy, which is minimized during the folding process as a result of interplay of enthalpic and entropic contributions. The folded structure is only marginally more stable than unfolded. For a small protein (<200 residues) under physiological conditions the folded state is typically only 4 to 20 kcal/mol more stable than the unfolded. The energetically small difference in stability is a result of large contributions from several major forces. These forces are involved in the protein folding process by impacting enthalpic or entropic contributions to Gibbs free energy.[25] This section underlines the dominant energies and forces that guide the protein from the unfolded to the folded state.

The Hydrophobic Effect. Almost 50 years ago Kauzmann[5] recognized the hydrophobic effect as a principal driving force in protein folding. The hydrophobic effect

can be described as the tendency of nonpolar groups to stick together when surrounded with polar solvent. The major factor in protein stability is the lack of a hydrogen bond between a nonpolar residue and water, rather than an interaction between nonpolar molecules. Accordingly, a hydrophobic amino acid residue creates a hole in the surrounding water, forcing it to reorganize and become more ordered. As a result, the entropy of water decreases, which is a thermodynamically unfavorable process. To minimize the surface tension created by the reorganization of water and to release free energy confined in the hydrogen bond network, hydrophobic amino acid residues tend to pack together in the interior of the molecule. A number of experimental results and theoretical approaches confirm that the hydrophobic effect is a major force in protein folding that provides an ample amount of energy to the folding reaction.

Hydrogen Bonds. The hydrogen bond is a weak but very abundant interaction in proteins. On average there are 1.1 intramolecular hydrogen bonds per amino acid residue in a protein. The energy of a hydrogen bond in a protein varies between 3 and 9 kcal/mol, depending on the type. Initially, it was believed that hydrogen bonding is the most important force responsible for folding stability. Kauzmann[5] argued that the hydrogen bond can not be the leading force in protein folding since there was no proof that buried intramolecular hydrogen bonds in proteins have lower free energy than those of the unfolded chain to water. Hydrogen exchange experiments showed that the energy of the solvated hydrogen bond is almost equal to the energy of the buried hydrogen bond. Conversely, hydrogen exchange studies also showed that the rate-limiting step in unfolding can be associated with the disruption of the hydrogen bond network. A number

of experiments that involved site-directed mutations indicated that hydrogen bonds could have an overall positive contribution to the protein stability. Although the energetic role of hydrogen bonding in protein stability is still a matter of debate, it is clear that once the internal hydrogen bonds are formed, they cannot be broken easily. It would be energetically very expensive to bury the unsatisfied polar group inside the hydrophobic core. Hydrogen bonds can guide protein folding by making it energetically unfavorable to convert already built structures rich in hydrogen bonding into other, structurally less-organized conformations.[26,27]

Conformational Entropy. The major force that opposes the hydrophobic effect is conformational entropy. The number of conformational states accessible to the unfolded protein is enormous. The polypeptide chain of the unfolded protein is very flexible due to the large number of degrees of freedom. Of particular interest in the unfolded state are the degrees of freedom related to the side chain rotation around torsion angles. As the protein folds, parts of its structure are confined to the hydrophobic core, where free rotation around the torsional angles is hindered due to steric effects and formation of a large number of hydrogen bonds. This results in a limited number of conformations, and as a consequence, a substantial loss of entropy that accompanies the process of folding. The folding is favored only if the hydrophobic effect exceeds the loss of conformational entropy.[25]

Electrostatic Interactions. The electrostatic interactions that take place between charged particles are characterized by an energy change that is distance dependent, as described by Coulomb's law. The energy of electrostatic interaction depends on the

nature of the charges, the distance between them and the dielectric constant of the medium. The dielectric constant of the protein exhibits large variations due to the diversity of protein structure and the presence of the protein-water interface. The dielectric constant inside the protein is believed to be significantly lower than water (2-4, in comparison to 80, respectively). The dielectric constant at the water-protein interface is thought to be similar to the one at the lipid-water interface, which is less than 40. The fact that the exact values for the dielectric constants of the protein are not known makes the determination of the electrostatic interactions and their influence on protein stability very challenging.[5,26,27]

In general, it is believed that the electrostatic interactions can contribute to the protein stability in two ways, through classical effects or as specific charge interactions. The classical effects are related to the nonspecific repulsions that occur between the protein and the surrounding solvent. These are conditions of high pH and/or ionic strength when protein is highly charged. The increase in the total charge of the protein results in the increased repulsion between the protein and solvent and, consequently, the destabilization of the native protein. The acid or base denaturation of the protein results in a state with lower electrostatic free energy.

Specific charge interactions, such as the formation of ion pairs, are the result of attractive forces between two oppositely charged amino acids. Unlike the electrostatic interactions in the classical sense, these interactions stabilize the protein structure. The largest contribution to the stability of the native state comes from the ion pairing on the surface of the protein. [26,27]

Van der Waals Interactions. Van der Waals interactions are nonpolar interactions between two dipoles, fixed or induced. The energy of these interactions is usually described with the Lennard-Jones potential, where the distance between atoms is defined as the sum of the Van der Waals radii. These interactions are generally very weak and characterized by low energies, so the resulting effect on protein stability is small but additive.[5,26,27]

All the interactions described above play a part in the stabilization of the native structure. How these interactions balance one another to create a stable native structure remains a puzzle. In the following we review theoretical models and experimental methods that have been applied to address this question.

1.1.2. Mechanisms

Almost 40 years ago, Anfinsen showed that proteins can fold reversibly without any help from other biological molecules. Anfinsen suggested that the amino acid sequence of a protein fully determines the three-dimensional structure. He proposed that the native state is the conformation corresponding to the lowest possible free energy. This idea is known as the *thermodynamic model* of protein folding.[28] However, Levinthal showed that the number of accessible conformations that a protein would have to search through in order to find the native state is endless. He showed that it would be impossible even for a very small protein to fold in a reasonable time frame if it had to sample them all.[29] Yet, many proteins fold on the millisecond to second timescale. This disagreement in actual and calculated time required for protein folding is known in literature as

Levinthal's paradox. As a solution, Levinthal proposed that the protein folds into the native state that does not necessarily correspond to the global free energy minimum. It does so by following a limited number of well-defined pathways. This is in contradiction to Anfinsen's thermodynamical model, and implies that protein folding is a kinetically controlled process. Levinthal's work initiated the development of several models for protein folding that involved a limited number of pathways.

The *nucleation model* of protein folding was based on the hypothesis that the amino acid sequence of each protein contains several residues that serve as markers. These residues are capable of forming initial contacts from which parts of the native secondary structure are built. They can act as a nucleus from which the structure can propagate further, in a stepwise manner, towards the native state. This model implies that there are no intermediates in the folding, and was abandoned with the first experimentally detected intermediates.[25] The updated version of this model is called the *search nucleation.*[30] In this model protein folding is envisioned as the search for the minimal number of contacts needed to achieve the native state. The search is performed through a trial-and-error process that traps critical, structure-formative hydrogen bonds. This leads to the formation of a nucleus with native-like topology which rapidly proceeds to the fully folded state.[31,32]

The *diffusion-collision model*, also known as the *framework model*, proposes that the formation of the secondary and tertiary structures occurs independently. In this model the conformational search is reduced by the formation of early-time secondary structures. These structures diffuse until they collide and reorganize into the tertiary structure.

The main hypothesis of the *hydrophobic-collapse model* was that the rapid collapse around the hydrophobic side chains of the protein creates an intermediate with restricted conformational space and far-off tertiary contacts. From this intermediate state the structure can rearrange further, governed by the native tertiary interactions.[25]

The experimental observation of intermediates in protein folding raised questions about their role in the process. One opinion is that their presence increases the rate of folding but it is clearly inconsistent with the experimental finding that many small globular proteins are fast-folders that follow two-state kinetics. The other opinion is that folding intermediates correspond to traps, which slow down the folding process. Even though the models discussed above provide an explanation for some of the experimental results, none of them provide a unified explanation for very complex experimental findings that went in favor of both thermodynamic and kinetic control of folding.

1.1.3. Energy Landscape and Funnels

In the *new view* advanced especially by Wolynes, Onuchic, Brooks and their coworkers, folding proteins are steered towards the native state as they fold by the funnel-shaped topology of the potential-energy hypersurface, also called the *energy landscape*.[33-37] This view requires consideration of the dynamics of an ensemble of folding trajectories, rather than the standard single-path reaction-coordinate picture with few well-defined intermediates that is suggested by most biochemical and spectroscopic experiments.[34] The hypothetical funnel shaped energy landscape for a small protein is shown in Figure 1.1 in a two-dimensional representation. The reader should keep in mind

that the real energy landscape is a complex multi-dimensional surface, with as many independent coordinates as there are internal degrees of freedom.[34] The vertical coordinate on the funnel-shaped surface is internal energy, E, defined as the total free energy without the entropy contribution. The entropy is represented by the width of the funnel. One additional parameter is proposed in this representation of the protein folding energy surface, and that is the measure of the native-like contacts, Q. The position of the ensemble of states within the funnel is described by the E and Q parameters. At the very top of the funnel is an ensemble of conformations for an unfolded protein. The unfolded state of the protein can be characterized as a state with large conformational freedom where individual groups and parts of the polypeptide chain can freely rotate relative to one another. As a consequence, the number of accessible conformational states for an unfolded protein is very large and has high entropy. As the protein folds into an ordered native structure, the number of different conformational states decreases and, consequently, entropy decreases, too. The decrease in the number of different conformational states is a direct consequence of the formation of the larger number of correct native contacts. When the number of correct native contacts becomes significant (about 25% or more), a partially folded protein reaches the ensemble of states called *molten globule*. Structural characteristics of the molten globule state are the presence of

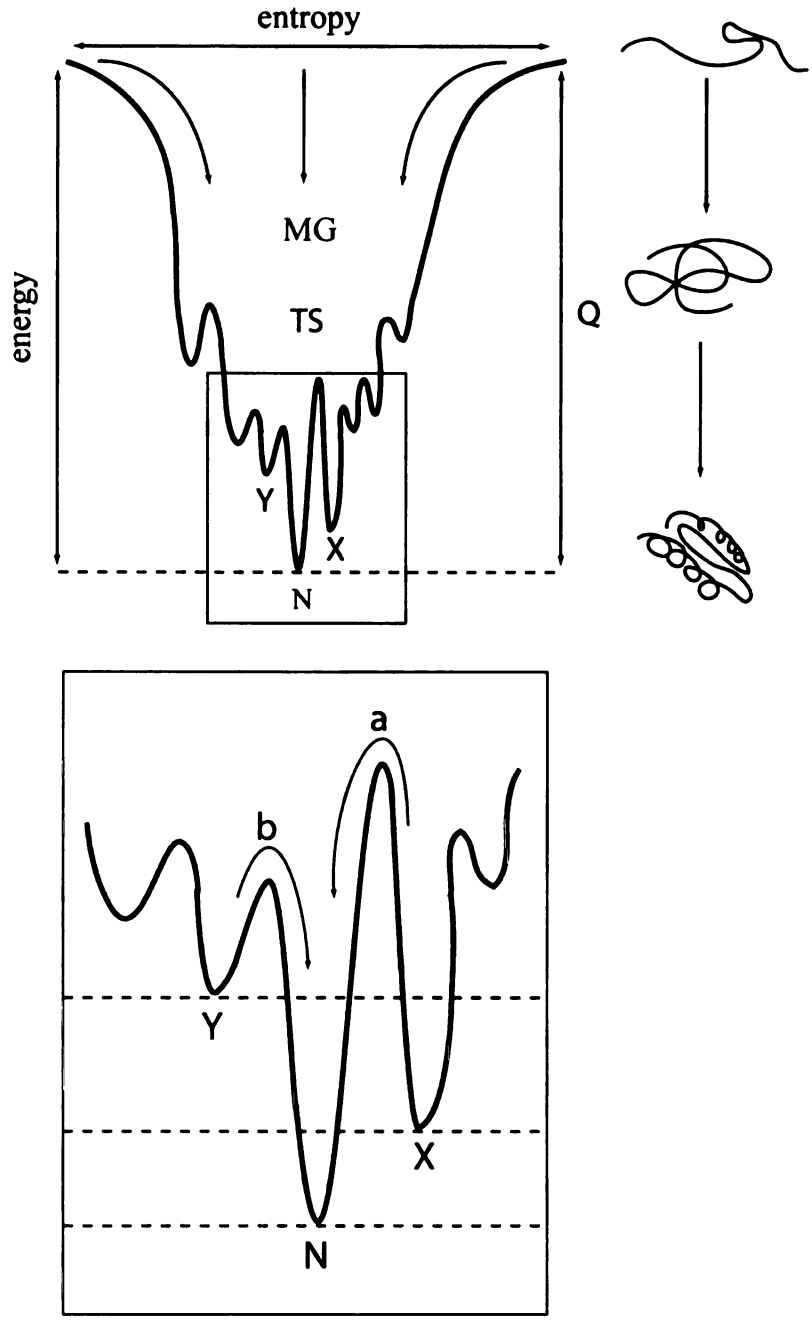

Figure 1.1 *Top panel.* Hypothetical funnel-shaped energy landscape. During the folding process protein moves down the funnel from the unfolded structure to the folded at the bottom of the funnel which is accompanied by a decrease in energy E and entropy, and with increase in native contacts Q. On its way to the native state protein goes through the region of molten globule MG and overcomes the transition state TS barrier before it finally reaches the native state. After Onuchic and Wolynes[34] *Bottom panel.* Enlarged view of near vicinity of a native state position in the funnel depicting the thermodynamic (*a*) and kinetic (*b*) paths.[38]

some secondary structure and some tertiary interactions and also the presence of the hydrophobic core. This state is very similar in structure to the native state, but less compact and energetically less stable. After the molten globule state, the folding process reaches the transition state region or so-called energy bottleneck on the potential energy landscape, after which the structure collapses into the compact and stable native state.[25]

The idea of the funnel-shaped potential energy landscape overcomes Levinthal's paradox by seeing the folding process as an ensemble average of a process that is in reality very heterogeneous. In this representation every molecule that undergoes folding can choose a different trajectory, but all molecules in the process will reach the same final state. Unlike the other models of protein folding, the energy landscape model explains folding as a process that is thermodynamically and/or kinetically controlled. [35]

1.1.4. Thermodynamic and kinetic control

The thermodynamically controlled folding process is the one defined by the energy of the conformational states and guided by the tendency to reach the state that corresponds to the global minimum on the energy landscape. In contrast, the kinetically controlled process is guided by the rate of the transformation from some random conformation to the native state, where the fastest route would be preferable.[35,39] In the potential energy landscape, the shape of the folding funnel and presence of the final state signify the thermodynamical control of protein folding. The final state is defined as the conformation with lowest energy. The ruggedness of the potential energy funnel implies kinetic control of protein folding by introducing a number of local minima where the

protein can temporarily or finitely reside depending on the height of the barrier.[35]

The comparison of two types of control can be seen at the bottom of Figure 1.1, which represents an enlarged view of the vicinity of the native state in the folding funnel. State X is obviously thermodynamically preferred, since it is energetically closer to the native state. However, state Y is kinetically preferred since it implies a smaller barrier to cross on the way to the native state. Depending on whether the system chooses path *a* or path *b*, the folding can be either thermodynamically or kinetically controlled.[35,40] The proteins that have smooth funnels show a preference towards the folding process which is mostly thermodynamically controlled, while the proteins with rugged folding funnels could fold via the kinetically controlled process. This implies that the native state does not necessarily have to be the state corresponding to the global energy minimum; it can be the state close to the global energy minimum that is kinetically preferred.

1.1.5. Experimental and Theoretical Approach

Protein folding reactions have been examined using NMR linewidth measurements from which structural information can be obtained.[41,42] The protein stability and structural dynamics are extensively studied with NMR methods coupled to hydrogen exchange.[43-45] Temperature jump methods were applied to studies of small peptides, and protein unfolding and refolding dynamics.[46-49]

Protein folding free energy surfaces can be sampled with molecular dynamics (MD) simulations. The MD simulations are based on Newton's laws of motion that are applied to every atom in the protein and surrounding solvent.[25,50] This requires

calculations of the large number of conformational states over a long period of time. As a result the calculations of folding reactions are limited to relatively short timescales. MD studies are suitable for the characterization of unfolding reactions since the initial parameters can be obtained from X-ray and NMR structural studies. Furthermore, simulating denaturants or increasing temperature can accelerate the unfolding reaction and reduce calculation time. The folding reaction can be examined by running the MD simulations for the unfolding reaction in reverse. MD simulations were successfully used for characterization of transition states and intermediate and denatured states in a variety of proteins including chymotrypsin inhibitor 2,[51] bovine pancreatic trypsin inhibitor,[52] barnase[53] and myoglobin.[54] Recently MD simulations were applied for studying conformational transition of amyloid *b*-peptide, a small protein related to Alzheimer's disease[55] and prion protein related to transmissible spongiform encephalopathies.[56]

1.1.6. Role of Intrinsic and Surface Water

Water plays an important role in the dynamics, function, structure and stability of proteins. Several different types of biological water can be recognized, depending on their position with respect to the protein molecule: structural or buried water, hydration water located in the vicinity of the protein surface and bulk water. Structural water is an integrated part of the protein structure; it interacts with the protein side chains and can organize in clusters in the hydrophobic regions inside of the protein. Hydration water interacts with the protein surface, resulting in the coupling of fluctuations of hydration water to the protein dynamics. This interaction stabilizes the folded structure but can also have a large effect on protein dynamics, increasing the complexity.

The most obvious reason why water has to be involved in studies of the protein folding process is its role in the hydrophobic effect, one of the main effects that govern folding.[57] One approach to studying water involvement in protein folding is to examine desolvation during the folding process starting with a fully solvated unfolded polypeptide chain. Onuchic and coworkers[58] used the minimalist model to investigate the desolvation of the SH3 protein during the folding process by including the effects of expulsion of water in the energy landscape theory. They found the presence of an intermediate with a partially solvated hydrophobic core that is structurally very close to the collapsed structure of the native state. These results are in agreement with Zhang et al[59-61] and Mok et al.,[62] who confirmed experimentally the existence of an intermediate SH3 structure with a hydrated hydrophobic core. The formation of this near-native structure precedes the final step in the folding of the protein, which according to Onuchic and coworkers is the desolvation of the hydrophobic core. In another contribution,[63] authors performed a detailed theoretical and experimental study of folding rates using mutations in the hydrophobic core on an a-spectrin SH3 protein. These studies suggested that the desolvation of the hydrophobic core in this protein is the most important step in overcoming the transition state barrier for folding.

Wolynes and coworkers suggested that the smooth regions of the potential energy funnel result from long-range water-mediated interactions. Hence, the water is directly involved in the folding process by insuring proper steering through the funnel and increasing the efficiency of folding.[64] Similar results were obtained for proteins A and G from atomistic simulation studies.[64-66]

The experimental studies of the dynamics of biological water report wide range of time scales depending on the method used, ranging from the several hundreds of picoseconds determined by NMR,[67,68] to several nanosecond as determined by dielectric relaxation experiments. Zewail and coworkers used surface tryptophan as a natural probe in solvation dynamics studies of surface water.[69,70] They observed a bimodal hydration response with time constants on the order of ps. The slower component of the response was attributed to the surface-bound water; the fast component was attributed to the free water. In the unfolded protein both time constants significantly lengthened. The authors proposed that the longest time constant (~60 ps) observed in the study with unfolded protein involves motions of the protein backbone.

1.2. Structural Fluctuations and Time-Correlation Function

Proteins are characterized by a high level of order but this does not mean that they are static structures. Even in the native state proteins exhibit motions over a wide range of timescales, amplitudes and energies. The motions can span from the global motions of the entire protein to local motions related to the atomic fluctuations and rotation of the amino-acid side chains. The high level of dynamics in proteins implies that in the native state protein fluctuates around some average structure, so even at room temperature it can sample a large number of conformations. Water also has a large impact on the motions of proteins and their dynamics. Fenimore et al.[71] argued that motions in the protein can be coupled to fluctuations in surrounding water. The protein motions are affected by the surrounding solvent mainly because of the difference in the dielectric coefficients of protein and water. The desolvated protein has a significantly smaller dielectric coefficient

than water. The fluctuations of the water dipoles surrounding the protein couple to the fluctuations of the water dipoles in the hydration shell and with charged residues at the protein surface, affecting the dynamics of the protein. This suggests that it could be possible to monitor solvent-protein interaction by detecting the dipole moment fluctuations of a carefully chosen probe molecule attached to the protein. The work presented in this dissertation utilizes that idea by experimentally observing protein dynamics in the folded and unfolded state through measurement of a solvent response function.

Upon excitation with light, the chromophore experiences an instantaneous transition from the equilibrium in the ground state to a higher electronic state (see Figure 1.2). This transition is accompanied by a fast change in the dipole moment of the chromophore. The solvent molecules that surround the chromophore cannot reorganize instantaneously in order to adapt to the new dipole moment of the chromophore, which as a consequence has a different chromophore-solvent interaction in the excited state than in the ground state. The energy released by the solvent molecules as they equilibrate within the excited state after Franck-Condon transition is called solvent reorganization energy, l. As the system equilibrates in the excited state, the energy gap between the two states will decrease in time and transition frequency ω_{eg} red-shifts.

In the condensed phase, the ground-to-excited-state transition frequency ω_{eg} of an electronic chromophore fluctuates with respect to time, owing to collisions and to the electrostatic interactions with molecules in motion outside the first solvation shell.

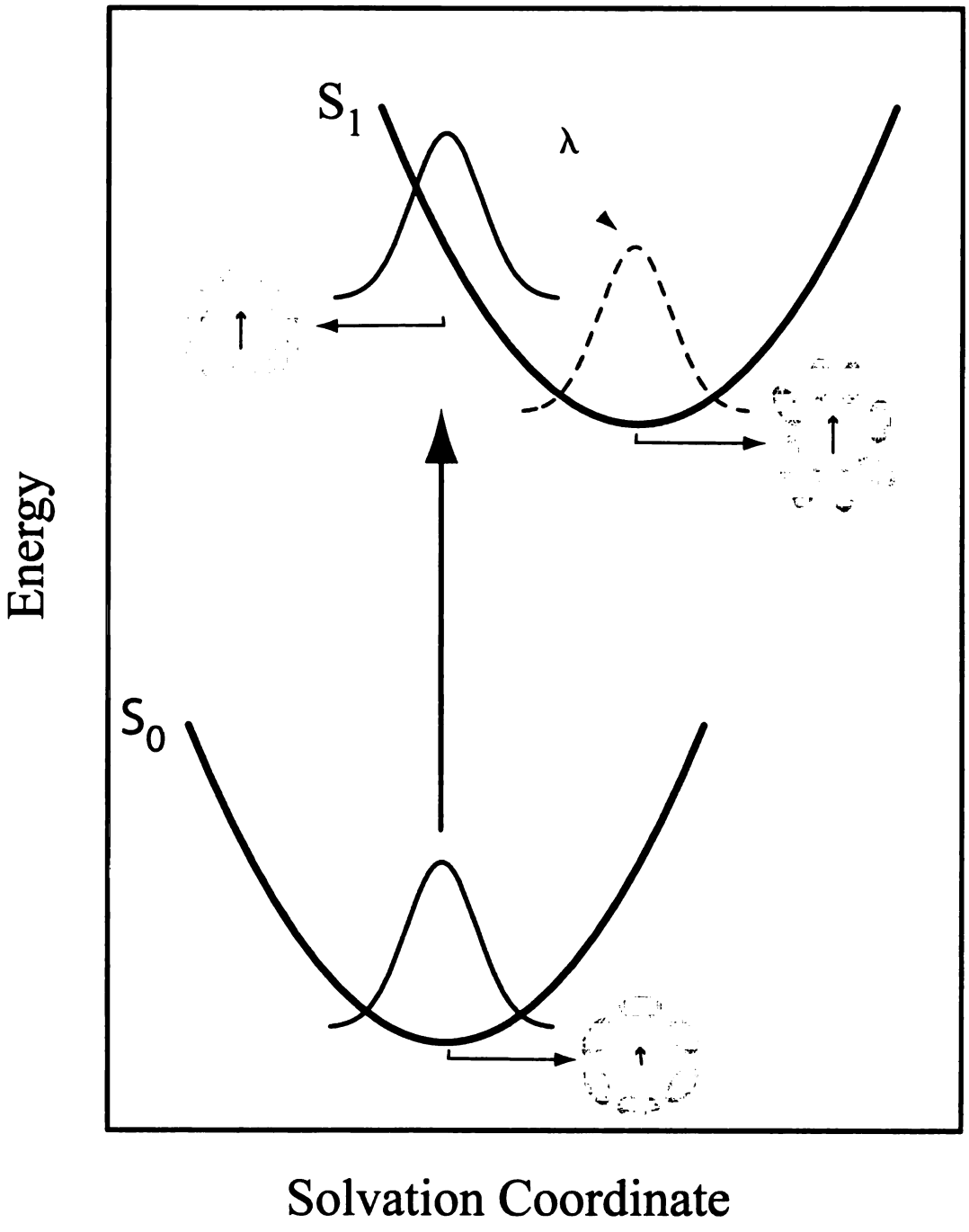

Figure 1.2 Solvation dynamics and the dynamic Stokes shift. Following electronic excitation of a solute chromophore, the solvent molecules still reside in the configuration that was reached at equilibrium with the ground state solute's dipole moment. Over time, the solute molecules reorganize in response to the change in the solute's dipole moment; the fluorescence spectrum shifts to the red as the system approaches equilibrium. After Stratt and Maroncelli.[72]

The fluctuation can be expressed in terms of the difference $\delta\omega_{eg}(t)$ between the transition frequency for a certain molecule at a given instant in time and that frequency averaged over the ensemble, $\langle\omega_{eg}\rangle$:[73-77]

$$\omega_{eg}(t) = \langle\omega_{eg}\rangle + \delta\omega_{eg}(t) + \varepsilon \tag{1.1}$$

The parameter ε is that part of the difference from the average for a given chromophore–solvent site that does not vary with time. The time correlation function $M(t)$ describes the loss of memory of the transition energy owing to the solvent-induced fluctuations:

$$M(t) = \frac{\langle\delta\omega_{eg}(0)\delta\omega_{eg}(t)\rangle}{\langle\delta\omega_{eg}{}^2\rangle} \tag{1.2}$$

The time evolution of the fluorescence spectrum defines a normalized solvent-response function, $S_\nu(t)$, defined usually in terms of the frequency at the fluorescence intensity maximum, n(t).[72]

$$S_\nu(t) = \frac{\nu(t) - \nu(\infty)}{\nu(0) - \nu(\infty)} \tag{1.3}$$

$M(t)$ and $S_\nu(t)$ are equivalent in the high-temperature limit, where the breadth of the energy fluctuations is much less than k_BT, and in the linear-response regime, where the perturbation caused by the ground-to-excited-state electronic excitation of the probe is

not so large that the motions of the solvent are different in the two electronic states.[72,75,76,78]

1.2.1. Molecular Liquids

Extensive studies performed on molecular liquids showed that it is possible to extract information about the time evolution of the solvent-solute interaction energy by detecting the time-resolved emission spectrum from an electronically excited chromophore.[79-81] The obtained experimental data suggests that the solvation dynamics in liquids are biphasic in nature. Fleming and coworkers[82] observed the fast inertial phase of solvation dynamics that occurred on 100 fs timescale. Maroncelli and Stratt attributed this fast phase of solvation dynamics to the librational motions of the solvent molecules surrounding the probe molecule.[81,83] Fleming and Barbara associated the slower, diffusive component with reorientational motions[74,79,84] The experimental results of Maroncelli[81] and theoretical work of Ladanyi and Stratt[85] suggest that solvation dynamics in both polar and nonpolar media result from the coupled rotational and/or translational dynamics chromophore-solvent system. While the polar solvation response is the result of a change in the probe's dipole moment, the non-polar solvation response is the result of a change in the probe's size or structure. The details of solvation dynamics in two media can vary due to the differences in the intermolecular interactions between the chromophore and solvent and solvent and solvent, but the solvation response exhibits a fast decay due to the inertial dynamics, followed by the slow diffusive dynamics in both polar and nonpolar media.

1.2.2. Polypeptide and Folded Proteins

The fluctuations that contribute to the decay of $M(t)$ and $S_\nu(t)$ in proteins might involve collision-like interactions between the probe and the surrounding polypeptide host and any intrinsic water molecules. Owing to the low effective dielectric constant in the interior of a protein,[86] however, the fluctuations may also involve more distant interactions of the chromophore's dipole moment with dipoles in the protein structure or, perhaps, on the surface of the protein than are possible in a molecular solvent with a high dielectric constant, where the interactions with the distant dipoles are attenuated. A consensus has not been reached on how a protein's structure and the included solvent contribute to $M(t)$ and $S_\nu(t)$.

In previous work in this laboratory, an intrinsic extended tetrapyrrole chromophore was used in transient-hole burning and stimulated photon-echo peak-shift experiments to sense the dynamics of a small globular protein, the alpha subunit of *C*-phycocyanin. A large fraction (90 %) of the decay of $M(t)$ in *C*-phycocyanin was observed on the <100 fs scale.[87,88] In molecular liquids, a probe's energy gap exhibits fluctuations on this time scale owing to the *inertial* (free-steaming, free-rotor or librational) motions of the surrounding solvent molecules.[87,88] The *diffusive* portion of the decay of $M(t)$ in *C*-phycocyanin extends, perhaps, even to the ns time scale, as it might in a slow-relaxing, viscous solvent. This part of the time-correlation function arises from random reorientational motions in a molecular solvent. Both the inertial and diffusive parts of $M(t)$ were assigned to motions of the surrounding protein structure and intrinsic water molecules.[88,89] A large inertial solvation component was also observed by Fleming

and co-workers in a chicken egg-white lysozyme, which was extrinsically probed with the fluorescent dye eosyn. The results indicated that the protein may make a contribution to the diffusive part of $M(t)$, but the large inertial component was strongly correlated with motions of the bulk aqueous solvent.[74] The solvation response observed by the same group in bacteriorhodopsin using the intrinsic retinal chromophore as the probe consists solely of an inertial component, with the bulk of the decay confined to the sub-50 fs regime; no diffusive decay was observed over the 1 ps-window in which stimulated photon echoes could be observed.[73]

Hochstrasser and co-workers[78] probed the solvation dynamics of calmodulin in pump–probe studies of the dynamic Stokes shift of the stimulated-emission spectrum of coumarin 343, which was used to label the protein. The inertial component that they observed on the sub-100-fs time scale was followed by a smaller diffusive component on the ps time scale. Both solvation components were assigned to motions of the surrounding protein rather than to the bulk solvent molecules.

Cohen et al.[86] observed a generally biphasic solvation response in the B1 domain of protein G using the fluorescent synthetic amino acid aladan incorporated at specific sites in the amino-acid sequence. The femtosecond fluorescence upconversion technique was employed in this work. The dynamic Stokes shift response that was detected both at the buried and solvent-exposed sites has a prominent sub-ps component followed by an exponential or multiexponential diffusive response that reached to the end of the reported 150-ps decay window. The magnitude of the solvation response was dependent on the degree of solvent exposure, with the exposed sites exhibiting a larger reorganizational

energy, but a substantial fraction of the reorganization was observed in the sub-ps portion at all of the probed sites. An important conclusion from this work is that the solvation response should be expected to be heterogeneous and strongly dependent on the location of the probe in the folded protein. For that reason it might be suitable to study solvation response with proteins that have naturally present chromophore, such as heme proteins.

1.3. Structure, Dynamics and Folding Reactions of Cytochrome *c*

1.3.1. Structure

Cytochrome *c* is an electron-transfer protein present in the mitochondrial membrane of all aerobic organisms. The role of cytochrome c is to carry electron between the cytochrome *c* reductase and cytochrome *c* oxidase in the final steps of the respiratory chain. It is a small globular protein with a single polypeptide chain of 103 to 111 amino acid residues, depending on the species. Cytochrome *c* contains a prosthetic group, an iron protoporphyrin IX ring (heme) (see Figure 1.3).

Unlike in some other heme proteins, myoglobin and hemoglobin for example, heme in cytochrome *c* is covalently bonded to the polypeptide chain via thioether bonds to the invariant Cys 14 and Cys 17. The Fe(II) in the heme is octahedrally liganded and can be in either the Fe(II) or Fe(III) oxidation state. Four octahedral ligands to the iron atom are supplied by the porphyrin ring. Axial ligands to the iron atom are contributed by the nitrogen of the His 18 side chain and the sulfur of Met 80. Hydrophobic residues occur in clusters, mostly in the heme region. The heme-binding region, hydrophobic

residues in its vicinity and two water molecules are highly conserved in cytochrome *c* molecules from different species. The small size of this protein and the presence of the natural chromophore, which is well-enveloped by the protein matrix and stays bonded to the polypeptide chain even when the protein is fully unfolded, makes cytochrome *c* a very attractive target for protein folding studies.

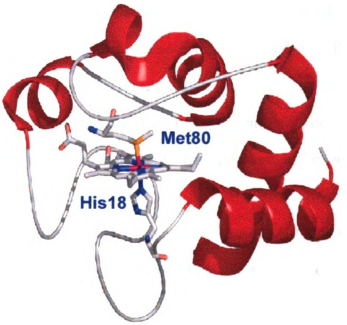

Figure 1.3 The structure of horse-heart[90] ferricytochrome *c*, rendered using PyMOL.[91]

1.3.2. Folding Intermediates

The unifying picture of the cytochrome c folding process is a result of experimental studies performed with a variety of methods. The results suggest that the bottleneck for the folding reaction of cytochrome *c* has its origin in the final steps in the search for the native structure and not in the initial condensation of the polypeptide chain.

Cytochrome *c* folding starts with formation of an early intermediate species characterized by a more compact polypeptide chain.[92,93]

When initiated from the acid-denatured state, folding of cytochrome *c* is rapid and occurs on two distinct time scales of 500 ms and about 15 ms. Biphasic folding in this case is attributed to the formation of helices, which occurs stepwise.[94] The same authors found two distinct intermediates that occur on-pathway during refolding of cytochrome c (at 160 ms and 500 ms). The faster time constant is related to the rapidly formed intermediate, which has some helix content and is almost two times larger in radius than the native state. This structure evolves into the second intermediate at 500 ms, which is more compact and in which the majority of helical content is formed. The presence of these two distinct intermediate forms was also confirmed by small angle X-ray scattering.[95] The native state is formed at a much slower rate (10-100 ms), which strongly depends on the refolding conditions and the formation of intermediates that involve the improper coordination of heme.

1.3.3. Role of Heme Ligation in the Folding Reaction

Denaturation of cytochrome *c* causes the displacement of the Met 80 ligand while His 18 stays coordinated to the iron in the heme. Spectral data showed that Met 80 is most commonly replaced with another His residue.[96] The non-natively ligated His residues in horse heart cytochrome *c* are typically His 26 or His 33, and their ligation to the heme iron can effect the overall rate of the folding of cytochrome *c*. Roder and coworkers[97] showed that folding initiated from the base-denatured state of cytochrome c

is slowed to several hundred milliseconds. The slow folding is attributed to the formation of an off-pathway intermediate due to the mis-coordination of iron in a heme group by His 26 or His 33. They[98] proposed the kinetic mechanism for the folding/unfolding of oxidized cytochrome *c*, which involves heme ligand exchange coupled to structural changes. In the early stages of folding several intermediate species are present that involve bounding of the non-native histidine. The misligation of the histidine represents a trap on the folding pathway and is the rate-limiting step. This mechanism is supported by experiments performed by a variety of methods: resonance Raman spectroscopy,[93] stopped-flow measurements monitored by fluorescence, heme absorbance, and CD over a range of conditions.[99-102] In contrast, the reduced form of cytochrome *c* seems to exhibit a two-state folding mechanism. The ligand exchange reactions were detected in the folding mechanism of reduced cytochrome *c* by triggering refolding with laser-induced photolysis of the CO ligand. These reactions involved alternative His and Met ligands and occurred on time scales much faster than in the oxidized form of cytochrome *c*, and long-lived intermediate species were not detected.

1.4. Proposed work

The investigation of the molecular mechanism involved in creation of the disease related species along the folding trajectory needs to start with a detailed evaluation of the native state. The protein in the native state is a highly dynamic structure that exhibits a wide range of motions while switching from one low energy conformation to another. Some of these motions might be responsible for trapping the protein in undesirable conformations which could ultimately result in a misfolded, toxic form. We will

investigate motions that protein exhibits in the native state by employing picosecond time-resolved fluorescence studies of solvent response from a Zn(II) substituted cytochrome *c*.

The native cytochrome c is not suitable for studies of the dynamics of a solvated protein with time resolved fluorescence, since the naturally present chromophore with the Fe(II) ion has a very short fluorescence lifetime. However, substitution of the Fe(II) ion in the heme with the Zn(II) ion provides the chromophore with long-lived fluorescence[103] and makes it a suitable probe for solvation dynamics. The studies of the Zn-substituted cytochrome *c* (ZnCytc) with continuous absorption and fluorescence spectra and 2D-NMR showed that replacement of the Fe(II) ion with Zn(II) in the heme does not result in a different structure.[104,105] Vanderkooi and coworkers applied fluorescence line narrowing spectroscopy to study ZnCytc in the native and denatured states.[106] Winkler and coworkers probed the environment of the heme chromophore in the native and denatured states of ZnCytc by monitoring triplet state decay kinetics.[107]

We will use this spectroscopically well characterized protein to probe not only solvation response in the native state but also near the transition for unfolding, since the chromophore stays bound to the protein even when it is fully unfolded. In the studies of the various diseases it has been indicated that toxicity of the misfolded species might be caused with increased exposure of the inside of the protein to the surrounding solvent and inappropriate hydrophobic interactions. The importance of water in the folding mechanism is well established, but the influence of water on the dynamics of proteins is not fully understood. Of particular interest is entrance or exit of water into and from

hydrophobic core since it is directly involved in the hydrophobic collapse of the protein structure. While the dynamics of the surface water is studied to the certain extent, the direct observation of the water entrance or exit into the hydrophobic core, its dynamics and its effect on the protein motions are not known.

So far, the studies of protein folding, unfolding and misfolding reactions were limited to the applications of methods that involve significant manipulation of the protein solution conditions or the temperature. We intend to address the above questions by studying the protein folding, unfolding and misfolding reactions triggered without imposing external manipulation of the solvent, or without the direct change of the temperature of the protein solution.

1.5. References

(1) Prusiner, S. B. *Proc. Natl. Acad. Sci. USA* **1998**, *95*, 13363–13383.

(2) Dobson, C. M. *Trends Biochem.Sci.* **1999**, *24*, 329–332.

(3) Caughey, B.; Lansbury, P. T. *Annu. Rev. Neurosci.* **2003**, *26*, 267–298.

(4) Dobson, C. M. *Nature* **2003**, *426*, 884–890.

(5) Kauzmann, W. *Adv. Protein. Chem.* **1959**, *14*, 1–63.

(6) Dobson, C. M. Philos. Trans. R. Soc. Lond. Ser. B-Biol. Sci. **2001**, 356, 133–145.

(7) Sunde, M.; Blake, C. The structure of amyloid fibrils by electron microscopy and X-ray diffraction. In *Adv. Prot. Chem.*, 1997; Vol. 50; pp 123–159.

(8) Chiti, F.; Stefani, M.; Taddei, N.; Ramponi, G.; Dobson, C. M. *Nature* **2003**, *424*, 805.

(9) Blake, C. C. F.; Geisow, M. J.; Oatley, S. J.; Rerat, B.; Rerat, C. *J. Mol. Biol.* **1978**, *121*, 339–356.

(10) Coelho, T. *Curr. Opin. Neurol.* **1996**, *9*, 355–359.

(11) Plante-Bordeneuve, V.; Said, G. *Curr. Opin. Neurol.* **2000**, *13*, 569–573.

(12) Chiti, F.; Webster, P.; Taddei, N.; Clark, A.; Stefani, M.; Ramponi, G.; Dobson, C. M. *Proc. Natl. Acad. Sci. USA* **1999**, *96*, 3590–3594.

(13) Selkoe, D. J. *Nature* **2003**, *426*, 900–904.

(14) Pertinhez, T. A.; Bouchard, M. L.; Tomlinson, E. J.; Wain, R.; Ferguson, S. J.; Dobson, C. M.; Smith, L. J. *Febs Lett.* **2001**, *495*, 184–186.

(15) Fandrich, M.; Forge, V.; Buder, K.; Kittler, M.; Dobson, C. M.; Diekmann, S. *Proc. Natl. Acad. Sci. USA* **2003**, *100*, 15463–15468.

(16) Guijarro, J. I.; Sunde, M.; Jones, J. A.; Campbell, I. D.; Dobson, C. M. *Proc. Natl. Acad. Sci. USA* **1998**, *95*, 4224–4228.

(17) Chiti, F.; Bucciantini, M.; Capanni, C.; Taddei, N.; Dobson, C. M.; Stefani, M. *Prot. Sci.* **2001**, *10*, 2541–2547.

(18) Lambert, M. P.; Barlow, A. K.; Chromy, B. A.; Edwards, C.; Freed, R.; Liosatos, M.; Morgan, T. E.; Rozovsky, I.; Trommer, B.; Viola, K. L.; Wals, P.; Zhang, C.; Finch, C. E.; Krafft, G. A.; Klein, W. L. *Proc. Natl. Acad. Sci. USA* **1998**, *95*, 6448–6453.

(19) Walsh, D. M.; Townsend, M.; Podlisny, M. B.; Shankar, G. M.; Fadeeva, J. V.; El Agnaf, O.; Hartley, D. M.; Selkoe, D. J. *J. Neurosci.* **2005**, *25*, 2455–2462.

(20) Hartley, D. M.; Walsh, D. M.; Ye, C. P. P.; Diehl, T.; Vasquez, S.; Vassilev, P. M.; Teplow, D. B.; Selkoe, D. J. *J. Neurosci.* **1999**, *19*, 8876–8884.

(21) Bucciantini, M.; Giannoni, E.; Chiti, F.; Baroni, F.; Formigli, L.; Zurdo, J. S.; Taddei, N.; Ramponi, G.; Dobson, C. M.; Stefani, M. *Nature* **2002**, *416*, 507–511.

(22) Bucciantini, M.; Calloni, G.; Chiti, F.; Formigli, L.; Nosi, D.; Dobson, C. M.; Stefani, M. *J. Biol. Chem.* **2004**, *279*, 31374–31382.

(23) Cleary, J. P.; Walsh, D. M.; Hofmeister, J. J.; Shankar, G. M.; Kuskowski, M. A.; Selkoe, D. J.; Ashe, K. H. *Nat. Neurosci.* **2005**, *8*, 79–84.

(24) Volles, M. J.; Lansbury, P. T. *Biochemistry* **2003**, *42*, 7871–7878.

(25) Fersht, A. Structure and mechanism in protein science: aguide to enzyme catalysis and protein folding.; W. H. Freeman and Company: New York, 1997.

(26) Dill, K. A. *Biochemistry* **1990**, *29*, 7133.

(27) Pace, C. N.; Shirley, B. A.; McNutt, M.; Gajiwala, K. *Faseb Journal* **1996**, *10*, 75.

(28) Anfinsen, C. B. *Science* **1973**, *181*, 223.

(29) Levinthal C. Journal De Chimie Physique Et De Physico-Chimie Biologique **1968**, 65, 44.

(30) Sosnick, T. R.; Mayne, L.; Englander, S. W. *Proteins* **1996**, *24*, 413–426.

(31) Plaxco, K. W.; Simons, K. T.; Baker, D. *J. Mol. Biol.* **1998**, *277*, 985–994.

(32) Krantz, B. A.; Sosnick, T. R. *Biochemistry* **2000**, *39*, 11696–11701.

(33) Frauenfelder, H.; Sligar, S. G.; Wolynes, P. G. *Science* **1991**, *254*, 1598–1603.

(34) Onuchic, J. N.; Luthey-Schulten, Z.; Wolynes, P. G. *Annu. Rev. Phys. Chem.* **1997**, *48*, 545–600.

(35) Chan, H. S.; Dill, K. A. *Proteins: Struct. Funct. Genet.* **1998**, *30*, 2–33.

(36) Brooks III, C. L.; Onuchic, J. N.; Wales, D. J. *Science* **2001**, *293*, 612.

(37) Shea, J.-E.; Brooks III, C. L. *Annu. Rev. Phys. Chem.* **2001**, *52*, 499–535.

(38) Dill, K. A. *Protein Sci.* **1999**, *8*, 1166–1180.

(39) Baker, D.; Agard, D. A. *Biochemistry* **1994**, *33*, 7505–7509.

(40) Dill, K. A.; Chan, H. S. *Nature Struct. Biol.* **1997**, *4*, 10–19.

(41) Burton, R. E.; Huang, G. S.; Daugherty, M. A.; Fullbright, P. W.; Oas, T. G. *J. Mol. Biol.* **1996**, *263*, 311.

(42) Huang, G. S.; Oas, T. G. *Proc. Natl. Acad. Sci. U. S. A.* **1995**, *92*, 6878.

(43) Englander, S. W.; Sosnick, T. R.; Mayne, L. C.; Shtilerman, M.; Qi, P. X.; Bai, Y. W. *Acc. Chem. Res.* **1998**, *31*, 737.

(44) Englander, S. W.; Mayne, L. *Annu. Rev. Biophys. Biol. Struc.* **1992**, *21*, 243–265.

(45) Englander, S. W. *Annu. Rev. Biophys. Biol. Struc.* **2000**, *29*, 213–238.

(46) Gruebele, M. *Annu. Rev. Phys. Chem.* **1999**, *50*, 485–516.

(47) Callender, R.; Dyer, R. B. *Curr. Opin. Struc. Biol.* **2002**, *12*, 628.

(48) Ballew, R. M.; Sabelko, J.; Gruebele, M. *Proc. Natl. Acad. Sci. U. S. A.* **1996**, *93*, 5759–5764.

(49) Williams, S.; Causgrove, T. P.; Gilmanshin, R.; Fang, K. S.; Callender, R. H.; Woodruff, W. H.; Dyer, R. B. *Biochemistry* **1996**, *35*, 691–697.

(50) Daggett, V.; Levitt, M. *J. Mol. Biol.* **1993**, *232*, 600.

(51) Day, R.; Daggett, V. *Protein Science* **2005**, *14*, 1242.

(52) Daggett, V.; Levitt, M. *Proc. Natl. Acad. Sci. U. S. A.* **1992**, *89*, 5142.

(53) Caflisch, A.; Karplus, M. *Proc. Natl. Acad. Sci. U. S. A.* **1994**, *91*, 1746.

(54) Onufriev, A.; Case, D. A.; Bashford, D. *J. Mol. Biol.* **2003**, *325*, 555.

(55) Xu, Y. C.; Shen, J. J.; Luo, X. M.; Zhu, W. L.; Chen, K. X.; Ma, J. P.; Jiang, H. L. *Proc. Natl. Acad. Sci. U. S. A.* **2005**, *102*, 5403.

(56) Barducci, A.; Chelli, R.; Procacci, P.; Schettino, V. *Biophys. J.* **2005**, *88*, 1334.

(57) Harano, Y.; Kinoshita, M. *Chem. Phys. Lett.* **2004**, *399*, 342.

(58) Cheung, M. S.; Garcia, A. E.; Onuchic, J. N. *Proc. Natl. Acad. Sci. USA* **2002**, *99*, 685–690.

(59) Zhang, O. W.; FormanKay, J. D. *Biochemistry* **1997**, *36*, 3959.

(60) Farrow, N. A.; Zhang, O. W.; FormanKay, J. D.; Kay, L. E. *Biochemistry* **1997**, *36*, 2390.

(61) Zhang, O.; Formankay, J. D. *Biochemistry* **1995**, *34*, 6784.

(62) Mok, Y. K.; Kay, C. M.; Kay, L. E.; Forman-Kay, J. *J. Mol. Biol.* **1999**, *289*, 619.

(63) Fernandez-Escamilla, A. M.; Cheung, M. S.; Vega, M. C.; Wilmanns, M.; Onuchic, J. N.; Serrano, L. *Proc. Natl. Acad. Sci. USA* **2004**, *101*, 2834.

(64) Papoian, G. A.; Ulander, J.; Eastwood, M. P.; Luthey-Schulten, Z.; Wolynes, P. G. *Proc. Natl. Acad. Sci. USA* **2004**, *101*, 3352.

(65) Sheinerman, F. B.; Brooks, C. L. *J. Mol. Biol.* **1998**, *278*, 439.

(66) Garcia, A. E.; Onuchic, J. N. *Proc. Natl. Acad. Sci. USA* **2003**, *100*, 13898.

(67) Otting, G.; Liepinsh, E.; Wuthrich, K. *Science* **1991**, *254*, 974.

(68) Halle, B.; Andersson, T.; Forsen, S.; Lindman, B. *Journal of the American Chemical Society* **1981**, *103*, 500.

(69) Pal, S. K.; Peon, J.; Bagchi, B.; Zewail, A. H. *J. Phys. Chem. B* **2002**, *106*, 12376–12395.

(70) Peon, J.; Pal, S. K.; Zewail, A. H. Proceedings of the National Academy of Sciences of the United States of America **2002**, 99, 10964.

(71) Fenimore, P. W.; Frauenfelder, H.; McMahon, B. H.; Parak, F. G. *Proc. Natl. Acad. Sci. USA* **2002**, *99*, 16047.

(72) Stratt, R. M.; Maroncelli, M. *J. Phys. Chem.* **1996**, *100*, 12981–12996.

(73) Kennis, J. T. M.; Larsen, D. S.; Ohta, K.; Facciotti, M. T.; Glaeser, R. M.; Fleming, G. R. *J. Phys. Chem. B* **2002**, *106*, 6067–6080.

(74) Jordanides, X. J.; Lang, M. J.; Song, X.; Fleming, G. R. *J. Phys. Chem. B* **1999**, *103*, 7995–8005.

(75) Cho, M.; Yu, J.-Y.; Joo, T.; Nagasawa, Y.; Passino, S. A.; Fleming, G. R. *J. Phys. Chem.* **1996**, *100*, 11944–11953.

(76) Fleming, G. R.; Cho, M. *Annu. Rev. Phys. Chem.* **1996**, *47*, 109–134.

(77) Joo, T.; Jia, Y.; Yu, J.-Y.; Lang, M. J.; Fleming, G. R. *J. Chem. Phys.* **1996**, *104*, 6089–6108.

(78) Changenet-Barret, P.; Choma, C. T.; Gooding, E. F.; DeGrado, W.; Hochstrasser, R. M. *J. Phys. Chem. B* **2000**, *104*, 9322–9329.

(79) Jarzeba, W.; Walker, G. C.; Johnson, A. E.; Barbara, P. F. *Chem. Phys.* **1991**, *152*, 57–68.

(80) Maroncelli, M.; MacInnis, J.; Fleming, G. R. *Science* **1989**, *243*, 1674–1681.

(81) Maroncelli, M. *J. Mol. Liq.* **1993**, *57*, 1–37.

(82) Rosenthal, S. J.; Xie, X.; Du, M.; Fleming, G. R. *J. Chem. Phys.* **1991**, *95*, 4715–4718.

(83) Stratt, R. M.; Cho, M. *J. Chem. Phys.* **1994**, *100*, 6700–6708.

(84) Kahlow, M. A.; Jarzeba, W.; Kang, T. J.; Barbara, P. F. *J. Chem. Phys.* **1989**, *90*, 151.

(85) Ladanyi, B. M.; Stratt, R. M. *J. Phys. Chem.* **1995**, *99*, 2502–2511.

(86) Cohen, B. E.; McAnaney, T. B.; Park, E. S.; Jan, Y. N.; Boxer, S. G.; Jan, L. Y. *Science* **2002**, *296*, 1700–1703.

(87) Riter, R. E.; Edington, M. D.; Beck, W. F. Inertial protein-matrix solvation of a light-harvesting chromophore. In *Ultrafast Phenomena X*; Barbara, P., Knox, W., Zinth, W., Fujimoto, J., Eds.; Springer-Verlag: Berlin, 1996; pp 324–325.

(88) Homoelle, B. J.; Edington, M. D.; Diffey, W. M.; Beck, W. F. *J. Phys. Chem. B* **1998**, *102*, 3044–3052.

(89) Homoelle, B. J.; Beck, W. F. *Biochemistry* **1997**, *36*, 12970–12975.

(90) Bushnell, G. W.; Louie, G. V.; Brayer, G. D. *J. Mol. Biol.* **1990**, *214*, 585–595.

(91) Delano, W. L. *The PyMOL molecular graphics system*; DeLano Scientific: San Carlos, California, 2002.

(92) Shastry, M. C. R.; Roder, H. *Nature Struct. Biol.* **1998**, *5*, 385.

(93) Yeh, S.-R.; Han, S.; Rousseau, D. L. *Acc.Chem. Res.* **1998**, *31*, 727–736.

(94) Akiyama, S.; Takahashi, S.; Ishimori, K.; Morishima, I. *Nature Struct. Biol.* **2000**, *7*, 514.

(95) Pollack, L.; Tate, M. W.; Darnton, N. C.; Knight, J. B.; Gruner, S. M.; Eaton, W. A.; Austin, R. H. *Proc. Natl. Acad. Sci. USA* **1999**, *96*, 10115.

(96) Babul, J.; Stellwag.E. *Biopolymers* **1971**, *10*, 2359.

(97) Colon, W.; Wakem, L. P.; Sherman, F.; Roder, H. *Biochemistry* **1997**, *36*, 12535.

(98) Colon, W.; Elove, G. A.; Wakem, L. P.; Sherman, F.; Roder, H. *Biochemistry* **1996**, *35*, 5538.

(99) Colon, W.; Roder, H. *Nature. Struct. Biol.* **1996**, *3*, 1019.

(100) Elove, G. A.; Chaffotte, A. F.; Roder, H.; Goldberg, M. E. *Biochemistry* **1992**, *31*, 6876.

(101) Elove, G. A.; Bhuyan, A. K.; Roder, H. *Biochemistry* **1994**, *33*, 6925.

(102) Sosnick, T. R.; Mayne, L.; Hiller, R.; Englander, S. W. *Nature Struct. Biol.* **1994**, *1*, 149.

(103) Vanderkooi, J. M.; Adar, F.; Erecìnska, M. *Eur. J. Biochem.* **1976**, *64*, 381.

(104) Anni, H.; Vanderkooi, J. M.; Mayne, L. *Biochemistry* **1995**, *34*, 5744–5753.

(105) Quian, C.; Yao, Y.; Tong, Y.; Wang, J.; Tang, W. *J. Biol. Inorg. Chem.* **2003**, *8*, 394–400.

(106) Logovinsky, V.; Kaposi, A. D.; Vanderkooi, J. M. *Biochim. Biophys. Acta* **1993**, *1161*, 149–160.

(107) Kim, J. E.; Pribisko, M. A.; Gray, H. B.; Winkler, J. R. *Inorg. Chem.* **2004**, *43*, 7953.

2. Experimental Procedure

2.1. Introduction

In order to study protein and solvent dynamics on the picosecond–nanosecond timescale by time resolved fluorescence spectroscopy, we have employed the time-correlated, single-photon counting (TCSPC) method. This method has been used for many years with a wide span of applications, including fluorescence lifetime measurements and anisotropies,[1] fluorescence resonant energy transfer (FRET), fluorescence correlation spectroscopy (FCS),[2,3] and determination of solvation dynamics in polar and nonpolar liquids.[4] Today the TCSPC method is widely used in combination with scanning microscopes for cell imaging.[5]

With the development of femtosecond laser techniques such as photon echo peak-shift spectroscopy, solvation dynamics measurements employing the picosecond TCSPC method have appeared in the literature less frequently because the focus in liquids has been on the very short timescales. In this dissertation we show that the TCSPC method can be of exceptional value for sensing the protein and solvent dynamics of diffusive character on the 100 ps to 50 ns time scale, when used with an intrinsic electronic chromophore in a globular protein. This chapter provides information about the preparation of ZnCytc, the protein of interest in this dissertation. We also outline the basics of TCSPC and provide details of the experimental apparatus and data analysis.

2.2. Sample Preparation

ZnCytc samples were prepared in the Vanderkooi laboratory at the University of Pennsylvania School of Medicine in Philadelphia. The procedure of Vanderkooi and co-workers[6] was employed to remove the native Fe(II) ion and replace it with a Zn(II) ion. A horse-heart cytochrome *c* (Sigma) was treated with anhydrous hydrogen fluoride in order to extract the Fe(II) ion from the porphyrin ring. The change in color of the protein solution from red to purple indicates completion of this reaction. The protein solution contained free porphyrin and intact protein, which were separated on the Sephadex G50 gel-filtration column. The absorption spectrum of an iron-free cytochrome *c* sample obtained in the Vanderkooi laboratory is presented in Figure 2.1.

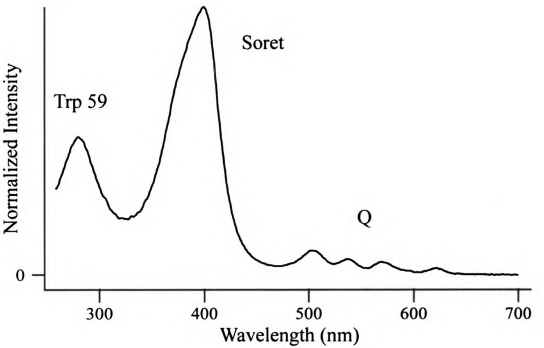

Figure 2.1. Continuous-wave absorption spectrum from iron-free cytochrome *c*, in water at room temperature. The spectrum shows the characteristic four bands in the Q region.

The band arising from Trp 59 is observed at 280 nm. The very intense Soret (or B) band occurs at 404 nm. The Soret band arises from porphyrin $\pi \rightarrow \pi^*$ transitions to the manifold of higher excited states, S_n ($n \geq 2$). The four Q bands, arising from porphyrin $\pi \rightarrow \pi^*$ transitions to the S_1 state, occur further to the red, in the 500–630 nm region of the spectrum. The ZnCytc was prepared by adding zinc acetate to a solution of iron-free cytochrome c followed by heating in water bath at 50° C. Measuring the absorption spectrum of the solution in short time intervals allows monitoring of the progress of reaction. The four Q bands, characteristic for absorption spectrum of iron-free cytochrome c, collapse into two bands upon the introduction of the Zn(II) ion into the porphyrin ring (see Figure 2.2). The Soret band red shifts in comparison to iron-free species, and occurs at 420 nm. The lower energy Q band in the absorption spectrum of

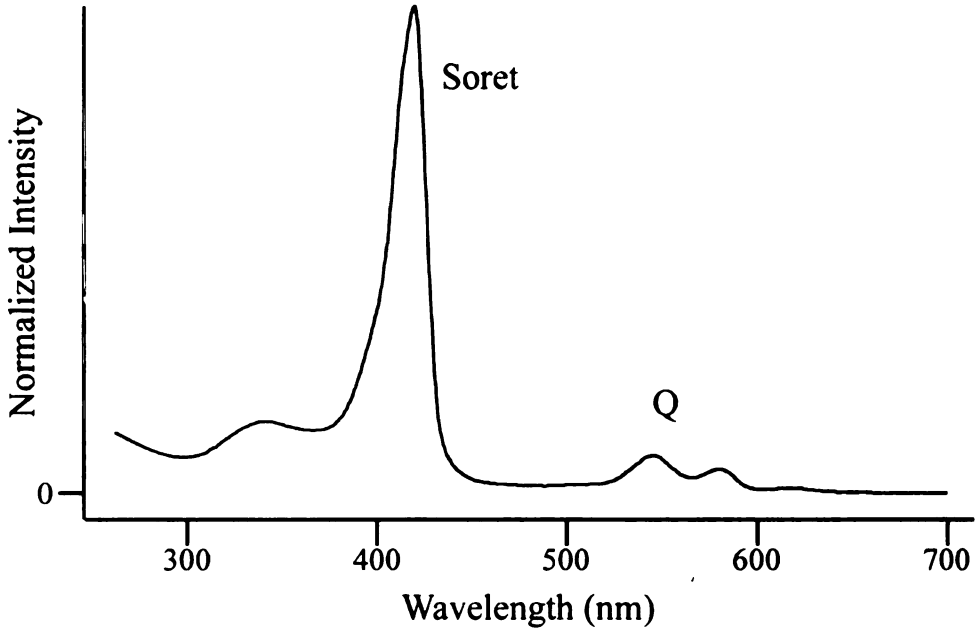

Figure 2.2 Continous-wave absorption spectrum from ZnCytc, in water at room temperature. The spectrum shows characteristic two bands in the Q region.

ZnCytc arises from the $S_0(\nu = 0) \rightarrow S_1(\nu = 0)$ vibronic transition and occurs at 580 nm. The higher energy Q band arises from $S_0(\nu = 0) \rightarrow S_1(\nu = 1)$ transition and occurs at 547 nm.

The purity of the Zn(II)-substituted species following the reaction of the metal-free form with Zn(II) was determined from a characterization of the absorption and fluorescence spectra. The sample was dialyzed to remove ammonium acetate, concentrated, lyophilized and stored in the dark at −10° C prior to use.

2.3. Modeling of Continuous Wave Absorption and Fluorescence Emission Spectra of ZnCytc

The representative absorption and fluorescence spectra of ZnCytc (see Figure 2.3) are plotted with respect to the wavenumber ν as $A(\nu)/\nu$ and $F(\nu)/\nu^3$, respectively, with normalization to the unit area. The integrals of these quantities report the dipole strength, the square of the transition-dipole moment.[3,7] The spectral region shown in Figure 2.3 features the Q bands, which arise from $\pi \rightarrow \pi^*$ transitions between the ground and first-excited singlet states. The Q bands exhibit a resolved vibronic structure arising from a progression in a methane-stretching mode that is polarized in the plane of the porphyrin macrocycle.[8]

The absorption dipole-strength spectra $D_A(\nu)$ from ZnCytc can be effectively described as a vibronic progression in one mode of frequency ν_A:

$$D_A(\nu) = A_{00}L_{00}(\nu,\nu_{00}) + A_{01}L_{01}(\nu,\nu_{00}+\nu_A) + A_{02}L_{02}(\nu,\nu_{00}+2\nu_A) \qquad (2.1)$$

The scaling parameters A_{0i} represent the dipole strengths for the 0–i vibronic transitions, each of which is described by a normalized log-normal (asymmetric Gaussian)[9] line-shape function $L_{0i}(\nu,\nu_0)$, with ν_0 defining the center of the line. Similarly, a good model for the fluorescence dipole-strength spectrum $D_F(\nu)$ from ZnCytc employs a vibronic progression in one mode of frequency n_F, with the normalized log-normal line shape $L_{0i}(\nu,\nu_0)$ oriented so that the broader side points to lower energy:

$$D_F(\nu) = F_{00}L_{00}(\nu,\nu_{00}) + F_{01}L_{01}(\nu,\nu_{00}-\nu_F) + F_{02}L_{02}(\nu,\nu_{00}-2\nu_F) \qquad (2.2)$$

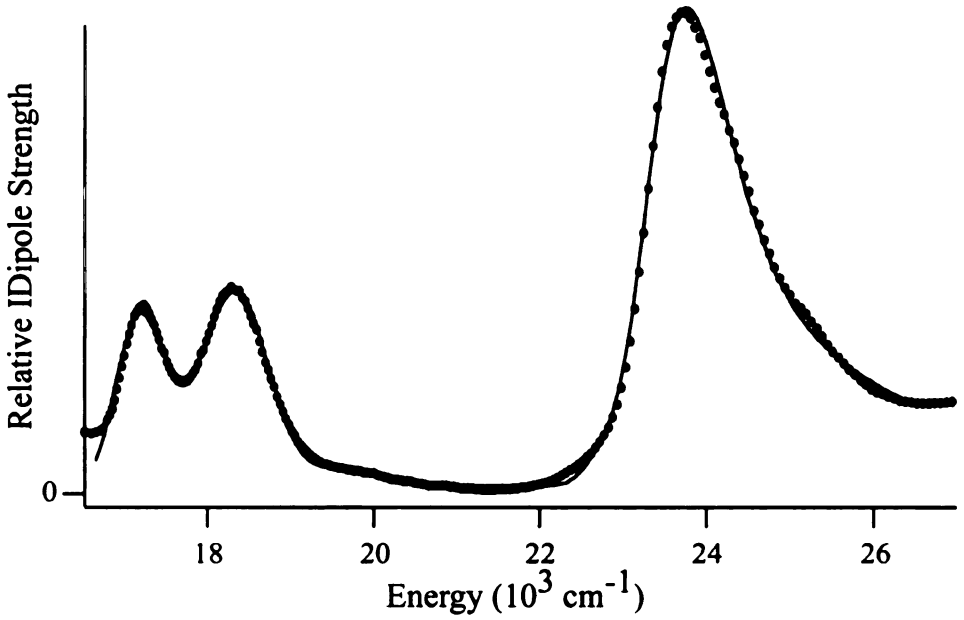

Figure 2.3. Continous-wave absorption spectrum (dots) from ZnCytc, in water at room temperature. The spectrum is plotted as relative dipole strength and normalized to unit area. Superimposed with the absorption spectrum is a model (line) described with equation 2.1.

The scaling parameters F_{0i} are the integrated dipole strengths for the vibronic lines in the fluorescence spectrum. Figure 2.4 shows the normalized fluorescence spectrum of ZnCytc.

The spectra shown in Figures 2.3 and 2.4 are superimposed with fitted curves that were obtained by a nonlinear least-squares regression to the models defined by equations 2.1 and 2.2. We find that an adequate description of the absorption or fluorescence spectra from ZnCytc can be obtained by using the same line-width and asymmetry parameters for L_{0i} in all three vibronic components. Good fits are obtained with the asymmetry parameter set to 1, which corresponds to the Gaussian line shape. As will be discussed in the next section, we use the model for the fluorescence spectrum as a starting point for a modeling of the time-resolved fluorescence spectra.

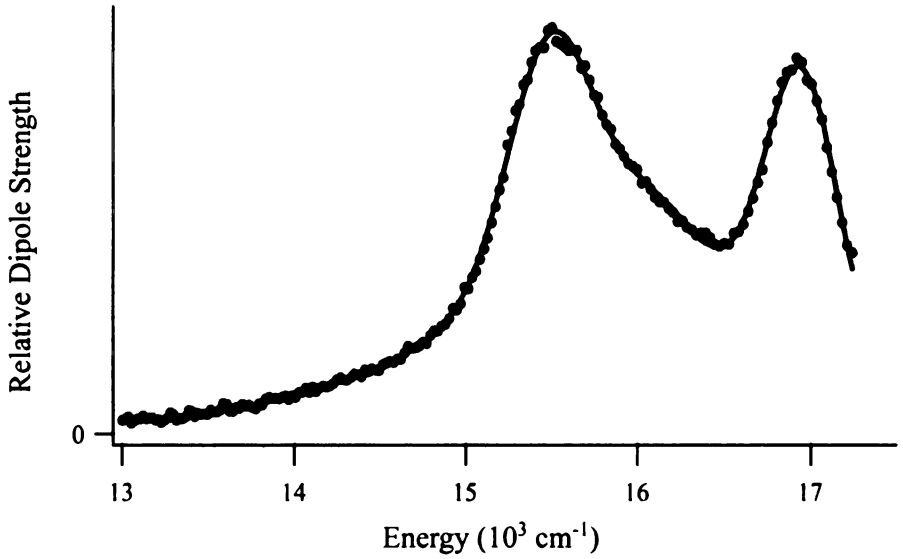

Figure 2.4. Continous-wave fluorescence spectrum (dots) from ZnCytc, in water at room temperature. The fluorescence spectrum was obtained with excitation at 585 nm. The spectrum is plotted as relative dipole strength and normalized to unit area. Superimposed with the fluorescence spectrum is a model (line) described with equation 2.2.

2.4. The TCSPC Method

TCSPC is a photon counting method that uses a pulsed light source, such as a mode-locked laser, to excite an ensemble of molecules in the sample. One of the basic prerequisites for this method is that it operates under the condition of low excitation power to insure only single photon absorption and detection of single emission events. The excited molecules relax by emitting fluorescence photons with an exponential distribution of time delays. The resulting fluorescence response function is commonly described with the equation

$$I_F(t) = \frac{1}{\tau} e^{-t/\tau}, \tag{2.3}$$

where $I_F(t)$ is the fluorescence intensity at some time t, and τ is fluorescence lifetime.[10]

In the TCSPC method the fluorescence response function is obtained by measuring the time delays of the fluorescence photons with respect to the excitation pulse. The excitation pulse is detected by a fast photodiode and serves as a start signal for counting photons that are time-correlated to the excitation pulse. This start signal triggers the voltage ramp in the time to amplitude converter (TAC), which is an essential part of the setup. It transforms the arrival time between a start and a stop pulse into a voltage. The ramping stops when the photomultiplier tube (PMT) registers the first fluorescence photon from the sample. The constant fraction discriminator (CFD) is used to minimize the noise and guarantee that the timing between the start and stop pulses is independent of the intensity of the signal pulse. The analog-to-digital converter (ADC) converts

output voltage from the TAC into a time channel in a multichannel analyzer (MCA). This process continues until the MCA builds up a probability histogram of the number of counts as a function of the time delay. For high repetition rate excitation sources, the TAC does not have enough time to reset between the two excitation pulses and the resulting fluorescence decay curve may be distorted. To avoid this, the TAC is usually operated in the reverse mode, where the first detected fluorescence photon serves as the start signal, and the subsequent excitation pulse as the stop signal.

With an infinitely narrow excitation pulse and infinitely fast detection electronics, the measured and real fluorescence response functions would be the same. In reality, the molecules in the sample that are excited at early times are still emitting fluorescence while the rest of the molecules are excited with the tail of the excitation pulse. This results in distortions of the measured fluorescence response at early times. To extract the early-time fluorescence response, it is necessary to deconvolute the instrument response function from the measurement. The instrument response function is collected under the same conditions as an actual measurement, but with a scattering solution instead of the sample. It represents the shortest time profile that can be measured with a given instrument. The TCSPC method is characterized by high resolution and sensitivity, and excellent signal-to-noise ratio.

2.4.1. The TCSPC Apparatus

The single-wavelength fluorescence transients were acquired with a time-correlated, single-photon-counting system operated in the reverse-triggered mode. The

schematic of the experimental apparatus is shown in Figure 2.5. The excitation source was a cavity-dumped rhodamine-6G dye laser (Coherent 702-1), which was synchronously pumped by the 532-nm second harmonic of a mode-locked Nd^{3+}-YAG laser (Coherent Antares 76-S). The saturable-absorber jet of the dye laser was not used. The cavity dumper was adjusted to produce a 4-MHz pulse-repetition rate; the zero-background autocorrelation width of the emitted pulses was 10 ps, as measured using an Inrad 5-14A autocorrelator.

The excitation laser light was passed through an attenuator composed of an achromatic half-wave retarder and a New Focus 5521 calcite/fused-silica polarizer; a BK7 lens (5-cm focal length) was used to focus the beam onto the sample position. The fluorescence emission was collected by another BK7 lens (5-cm focal length), passed through a Glan-Thompson calcite polarizer (CVI Laser CPLG-10.0), dispersed with a 0.125-m double-subtractive monochromator (CVI CM112), and detected with a microchannel-plate photomultiplier tube (Hamamatsu R3809U). The spectral band pass of the monochromator was 4 nm. To obtain dichroism-free signals, the plane of polarization of the excitation laser beam was rotated to the magic angle, 54.7°, with respect to the plane analyzed by the polarizer in the fluorescence beam.[3]

For timing of the fluorescence and excitation photons, reference pulses were split from the dye laser output, passed through a fused-silica neutral-density filter and an 80-m fiber optic delay line, and then focused onto a silicon avalanche photodiode (RCA C30902E). The arrival times of the reference and fluorescence photons were determined with a constant fraction discriminator (CFD, Oxford TC 454). The CFD

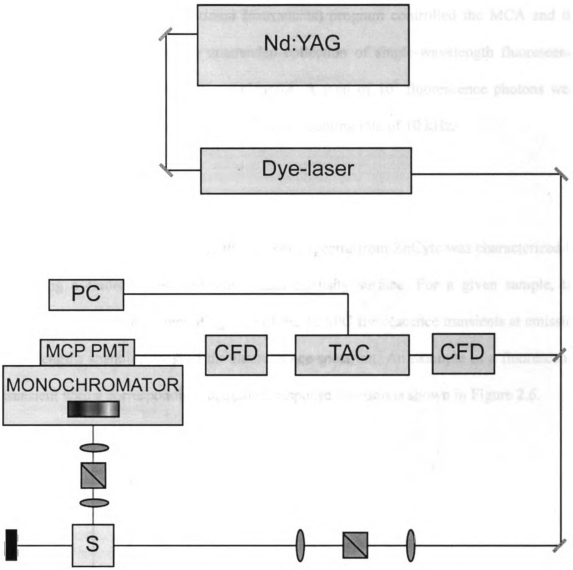

Figure 2.5 Schematic for the time-correlated single-photon-counting apparatus: CFD, constant fraction discriminator; TAC, time-to-amplitude converter; MCP PMT, multichannel plate photomultiplier; S, sample.

output pulses corresponding to the reference photons were sent to a time-to-amplitude converter (TAC, Canberra 2145). The CFD output pulses corresponding to the fluorescence photons were delayed (Tennelec 412A) and then sent to the TAC. The TAC output pulses were pulse-height analyzed by a multichannel analyzer (MCA, Canberra

MPT-16E). A LabVIEW (National Instruments) program controlled the MCA and the monochromator, allowing the unattended collection of single-wavelength fluorescence transients at different emission wavelengths. A total of 10^6 fluorescence photons were accumulated for each transient at an effective counting rate of 10 kHz.

2.4.2. Data Analysis

The time evolution of the fluorescence spectra from ZnCytc was characterized by acquiring a fluorescence time–wavelength–intensity surface. For a given sample, the surface was obtained by recording a set of the TCSPC fluorescence transients at emission wavelengths spanning most of the fluorescence spectrum. An example of a fluorescence transient with a corresponding instrument response function is shown in Figure 2.6.

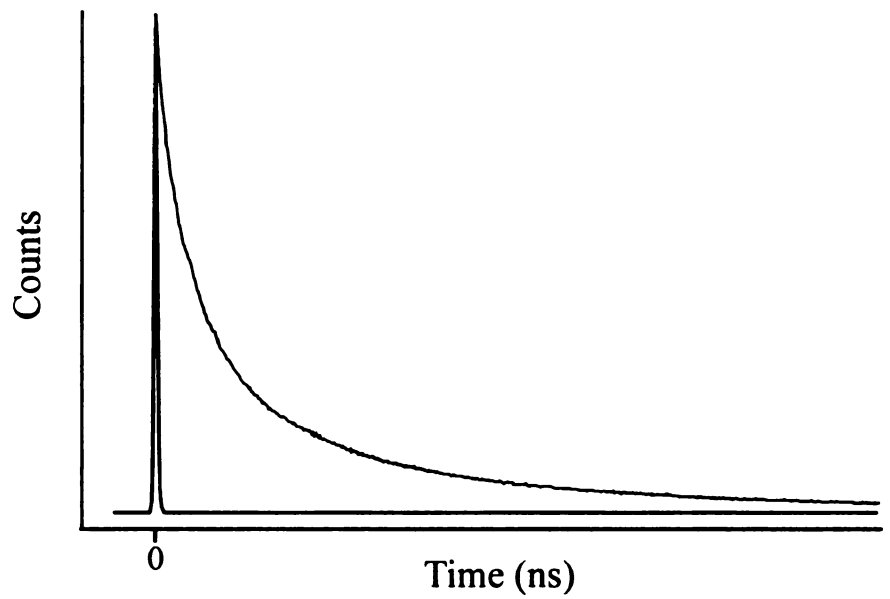

Figure 2.6 Typical single-wavelength transient and instrument response function obtained in TCSPC experiment.

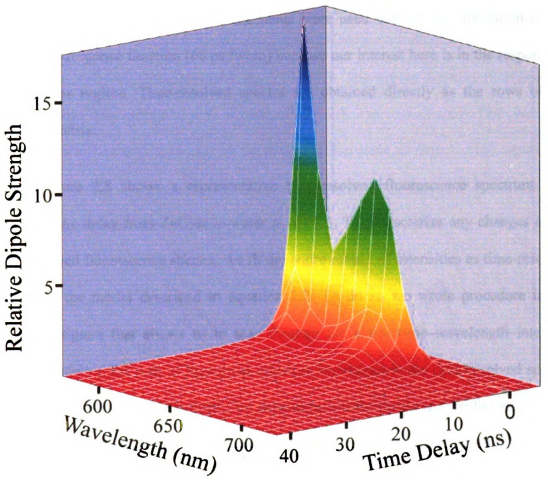

Figure 2.7 Typical time-wavelength-intensity surface constructed from the single wavelength transients collected in TCSPC experiment.

For each experimentally acquired data set, a given transient recorded at a certain emission wavelength contributes one column to a matrix of intensities that composes the time–wavelength–intensity surface (see Figure 2.7). The grid spacing along the wavelength direction corresponds to the band pass of the emission monochromator; the grid spacing along the time direction is 12 ps, the effective dwell time for the MCA. The

relative intensity of each transient is scaled so that its integral with respect to time is proportional to the relative intensity at the observation wavelength in the continuous-wave fluorescence spectrum.[11] The transients were used without deconvolution of the instrument-response function (60 ps fwhm) because our interest here is in the response in the >100-ps regime. Time-resolved spectra are obtained directly as the rows of the intensity matrix.

Figure 2.8 shows a representative time-resolved fluorescence spectrum at a selected time delay from ZnCytc in water at pH 7.5. To characterize any changes in the time resolved fluorescence spectra, we fit the entire matrix of intensities as time-resolved spectra to the model described in equation 2.2. To do so we wrote procedure in the IgorPro program that allows us to scan through the entire time–wavelength–intensity surface modeling the sum of lognormal emission lineshapes to the time-resolved spectra obtained from slices of the surface. For most experiments shown in this dissertation, the mode frequency (ν_F) and line-shape parameters were fixed to those obtained from the analysis of the continuous-wave spectrum. Allowing these parameters to vary during the analysis did not result in improved fits, nor were trends observed in the floating parameters with respect to time, so we conclude that the shape and separation of the vibronic components did not evolve significantly during the time course from 100 ps onward. Use of fixed line-shape and mode-frequency parameters in the modeling of the time-resolved spectra permits a relatively precise estimation of F_{00}, even when the spectral range does not include the entire width of the 0–0 vibronic feature. For the spectra obtained with Q-band excitation the analyzed spectral range begins one spectral

band pass to the red of the excitation wavelength. Examples of the fitted spectra are shown in Figure 2.8 superimposed with the data points of the three time-resolved spectra.

The analysis of the time-resolved spectra allows for tracking of the intensity and the position of the vibronic lines with respect to time. The change in the intensities of the vibronic lines with respect to time is discussed in detail in next chapter. The change of the position of the 0–0 fluorescence transition with respect to time, which reports the time-scales for the reorganization of the surrounding solvent in terms of Dynamic Stokes shift, is discussed in chapters 4 and 5.

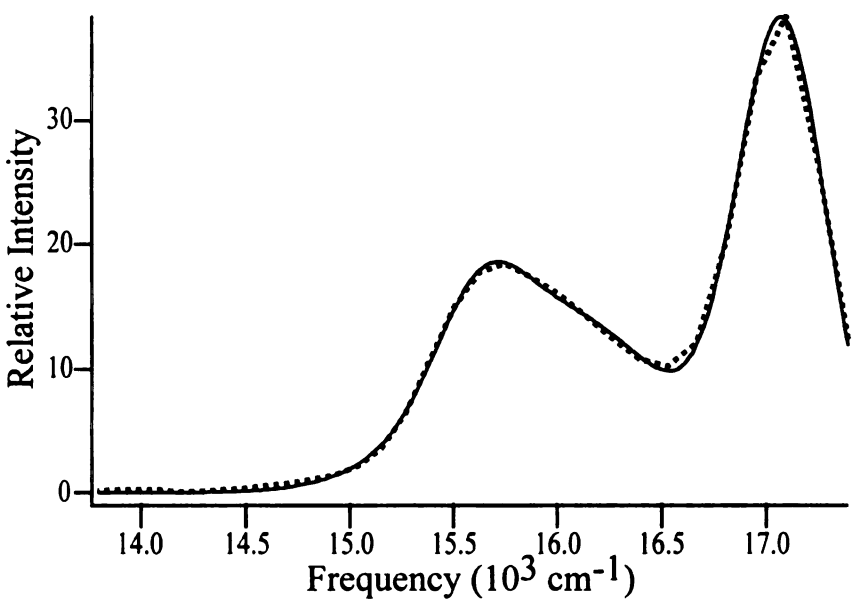

Figure 2.8 Typical time-resolved fluorescence spectrum obtained from time-wavelength-intensity surface (data points). Superimposed with the time-resolved fluorescence spectrum is a model (line) described with equation 2.2.

2.5. References

(1) Chen, L. X.-Q.; Petrich, J. W.; Fleming, G. R.; Perico, A. *Chem. Phys. Lett.* **1987**, *139*, 55–61.

(2) Fleming, G. R. *Chemical Applications of Ultrafast Spectroscopy*; Oxford University Press: New York, 1986.

(3) Lakowicz, J. R. *Principles of Fluorescence Spectroscopy*, Second ed.; Kluwer Academic/Plenum Publishers: New York, 1999.

(4) Maroncelli, M.; Fleming, G. R. *J. Chem. Phys.* **1987**, *86*, 6221–6239.

(5) Berland, K. M.; So, P. T. C.; Gratton, E. *Biophys. J.* **1995**, *68*, 694–701.

(6) Vanderkooi, J. M.; Adar, F.; Erecìnska, M. *Eur. J. Biochem.* **1976**, *64*, 381.

(7) Kantor, C. R.; Schimmel, P. R. Biophysical Chemistry, Part II: Techniques for the study of Biological Structure and Function; Freeman and Co: San Francisco, 1980.

(8) Gouterman, M. Optical spectra and electronic structure of porphyrins and related rings. In *The Porphyrins*; Dolphin, D., Ed.; Academic Press: New York, 1978; Vol. 3; pp 1–159.

(9) Siano, D. B.; Metzler, D. E. *J. Chem. Phys.* **1969**, *51*, 1856–1861.

(10) Lakowicz, J. R. *Principles of Fluorescence Spectroscopy*; Plenum Press, 1983.

(11) Pierce, D. W.; Boxer, S. G. *J. Phys. Chem.* **1992**, *96*, 5560.

3. Excited-State Axial-Ligand Photodissociation and Nonpolar Protein-Matrix Reorganization in Zn(II)-Substituted Cytochrome c[†]

3.1. Introduction

Even under conditions that favor the native structure, a protein fluctuates over a range of thermally accessible states and time scales. The work of Frauenfelder and co-workers showed early on that an intrinsic chromophore can be used as a probe of these fluctuations; the motions and structures that a protein accesses on its potential-energy surface control the probe's spectroscopic line-shape. The potential-energy surface (or *energy landscape*) of a protein resembles that of a glass in exhibiting a rugged profile,[2] at least over short displacements from the vicinity of a given folding state. A large number of possible paths and intermediate states should contribute to the dynamics of folding,[3-5] an ensemble view is to be favored over the older concept of a sequential pathway between a small number of intermediate states.[6]

Proteins also exhibit some of the properties of liquids, especially at physiological temperatures.[7] Ultrafast spectroscopic techniques have proven effective in the study of line shape and dynamics in liquids, specifically in studying what kinds of *larger-range* motions an ensemble of protein structures makes on its potential-energy surface.[8-11] The methods used, femtosecond transient-hole burning spectroscopy and stimulated photon-echo peak-shift spectroscopy, obtain the ground-excited-state energy-gap time-

[†] The work in this chapter has been published in other form[1]

correlation function, $M(t)$, from a probe molecule in condensed phases.[12-15]

In this chapter, we begin a discussion of the picosecond–nanosecond time-scale diffusive part of $M(t)$ in cytochrome *c*, which contains an intrinsic heme chromophore. To have access to an intrinsic fluorophore with a well-characterized surrounding protein structure, we have initially chosen to study the dynamics of the Zn(II)-substituted molecule[16-20] rather than that of the naturally occurring Fe(II,III)-containing molecule[21] The Zn(II)-porphyrin in ZnCytc exhibits a long fluorescence lifetime and a spectrum with resolved vibronic structure,[16] which permits measurement of $M(t)$ in terms of the dynamic Stokes shift of the time-resolved fluorescence spectrum despite the small reorganization energy (<200 cm^{-1}).

In performing an initial characterization of the time-resolved fluorescence spectrum from ZnCytc on the picosecond time scale, however, we were surprised to observe a pronounced biexponential time evolution of the vibronic structure. The mirror-image time evolution of the 0–0 and 0–1 transitions evidences a dissociation of the Zn(II)-ion's axial ligands, which are apparently derived in the native state from the side chains of the nearby Met 80 and His 18 amino acid residues,[20] as in the Fe(II,III) species (see Figure 3.1). The fast phase of the vibronic structure response that accompanies release of the first axial ligand is slowed when the external medium is changed from water to 50% glycerol; these results suggest a rate limitation involving reorganization of the protein matrix and surrounding solvent.

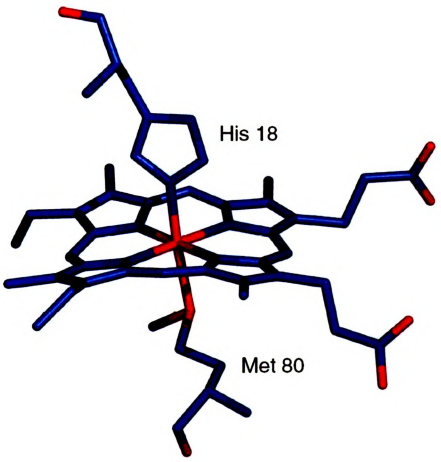

Figure 3.1. Structure of the heme and axial ligands from horse-heart ferricytochrome *c*, as rendered using PyMOL[22] from the pdb file 1HRC.[21]

3.2. Experimental

3.2.1. Zn(II)-Substituted Cytochrome *c*

ZnCytc samples were prepared by the method of Vanderkooi and coworkers, as described in detail in chapter 2. The ZnCytc samples were dissolved in a 50-mM *N*-(2-hydroxyethyl)piperazine-*N*'-2-ethanesulfonic acid (HEPES, Research Organics) buffer solution at pH 7.5 or in a 50% (v/v) glycerol/HEPES buffer solution mixture. The

samples were filtered and then diluted in the chosen solution so as to obtain a maximum absorption of 0.1 in the 0–0 transition of the Q-band for a 1-cm path length. The samples were held in quartz cuvettes with 1-cm path lengths and were purged with dry nitrogen prior to use.

3.2.2. Continuous-Wave Absorption and Fluorescence Instrumentation

Steady-state absorption spectra were acquired with 2-nm spectral band pass with Hitachi U-2000 spectrophotometer or an ATI Unicam UV2 spectrophotometer. Steady-state fluorescence spectra were acquired with a Hitachi F-4500 fluorescence spectrometer (5-nm excitation and emission band pass). The fluorescence intensities were corrected by the spectrofluorometer's data-acquisition program using a calibration curve obtained from a standard lamp. The intensities were recorded in terms of photons per nanometer band pass. When presented as a function of wavenumber, the fluorescence intensities are accordingly multiplied by the square of the wavelength to compensate properly for the fixed (in wavelength units) spectral band pass of the emission spectrometer.[23] Scattered excitation light was eliminated from the fluorescence spectra by subtraction of a blank, solvent-only sample held in the same cuvette.

3.2.3. Picosecond Time-Resolved Fluorescence Spectroscopy

Single-wavelength fluorescence transients were acquired with a TCSPC apparatus described in detail in chapter 2. The excitation wavelength used in these experiments was set to 585 nm so as to correspond to the 0–0 transition energy for ZnCytc spectra in

water. Samples used in time-resolved fluorescence measurements were held in 1-cm quartz cuvettes mounted in a temperature-controlled holder (Quantum Northwest TLC 50). All samples were filtered, kept at 22 °C, purged with dry nitrogen, and prepared at the same concentrations used in steady-state measurements. The instrument-response function of the detection system was approximately 60 ps (fwhm) in these experiments.

3.3. Results

3.3.1. Continuous-Wave Absorption and Fluorescence Emission Spectra

Figure 3.2. shows the absorption and fluorescence spectra obtained at 22 °C from ZnCytc at pH 7.5 in water. The spectra are normalized to unit area and plotted as dipole strength. The absorption and fluorescence dipole strength spectra can be modeled with line-shape functions described in detail in chapter 2 (equations 2.1 and 2.2). The spectra shown in Figure 3.2 are superimposed with fitted curves that were obtained by nonlinear least-squares regression to the models defined by equations 2.1 and 2.2 in chapter 2.

3.3.2. Time-Resolved Fluorescence Spectra

The time evolution of the fluorescence spectra from ZnCytc (see figures 3.3–3.5) was characterized by acquiring a fluorescence time–wavelength–intensity surface. For a given sample, the surface was obtained by recording a set of TCSPC fluorescence transients at emission wavelengths spanning most of the fluorescence spectrum. The details of this procedure are discussed in chapter 2. Figure 3.3 shows time-resolved fluorescence spectra at three selected time delays from ZnCytc in water at pH 7.5. During

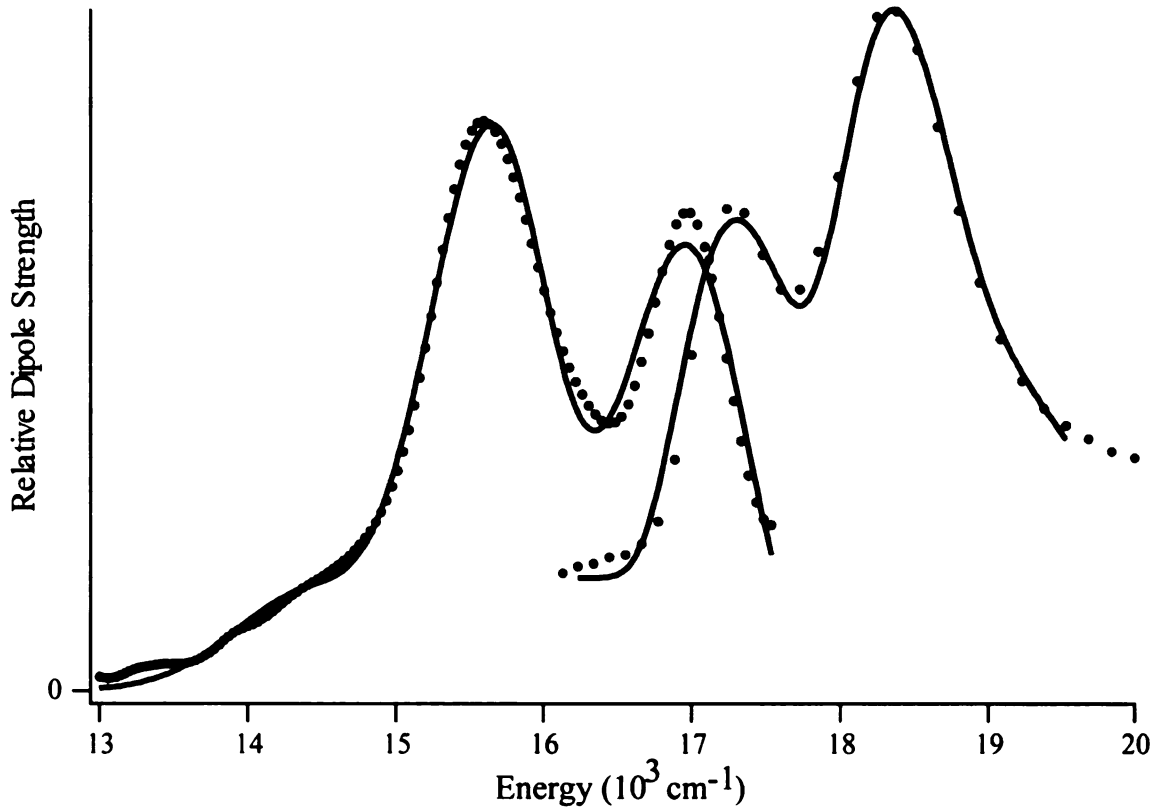

Figure 3.2. Continuous-wave absorption (right) and fluorescence (left) spectra from ZnCytc at 22°C. The spectra are plotted as dipole strengths, $A(\nu)/\nu$ and $F(\nu)/\nu^3$, respectively, and are normalized to unit area. The spectra are superimposed with fitted curves employing eqs 1 and 2 as models. The fluorescence spectrum was obtained with excitation tuned to the 0–0 transition energy, where the absorption and fluorescence spectra cross.

the fluorescence decay, the relative dipole strength of the 0–1 transition, Q_{01}, increases at the expense of that of the 0–0 transition, Q_{00}, which is initially larger. To characterize these and any other changes in the time-resolved fluorescence spectra, we fit the entire matrix of intensities as time-resolved spectra to the model described in the equation 2.2 chapter 2. The mode frequency (ν_F) and line-shape parameters were fixed to those obtained from the analysis of the continuous-wave spectrum. Allowing these parameters to vary during the analysis did not result in improved fits, nor were trends observed in the

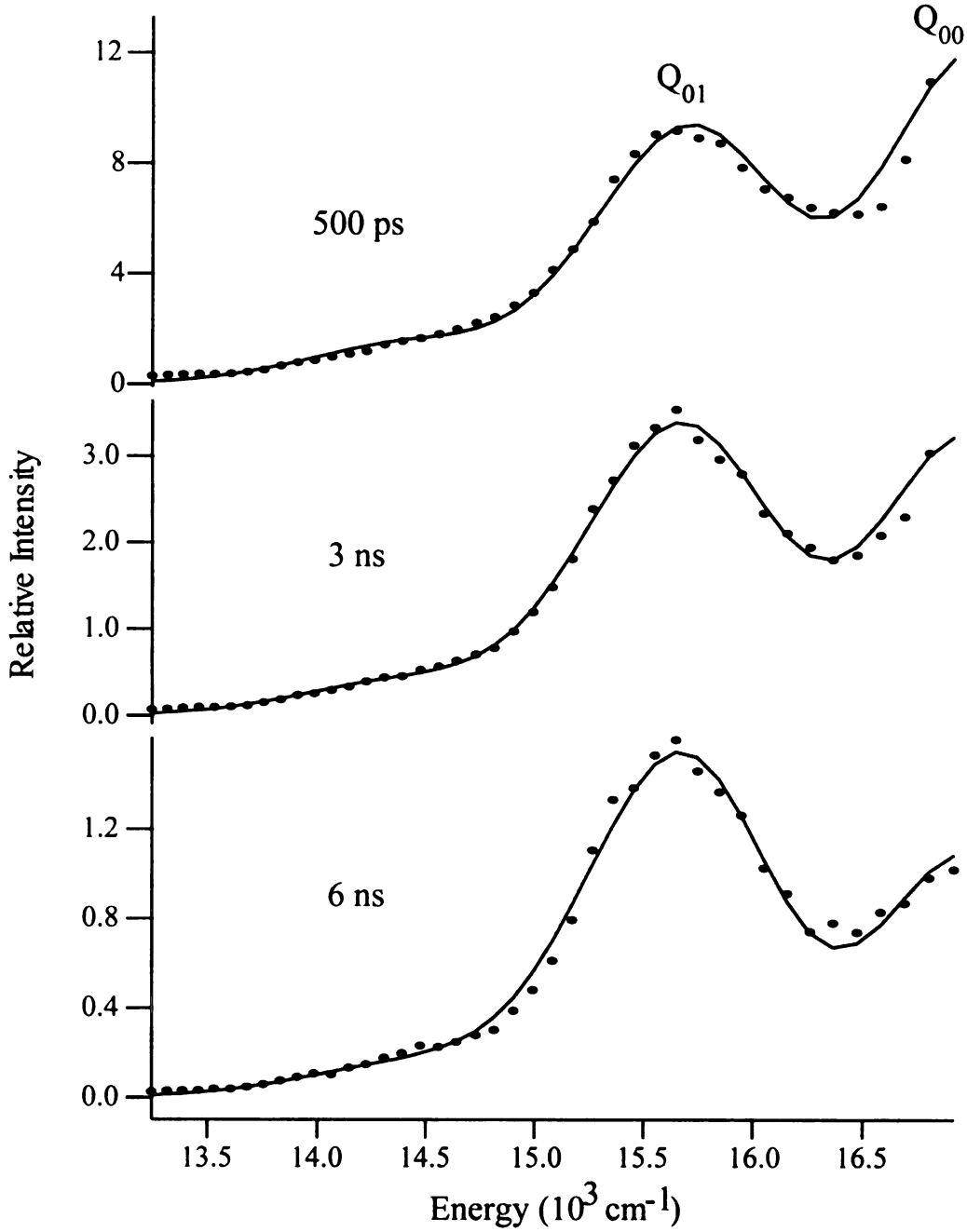

Figure 3.3. Time-resolved fluorescence spectra from ZnCytc in water at 22°C (data points) and fitted spectra (smooth curves, see eq 2) at three delays.

floating parameters with respect to time, so we conclude that the shape and separation of the vibronic components did not evolve significantly during the time course from 100 ps onward. Use of fixed line-shape and mode-frequency parameters in the modeling of the time-resolved spectra permits a relatively precise estimation of Q_{00} even though the spectral range does not include the entire width of the 0–0 vibronic feature. The analyzed spectral range begins one spectral band pass to the red of the excitation wavelength. Examples of the fitted spectra are shown in Figure 3.3 superimposed with the data points of the three time-resolved spectra.

The analysis also allows us to track the position of the 0–0 fluorescence transition, n_{00}, over the entire time scale. A plot of ν_{00} with respect to time reports the dynamic Stokes shift.[24,25] In ZnCytc, ν_{00} evidently reports the *polar* reorganizational dynamics of the protein that surrounds the Zn(II) porphyrin. We will discuss these details in the next chapter.

The time evolution of the intensities of the 0–0 and 0–1 vibronic components in the time-resolved fluorescence spectra is described by the dipole strengths Q_{00} and Q_{01} with respect to time. These parameters are plotted in Figure 3.4 for ZnCytc in water in terms of relative dipole strengths, $Q_{0i} / \sum_j Q_{0j}$, and as the ratio Q_{01} / Q_{00}. The former plot normalizes the intensity of the vibronic component with respect to the total dipole strength at a given time point, which decays proportionally to the excited-state population according to the fluorescence lifetime. The latter plot obtains in a single observable the relative intensity evolution of the two vibronic lines. A distinct biexponential response

was observed in both types of plots. The fit parameters for Q_{01}/Q_{00} obtained from $Q_{01}(t)/Q_{00}(t) = C - \sum_i A_i e^{t/t_i}$ are listed in Table 1. A similar model can be used to fit separately the normalized Q_{00} and Q_{01} responses.

Table 1.

solvent	a_1	τ_1, ps	a_2	τ_2, ps	C
water	0.50 ± 0.02	120 ± 50	1.50 ± 0.02	7 ± 1	2.1 ± 0.02
50% glycerol	0.30 ± 0.02	400 ± 50	0.90 ± 0.02	7 ± 1	1.66 ± 0.02

Table 1. The time evolution of Q_{01}/Q_{00} for ZnCytc in two solvent systems at 22 °C.

The plot of Q_{01}/Q_{00} for ZnCytc in 50% glycerol is shown in Figure 3.5. The time-resolved fluorescence spectra evidence a biexponential rise in the value of Q_{01}/Q_{00} over six-tenths of the range that was observed in water only (see Figure 3.4), and the time constant for the faster of the two exponentials is slowed by a factor of 4 (see Table 1). Note that the time constant for the slower exponential component and the relative magnitude of the two exponential components were not significantly affected by the presence of glycerol.

Although the time–wavelength–intensity surfaces that are described in Figures 3.3–3.5 and Table 1 were obtained with excitation close to 0–0 transition energy, where the fluorescence and absorption spectra cross each other (see Figure 3.2), additional experiments were conducted with the pump laser tuned farther to the blue by as much as 700 cm^{-1}. No effects on the time-resolved spectra nor trends in the fitted

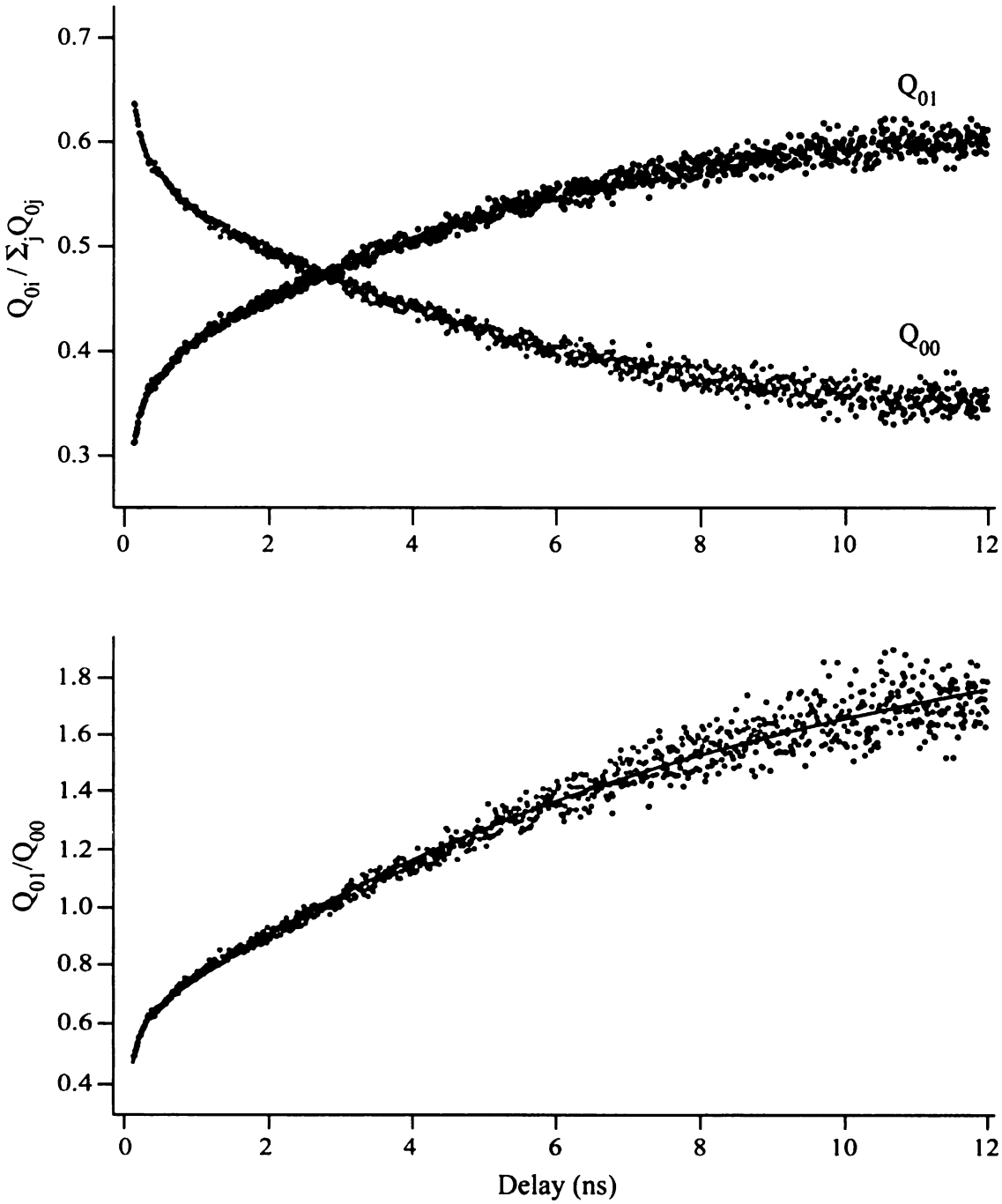

Figure 3.4 Time evolution of the dipole strengths for the 0-1 (Q_{01}) and 0-0 (Q_{00}) vibronic transitions in time-resolved fluorescence spectra from ZnCytc in water at 22°C. Top: As normalized by the total dipole strength $S_j Q_{0j}$. Bottom: As the ratio Q_{01} / Q_{00}. The parameters for the fit to the ratio are listed in Table 1.

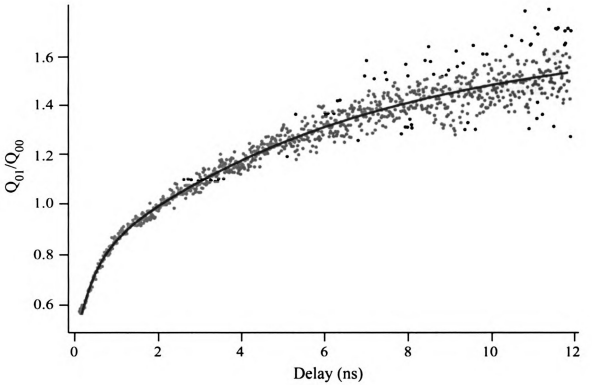

Figure 3.5. Time evolution of the ratio of the dipole strengths for the 0-1 (Q_{01}) and 0-0 (Q_{00}) vibronic transitions in time-resolved fluorescence spectra from ZnCytc in 50% glycerol at 22°C. The fit parameters are listed in Table 1.

parameters as a function of time were noted. These results show that the time evolution observed in the Q-band vibronic structure is not predominantly associated with vibrational relaxation or a redistribution of vibrational energy; either of these phenomena would be expected to occur on the < 100-ps time scale.

3.4. Discussion

We suggest that the time evolution of the vibronic structure of the Q-band fluorescence spectrum of ZnCytc can be explained by an excited-state release of axial ligands from the Zn(II) ion. This suggestion is based on the known effects of ligand

binding on the Q-band vibronic structure. In the following, we discuss a possible explanation for the biexponential response and the apparent rate limitation owing to protein-matrix and solvent reorganization that is implied by the experimental results.

3.4.1. Interpretation of Vibronic Structure in Zn(II)-Porphyrin Complexes

The presence of axial ligands in Zn(II)-porphyrin systems can be monitored using the partially resolved vibronic structure of the Q-band absorption and fluorescence spectra. The effect of binding axial ligands on the absorption and fluorescence spectra of Zn(II) porphyrins is a redistribution of dipole strength between 0–0 and 0–1 vibronic transitions. In equilibrium titration studies in which a ligand is added to a Zn(II)-porphyrin species dissolved initially in a noncoordinating solvent, the intensity of the absorption or fluorescence 0–1 transition decreases and the intensity of the 0–0 transition increases in response to an increase in the concentration of the ligand. Both intensity responses are initially linear with respect to the concentration of the ligand; at higher ligand concentrations, the responses saturate. The entire response as a function of ligand concentration defines the equilibrium constant for the ligand-binding reaction.[26-28]

The time-resolved fluorescence spectra from ZnCytc exhibit changes in vibronic structure that closely resemble the spectral evolution observed in the Zn(II)-porphyrin ligand-titration studies as the concentration of ligand decreases. Figure 3.4 shows that Q_{00} and Q_{01} dipole strengths mirror each other, with Q_{00} decreasing and Q_{01} increasing in intensity with respect to time. These results strongly suggest that a net photodissociation of the axial ligands occurs in the excited state. The spectral response

should be interpreted as a shift of the equilibria that link the ligated and deligated structures. The response shown in Figures 3.4 and 3.5 arises from the transient flow of population that accompanies relaxation toward the new equilibrium constant.

3.4.2. Origin of the Biexponential Axial-Ligand Photodissociation Response in ZnCytc

The simplest explanation for the biexponentiality of the kinetics observed for the time evolution of the Q_{01}/Q_{00} ratio involves a dissociation of two axial ligands:

$$L_a - Zn(P) - L_b \overset{K_1}{\rightleftharpoons} L_a + Zn(P) - L_b \overset{K_2}{\rightleftharpoons} L_a + Zn(P) + L_b \qquad (3.1)$$

In equation 3.1, the axial ligands L_a and L_b are initially coordinated to the Zn(II) porphyrin, Zn(P); the two equilibria govern the sequential dissociation of the two axial ligands. The exponential components observed for the time evolution of the Q_{01}/Q_{00} ratio report the relaxation time constants for the two equilibria.

This suggestion conflicts, however, with the standard picture that Zn(II) porphyrins can bind only one axial ligand. It is generally thought that Zn(II) porphyrins prefer a five-coordinate ligand environment in solution, with the Zn(II) ion domed from the plane of the porphyrin on the side of the single axial ligand,[26,29-31] but there are some structures in crystals that coordinate two axial ligands.[32-34] Crystal packing forces impose two axial ligands upon the Zn(II) ion, a nonplanar distortion of the porphyrin macrocycle results, and the Zn(II) ion is positioned closer to the nominal plane of the porphyrin.[20,33]

A similar situation is likely to exist in the native conformation of ZnCytc. The structure of the polypeptide chain in Zncytc has been characterized by two groups with 2D-NMR methods.[19,20] Anni et al.[20] conclude that the polypeptide in ZnCytc assumes the same configuration that exists in Fe(II) protein. The proton resonances for the polypeptide backbone and the side chains of His 18 and Met 80 indicate that these residues are located as they are in the Fe(II) protein; the resonances of residues elsewhere in the protein are the same in the Fe(II) and Zn(II) forms, showing that the configuration of the polypeptide is identical in the two forms. The same conclusion was reached recently by Quian et al.[19] Thus, the polypeptide projects the His 18 and Met 80 side chains in the correct configuration to permit them to serve as axial ligands to the Zn(II) ion, and importantly, no other amino acids are ligated to the Zn(II) ion. Anni et al. conclude on the basis of their NMR results and their studies of low-temperature absorption and fluorescence spectra that the Zn(II) ion is ligated by His 18 and Met 80 in the same geometry that is present in the Fe(II)-containing molecule.[20]

Resonance Raman measurements of porphyrin core marker bands by Kostić and co-workers, however, suggest that the porphyrin core is not sufficiently expanded in ZnCytc to permit an orthodox six-coordinate configuration.[18] The same group accounts for their finding that the Marcus reorganization energy for electron self-exchange between ZnCytc and $ZnCytc^{+}$ is lower than that obtained for the Fe(II) species by suggesting that Met 80 does not act as an axial ligand to the Zn(II) ion.[35]

Having considered all of these results, we conclude that it is probable that the ligand coordination sphere for the Zn(II) ion in ZnCytc is six-coordinate, as imposed by

the essentially native structure of the cytochrome *c* polypeptide. Incorporation of the Zn(II) ion in the porphyrin is, however, likely to result in axial-ligand bonding geometries that are somewhat different from those present in the Fe(II)-containing protein. The resulting porphyrin structure should be strained, as in the distorted six-coordinate Zn(II) porphyrins that have been observed in crystal structures.

We suggest that our results are consistent with this hypothesis. The two exponential components detected in the response of the Q_{01}/Q_{00} dipole-strength ratio are widely separated in time scale ($\tau_1 = 120$ ps, $\tau_2 = 7$ ns; see Figures 3.4 and 3.5 and Table 1). A six-coordinate ground-state species would yield a five-coordinate intermediate upon breaking the first axial-ligand bond, perhaps that to the Met 80 side chain. The five-coordinate intermediate would be expected to be less strained and accordingly less reactive than the six-coordinate starting structure. Owing to motion of the departing ligand away from the Zn(II) ion, the packing forces that were imposed upon the porphyrin by the two axial-ligand side chains would be relaxed, the Zn(II) ion would dome, and the porphyrin might be expected to assume a more stable, planar configuration. Thus, the relaxation of the second axial-ligand equilibrium in equation 3.1 might well be expected to occur on a much slower time scale.

3.4.3. Protein-Matrix and Solvent Reorganization Dynamics

The suggestion that the surrounding protein structure applies packing force upon the Zn(II) porphyrin in ZnCytc and establishes two axial ligands also implies that a reorganization of the protein structure would be required in response to axial-ligand

photodissociation events. The finding that the fast phase of the Q_{01}/Q_{00} dipole-strength response in ZnCytc is slowed by the presence of 50% glycerol in the surrounding solvent is consistent with this idea. As a result of the photodissociation of either of the two ligands, a displacement of the ligand donor atoms away from the plane of the porphyrin would be expected to occur only as fast as the surrounding protein and solvent could accommodate the change in the effective volume. The rate of reorganization of the protein and the surrounding solvent would be expected to be slower when glycerol is present, owing to the change in the bulk viscosity. It is interesting that only the 120-ps component of the Q_{01}/Q_{00} dipole-strength response is slowed by the addition of glycerol; it could be that the breaking of the second axial-ligand bond occurs so slowly from the more relaxed five-coordinate intermediate that reorganization of the surrounding solvent medium is not a significant rate limitation.

The effect of glycerol on the total range of change of the Q_{01}/Q_{00} ratio suggests that the overall equilibrium constant for the ligand-dissociation sequence is somewhat smaller in the presence of glycerol in the external solvent medium than in the presence of water only. One might expect that the forward, ligand-dissociating and reverse, ligand-binding reactions would exhibit a comparable dependence on the solution viscosity owing to microscopic reversibility. An observation of an effect of glycerol on the equilibrium constant suggests, then, that glycerol has an additional effect on the reaction that does not involve solvent friction. It is possible that the change in equilibrium constant reflects a subtle change in the structure of cytochrome *c* that is associated with the lowered polarity of the glycerol/water solvent mixture.

We suggest that the reorganization of protein and surrounding solvent that accompanies the excited-state dissociation of axial ligands in ZnCytc is an example of nonpolar solvation, a response of the medium to a change in size of the imbedded probe.[36-43] The effects noted here upon a change of the external solvent viscosity are probably rather different in character from those discussed by Eaton and co-workers(refs) and Fayer and coworkers[44] in their studies of protein dynamics associated with photolysis of carbon monoxide in myoglobin. These studies considered the effects of solvent and internal protein friction on the protein reorganization that accompanies the conformational relaxation of the Fe(II) porphyrin upon photodissociation of the axially coordinated carbon monoxide ligand. The axial-ligand response discussed in this chapter involves a direct displacement of the polypeptide backbone away from the porphyrin by the side chains of the amino acids that serve as ligands to the Zn(II) ion. An increase in the external solution viscosity would be expected to retard this process because the associated internal pressure increase would be expected to result in an expansion of the protein's solvated volume.

In addition to the nonpolar response, ZnCytc should also exhibit a polar response to the excited state change in dipole moment that occurs upon the ground-to-excited state $\pi \rightarrow \pi^*$ transition. We will discuss in the next chapter the details of polar salvation in ZnCytc and its possible coupling to the axial-ligand photodissociation dynamics.

3.5. References

(1) Lampa-Pastirk, S.; Beck, W. F. *J. Phys. Chem. B.* **2004**, *108*, 16288.

(2) Frauenfelder, H.; Sligar, S. G.; Wolynes, P. G. *Science* **1991**, *254*, 1598–1603.

(3) Onuchic, J. N.; Luthey-Schulten, Z.; Wolynes, P. G. *Annu. Rev. Phys. Chem.* **1997**, *48*, 545–600.

(4) Dill, K. A.; Chan, H. S. *Nature Struct. Biol.* **1997**, *4*, 10–19.

(5) Chan, H. S.; Dill, K. A. *Proteins: Struct. Funct. Genet.* **1998**, *30*, 2–33.

(6) Dill, K. A. *Protein Sci.* **1999**, *8*, 1166–1180.

(7) Vanderkooi, J. M. *Biochim. Biophys. Acta* **1998**, *1386*, 241–253.

(8) Riter, R. E.; Edington, M. D.; Beck, W. F. Inertial protein-matrix solvation of a light-harvesting chromophore. In *Ultrafast Phenomena X*; Barbara, P., Knox, W., Zinth, W., Fujimoto, J., Eds.; Springer-Verlag: Berlin, 1996; pp 324–325.

(9) Homoelle, B. J.; Edington, M. D.; Diffey, W. M.; Beck, W. F. *J. Phys. Chem. B* **1998**, *102*, 3044–3052.

(10) Homoelle, B. J.; Beck, W. F. *Biochemistry* **1997**, *36*, 12970–12975.

(11) Jordanides, X. J.; Lang, M. J.; Song, X.; Fleming, G. R. *J. Phys. Chem. B* **1999**, *103*, 7995–8005.

(12) Loring, R. F.; Yan, Y. J.; Mukamel, S. *J. Chem. Phys.* **1987**, *87*, 5840–5857.

(13) Joo, T.; Jia, Y.; Yu, J.-Y.; Lang, M. J.; Fleming, G. R. *J. Chem. Phys.* **1996**, *104*, 6089–6108.

(14) Fleming, G. R.; Cho, M. *Annu. Rev. Phys. Chem.* **1996**, *47*, 109–134.

(15) Everitt, K. F.; Geva, E.; Skinner, J. L. *J. Chem. Phys.* **2001**, *114*, 1326.

(16) Vanderkooi, J. M.; Adar, F.; Erecìnska, M. *Eur. J. Biochem.* **1976**, *64*, 381.

(17) Vanderkooi, J. M.; Landesberg, R.; Hayden, G. W.; Owen, C. S. *Eur. J. Biochem.* **1977**, *81*, 339.

(18) Ye, S.; Shen, C.; Cotton, T. M.; Kostìc, N. M. *J. Inorg. Biochem.* **1997**, *65*, 219–226.

(19) Quian, C.; Yao, Y.; Tong, Y.; Wang, J.; Tang, W. *J. Biol. Inorg. Chem.* **2003**, *8*, 394–400.

(20) Anni, H.; Vanderkooi, J. M.; Mayne, L. *Biochemistry* **1995**, *34*, 5744–5753.

(21) Bushnell, G. W.; Louie, G. V.; Brayer, G. D. *J. Mol. Biol.* **1990**, *214*, 585–595.

(22) Delano, W. L. *The PyMOL molecular graphics system*; DeLano Scientific: San Carlos, California, 2002.

(23) Lakowicz, J. R. *Principles of Fluorescence Spectroscopy*; Plenum Press, 1983.

(24) Maroncelli, M. *J. Mol. Liq.* **1993**, *57*, 1–37.

(25) Stratt, R. M.; Maroncelli, M. *J. Phys. Chem.* **1996**, *100*, 12981–12996.

(26) Humphry-Baker, R.; Kalyanasundaram, K. *J. Photochem.* **1985**, *31*, 105–112.

(27) Kadish, K. M.; Shiue, L. R. *Inorg. Chem.* **1982**, *21*, 3623–3630.

(28) Miller, J. R.; Dorough, G. D. *J. Am. Chem. Soc.* **1952**, *74*, 3977–3981.

(29) Nappa, M.; Valentine, J. S. *J. Am. Chem. Soc.* **1978**, *100*, 5075–5080.

(30) Vogel, G. C.; Beckmann, B. A. *Inorg.Chem.* **1976**, *15*, 483–484.

(31) Scheidt, R. W. Porphyrin stereochemistry. In *The Porphyrins*; Dolphin, D., Ed.; Academic Press: New York, 1978; Vol. 3; pp 463–511.

(32) Scheidt, R. W.; Eigenbrot, C. W.; Ogiso, M.; Hatano, K. *Bull. Chem. Soc. Jpn.* **1987**, *60*, 3529–3533.

(33) Schauer, C. K.; Anderson, O. P.; Eaton, S. S.; Eaton, G. R. *Inorg.Chem.* **1985**, *24*, 4082–4086.

(34) Fleischer, E. B.; Miller, C. K.; Webb, L. E. *J. Am. Chem. Soc.* **1964**, *86*, 2342–2347.

(35) Crnogorac, M. M.; Kostìc, N. M. *Inorg. Chem.* **2000**, *39*, 5028–5035.

(36) Berg, M. *J. Phys. Chem. A* **1998**, *102*, 17–30.

(37) Berg, M. *J. Chem. Phys.* **1999**, *110*, 8577–8588.

(38) Bagchi, B. *J. Chem. Phys.* **1994**, *100*, 6658–6664.

(39) Ladanyi, B. M.; Stratt, R. M. *J. Phys. Chem.* **1996**, *100*, 1266–1282.

(40) Saven, J. G.; Skinner, J. L. *J. Chem. Phys.* **1993**, *99*, 4391–4402.

(41) Kang, T. J.; Yu, J.; Berg, M. *Chem. Phys. Lett.* **1990**, *174*, 476–480.

(42) Fourkas, J. T.; Benigno, A.; Berg, M. *J. Chem. Phys.* **1993**, *99*, 8552–8558.

(43) Fourkas, J. T.; Berg, M. *J. Chem. Phys.* **1993**, *98*, 7773–7785.

(44) Rector, K. D.; Rella, C. W.; Hill, J. R.; Kwok, A. S.; Sligar, S. G.; Chien, E. Y. T.; Dlott, D. D.; Fayer, M. D. *J. Phys. Chem. B* **1997**, *101*, 1468–1475.

4. Polar Solvation Dynamics in Zn(II)-Substituted Cytochrome *c*: Diffusive Sampling of the Energy Landscape in the Hydrophobic Core and Solvent-Contact Layer[†]

4.1. Introduction

The potential-energy surface (or *energy landscape*) of a protein is thought to have a rugged profile like that of a glass,[2] at least over short displacements from a given folding state. But at physiological temperatures, proteins are comparable to molecular liquids in exhibiting local flexibility and in allowing internal diffusion of small molecules.[3] On a local scale, the amino acids and their side chains perform hindered internal reorientational motions and torsions with respect to the polypeptide backbone; over a longer range, the polypeptide undergoes conformational and folding motions. An additional complexity arises from the interface between the protein and the surrounding aqueous bulk, which hinders motions of the solvated regions of the polypeptide as it moves between folding states.

In this chapter, we show how picosecond time-resolved fluorescence spectroscopy can be used with an *intrinsic* electronic chromophore embedded in the hydrophobic core of a globular protein to sense the liquid-like diffusive polypeptide motions that contribute to the random search of the protein's potential-energy surface. We consider here the

[†] The work in this chapter has been published in other form[1]

polar protein and solvent dynamics in ZnCytc. The Zn(II) porphyrin in ZnCytc is fluorophore with a long lifetime $\tau_F > 2ns$,[4,5] which permits us to measure the dynamic Stokes shift, the red shift of the fluorescence spectrum with respect to time, over the 100-ps to 12-ns regime. The dynamic Stokes shift describes the reorganization of the protein and solvent dipoles that occurs in response to the ground-to-excited-state change in dipole moment of the Zn(II)-porphyrin chromophore. The fluorescence spectrum of ZnCytc exhibits some resolved vibronic structure,[4] which permits the solvent-response function to be measured with a good signal/noise ratio despite the small reorganizational energy (<200 cm^{-1}). The structure of ZnCytc has been studied with 2D-NMR methods,[6,7] and continuous absorption and fluorescence spectra from ZnCytc have been extensively characterized.[4,6,8,9] Wiersma and co-workers[5] used photon-echo spectroscopy to characterize the glass-like protein dynamics in ZnCytc that are observed at 2 K.

In the previous chapter we reported the changes in vibronic structure that are observed in ZnCytc's time-resolved fluorescence spectrum owing to excited-state photodissociation of the Zn(II) ion's axial ligands, which are provided by the side chains of Met 80 and His 18 (see Figure 4.1). The release of the ligands was shown to be sensitive to the external bulk viscosity; in 50% (v/v) glycerol, the time constant for the faster of two exponential components was slowed from 120 ps to 400 ps. The axial-ligand reactions are evidently rate limited by the reorganization of the protein and the surrounding solvent. The motions in question can be considered to be a *nonpolar* solvation response to a change in the *size* of an embedded probe.[10-16] In this chapter we report that *polar* reorganizational dynamics of ZnCytc are not strongly coupled to the

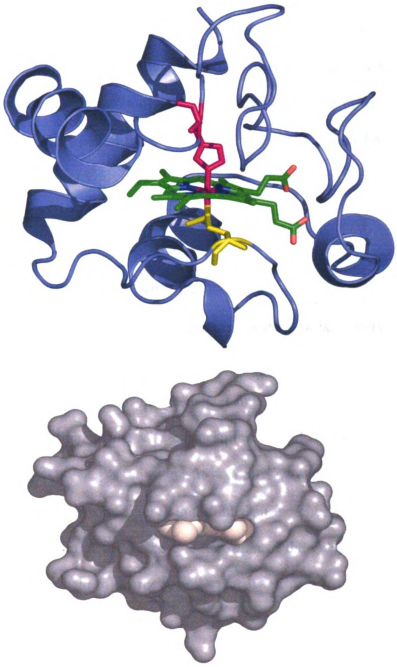

Figure 4.1 Structure of the horse-heart ferricytochrome c, as rendered using PyMOL[17] from pdb file 1HRC.[18] *Top*: Ribbon representation showing the polypeptide's secondary and folded structure, with heme and axial ligands to the Fe(III) ion, Met 80 and His 18, rendered as tube structures. *Bottom*: Solvent-contact surface, with the heme as a space-filling (CPK) representation.

nonpolar response because they occur on a significantly different time scale. The dynamic Stokes shift of the time-resolved fluorescence spectrum is biexponential, with only the slower phase of relaxation showing sensitivity to the presence of glycerol in the external solvent medium. We discuss the observed response in terms of the motions of the hydrophobic core and of the solvent-contact layer of the folded protein.

4.2. Experimental

4.2.1. Zn(II)-Substituted Cytochrome *c*

ZnCytc samples were prepared in the Vanderkooi laboratory at the University of Pennsylvania School of Medicine in Philadelphia by the method described in detail in chapter 2. For the experiments in this chapter ZnCytc samples were dissolved in a 50 mM *N*-(2-hydroxyethyl)piperazine-*N*'-2-ethanesulfonic acid (HEPES, Research Organics) NaOH buffer solution at pH 7.5 or in a 35% or 50% (v/v) glycerol/HEPES buffer solution mixture. The samples were filtered and diluted in the chosen solution so as to obtain a maximum absorption of 0.1 in the 0–0 transition of the Q-band for a 1-cm path length. The samples were held in quartz cuvettes with 1-cm path lengths and were purged with dry nitrogen prior to use.

4.2.2. Continuous Wave Absorption and Fluorescence Instrumentation

Steady-state absorption spectra were acquired with a 2-nm spectral band pass with a Hitachi U-2000 spectrophotometer or an ATI Unicam UV2 spectrophotometer. Steady-state fluorescence spectra were acquired with a Hitachi F-4500 fluorescence

spectrophotometer (5-nm excitation and emission band pass). The fluorescence intensities were corrected by the spectrofluorimeter's data acquisition program using a calibration curve obtained from a standard lamp. The intensities were recorded in terms of photons/nm band pass. When presented as a function of wavenumber, the fluorescence intensities are accordingly multiplied by the square of the wavelength in order to compensate properly for the fixed spectral band pass of the emission spectrometer. Scattered excitation light was eliminated from the fluorescence spectra by subtraction of the spectrum from a blank, solvent-only sample held in the same cuvette.

4.2.3. Picosecond Time-Resolved Fluorescence Spectroscopy

Single-wavelength fluorescence transients were acquired with a TCSPC apparatus operated in the reverse-triggered mode. The details of the method and apparatus were discussed in chapter 2. For the experiments discussed in this chapter the excitation wavelength was set to 585 nm , the 0–0 transition energy for ZnCytc spectra in water.

Samples used in time-resolved fluorescence measurements were held in 1-cm quartz cuvettes mounted in a temperature-controlled holder (Quantum Northwest TLC 50). All samples were filtered, kept at 22 °C, purged with dry nitrogen, and prepared at the same concentrations used in steady-state measurements. The instrument-response function of the detection system was approximately 60 ps (fwhm) in these experiments.

4.3. Results

4.3.1. Continuous-Wave Absorption and Fluorescence Emission Spectra

Figures 4.2 and 4.3 show the absorption and fluorescence spectra obtained at 22 °C from ZnCytc at pH 7.5 in water and in 50% (v/v) glycerol, respectively. The spectra are plotted with respect to wavenumber ν as A/ν and F/ν^3, respectively, with normalization to unit area. The integrals of these quantities report the dipole strength, the square of the transition-dipole moment.[19-21] The spectral regions shown in Figures 4.2 and 4.3 feature the Q bands, which arise from $\pi \rightarrow \pi^*$ transitions between the ground and

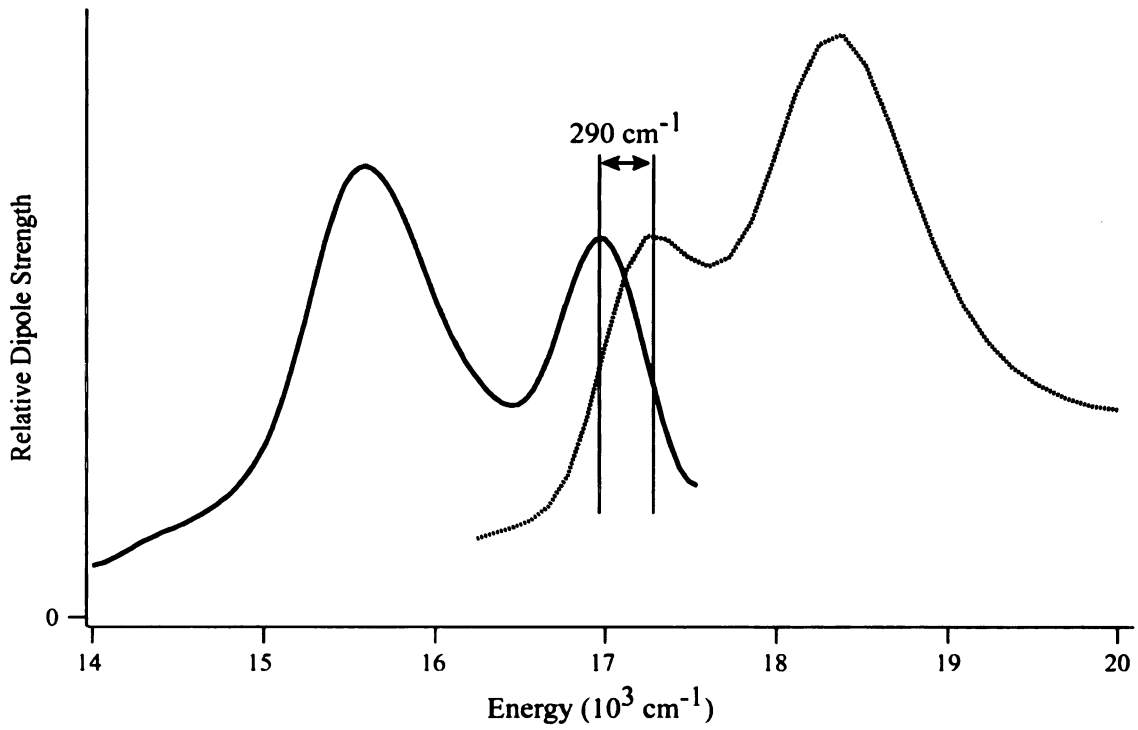

Figure 4.2. Continuous-wave absorption and fluorescence emission spectra from ZnCytc in water at room temperature. The spectra are plotted as relative dipole strengths and are normalized to unit area. The fluorescence spectrum was obtained with excitation tuned to the origin (0-0 transition energy), where the two spectra cross. The two spectra are displaced by $2\lambda = 290$ cm^{-1}, where λ represents the reorganization energy.

first-excited singlet states. The Q bands exhibit a partially resolved vibronic progression in methine-stretching mode that is polarized in the plane of the porphyrin macrocycle.[22] A comparison of Figures 4.2 and 4.3 shows that the absorption and fluorescence line shape is discernibly narrower in the presence of glycerol than observed in water alone. In both solvents, the energy distance ΔE_{00} between the 0–0 transitions in the absorption and fluorescence spectra, 290 cm^{-1}, allows an estimate of the reorganization energy, λ, of 145 cm^{-1}; if the ground-state and excited-state potentials are assumed to be harmonic and have the same normal-mode frequencies, then $\Delta E_{00} = 2\lambda$.[21,23] This estimate of the

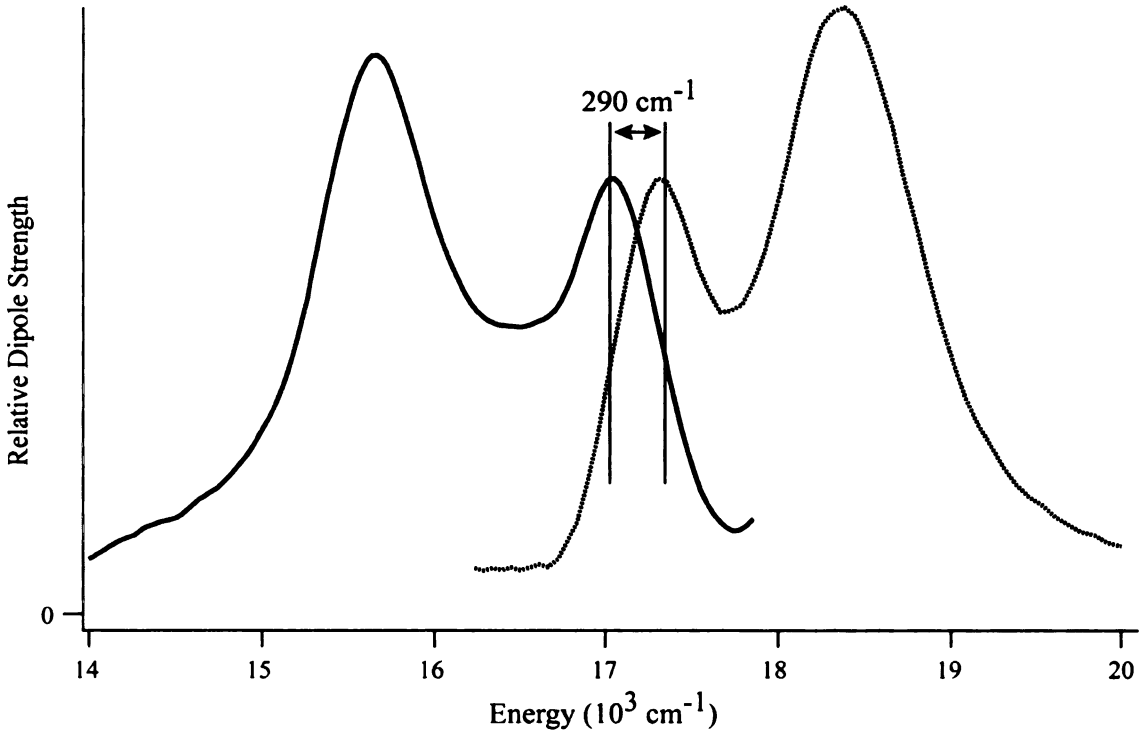

Figure 4.3. Continuous-wave absorption and fluorescence emission spectra from ZnCytc in 50% (v/v) glycerol at room temperature. The spectra are plotted as relative dipole strengths and are normalized to unit area. The fluorescence spectrum was obtained with excitation tuned to the origin (0-0 transition energy), where the two spectra cross. The two spectra are displaced by 2λ = 290 cm^{-1}, where λ represents the reorganization energy.

reorganization energy is valid in the limit of Gaussian line shapes,[24]as are essentially observed for the resolved vibronic components in the continuous spectra from ZnCytc.[25]

4.3.2. Dynamic Stokes Shift

Figures 4.4 and 4.5 present the time evolution of the fluorescence 0–0 transition energy, $\nu_{00}(t)$, from ZnCytc in water and in 50% (v/v) glycerol. These plots were obtained from an analysis of a set of time-resolved fluorescence spectra, which were obtained as described in the chapter 2. A set of TCSPC transients were recorded at discrete emission wavelengths spanning most of the fluorescence spectrum and spaced by

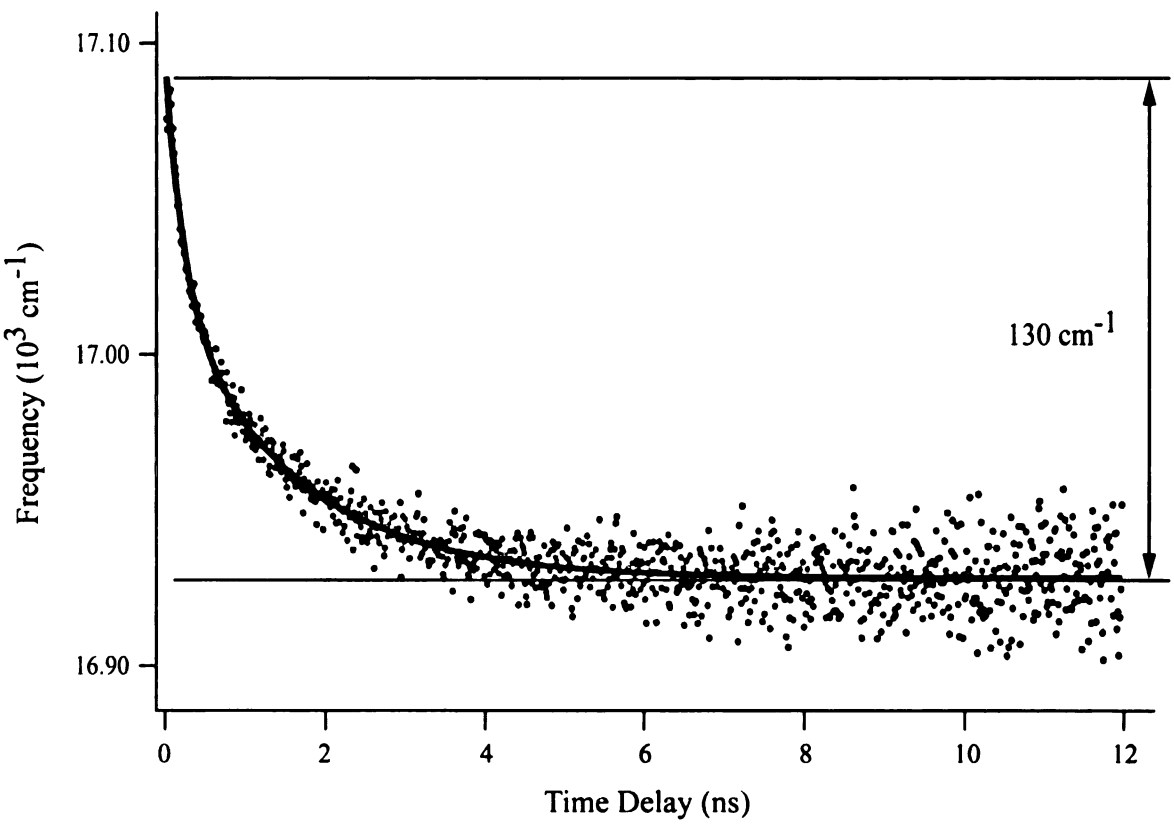

Figure 4.4. The time evolution ν_{00} (see eq 1) for ZnCytc in water. The fit parameters are listed in Table 2.

4 nm, the band pass of the emission monochromator. The transients were used without deconvolution of the instrument-response function. Time-resolved fluorescence-emission spectra were obtained directly as slices across the intensity–wavelength–time surface described by the set of transients at 12 ps intervals, the dwell time per point in the recorded transients.

To determine $\nu_{00}(t)$, we fit the time-resolved fluorescence spectra as dipole strengths $D_F = F(\nu)/\nu^3$ to a vibronic progression defined by the sum of three log-normal line shapes[26] $L_{0i}(\nu, \nu_0)$ offset by the mode frequency ν_F as described in detail in the chapter 2.

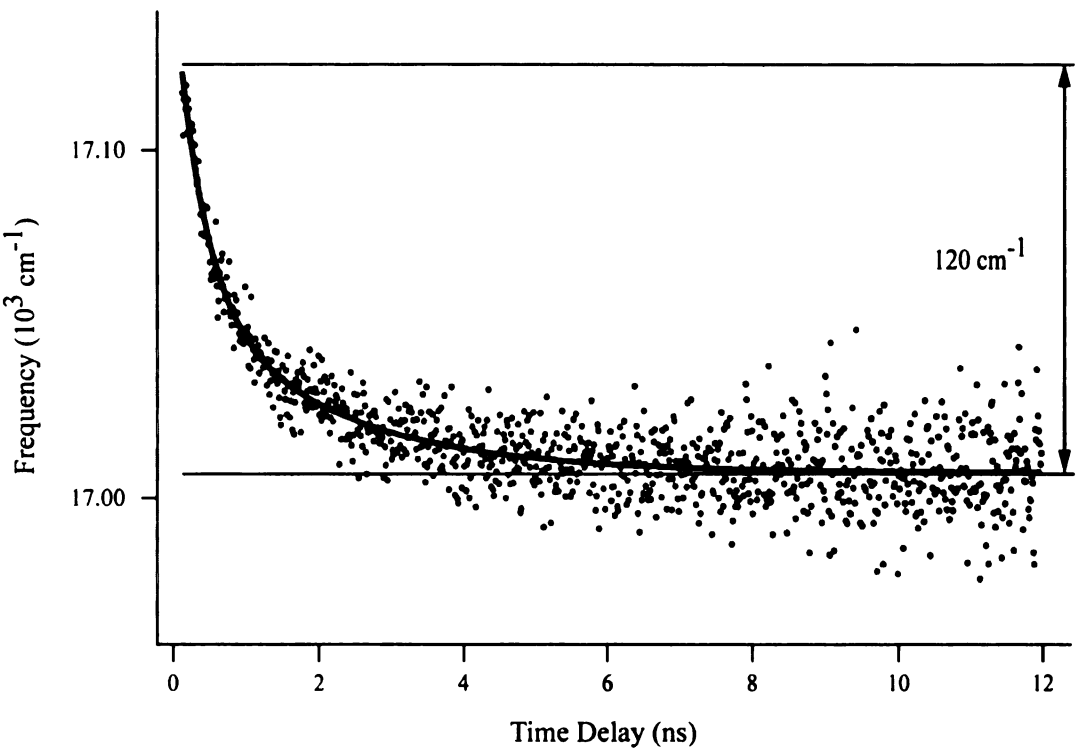

Figure 4.5. Time evolution ν_{00} (see eq 1) for ZnCytc in 50% (v/v) glycerol. The fit parameters are listed in Table 2

By fitting this model to the entire emission range covered in the time-resolved spectra, we obtain the time evolution of ν_{00} with a good signal/noise ratio despite the very small reorganization energy. The line shapes L_{0i} did not vary significantly in width or asymmetry over the 100-ps to 12-ns time window; Gaussians provide a satisfactory description of the line shapes. The mode frequency ν_F was also invariant. The scaling terms F_{0i} are the integrated dipole strengths for the vibronic lines in the fluorescence spectrum; as discussed in the previous chapter, these parameters change as a function of time owing to an excited-state dissociation of axial ligands from the Zn(II) ion.

Table 2

Solvent	a_1, cm^{-1}	τ_1, ps	a_2, cm^{-1}	τ_2, cm^{-1}	ν_∞, cm^{-1}
water	70±10	250±20	100±10	1450±100	16940±10
35% (v/v) glycerol	50±15	250±50	115±15	2000±100	16990±15
50% (v/v) glycerol	60±15	260±60	90±15	2200±100	17000±15

Table 2. Fit parameters for the time evolution of ν_{00} for Zn(II)-substituted cytochrome c in three solvents at 295 K.

The time evolution of ν_{00} observed from ZnCytc in Figures 4.4 and 4.5 is well described by an exponential model. The parameters obtained by fitting the data obtained in water, 35% (v/v) glycerol, and 50% (v/v) glycerol are compared in Table 2. (The corresponding plot of $\nu_{00}(t)$ obtained with 35% (v/v) glycerol is not shown.) The faster of the two components exhibits the same amplitude and time constant in the three solvent

mixtures, an average of 60 cm^{-1} and 253 ps, respectively. While the amplitude of the slow component is also independent of the solvent mixture, about 100 cm^{-1}, the time constant lengthens significantly from 1450 ps to 2200 ps in moving from water to 50% (v/v) glycerol. The slow component exhibits a time constant of 2000 ps in the presence of 35% (v/v) glycerol, so the trend for this component is monotonic as a function of the glycerol concentration. The change in the ν_∞ offset parameter that is obtained from the $\nu_{00}(t)$ profiles is consistent with the solvatochromic blue shift observed with continuous fluorescence spectra (see Figures 4.2 and 4.3) upon moving from water to 50% (v/v) glycerol. We did not observe any trend in the range of response nor was a faster component detected when the excitation wavelength was tuned as far as 700 cm^{-1} to the blue from the 0–0 transition, so vibrational relaxation and intramolecular vibrational redistribution do not make detectable contributions to the observed response functions over the reported time window.

4.4. Discussion

4.4.1. Solvent Response Functions in Proteins

The solvent-response function, $S_\nu(t)$, describes the time evolution of the fluorescence spectrum. It is usually defined in terms of the frequency of the fluorescence intensity maximum, $\nu(t)$, as discussed in chapter 1. The decay of $S_\nu(t)$ in proteins can reflect collision-like interactions between the chromophore and the surrounding polypeptide and any intrinsic water molecules.[27] As a consequence of the significantly

lower dielectric constant in the interior of a protein, $S_v(t)$ can involve more distant interactions of the chromophore and the protein structure, such as interactions with the surface of the protein.

The solvation response observed in proteins is a topic of current discussion. In most of the reported work in proteins the response is biexponential, exhibiting a large inertial phase followed by a smaller diffusive component. The large amplitude fast component is similar to the inertial phase in liquids that is attributed to the librational motions of the surrounding solvent molecules.[24,28,29] The slow component of the solvation response in liquids arises from random reorientational motions in a molecular solvent. The assignment of components observed in the solvation response in proteins strongly depends on the type of the protein and location of the chromophore.[27] The studies of the solvation response in proteins show that both the inertial and diffusive components of response can be attributed to the motions of the surrounding protein structure and intrinsic water molecules, or that both solvation components can be correlated to the motions of the surrounding protein matrix rather than to the bulk solvent molecules.[30] In some studies even the complete lack of a slow diffusive component was observed.[23] At the present time it is not fully understood how a protein's structure and the included solvent contribute to solvent response.

4.4.2. Dynamic Solvation in ZnCytc.

In this chapter, we have exploited the long-lived fluorescence of the intrinsic Zn(II) porphyrin in ZnCytc to focus on the diffusive part of the solvent-response

function. The methods we employed are similar to those that were used by Bashkin et al.[31] and by Pierce and Boxer[32] with solvatochromic dyes in the heme-binding pocket to obtain the solvation response in apomyoglobin. The results obtained by two groups were not in agreement. A single-exponential on the ns timescale was observed by Bashkin et al.[31] whereas a complex multiexponential decay spanning the ps-to-ns timescale was observed by Pierce and Boxer.[32] The most likely explanation for the different results obtained with myoglobin is that different dye-binding configurations in the heme-binding pocket are obtained with the two dyes. By exploiting the intrinsic Zn(II) porphyrin as a probe for ZnCytc, we avoid the various complications that can arise from the use of extrinsic probes, such as the presence of multiple binding sites and the possibility that the dye moves in its protein host during the excited-state lifetime. Because of its considerable size and surface area, however, the Zn(II) porphyrin is certainly not as spatially selective as the intrinsic aladan probe employed by Cohen et al.[27]

At delays longer than 100 ps, the dynamic Stokes shift response exhibited by ZnCytc is well described by a double exponential function, with only the slower of the two components exhibiting sensitivity to the nature of the external bulk solvent. It is clear that protein motions are mostly responsible for both phases of the response because the time constants are several orders of magnitude slower than those of the bulk solvent or of the solvent in the hydration layer itself. Consider that the diffusive part of the solvent-response function observed in water occurs on a sub-ps time scale;[33,34] the motions of water molecules in the hydration layer of a protein are thought to be slower than the bulk, with a prominent component observed on the 40-ps time scale.[24,35-38]

The slower of the two solvation components observed in ZnCytc evidently reports motion of the outer part of the protein that directly contacts and is frictionally hindered by the surrounding solvent. At least part of the solvent sensitivity is suggested by Figure 4.1, which includes rendering from the X-ray crystal structure of horse-heart ferricytochrome c[18] of the solvent-contact surface and its proximity to the porphyrin. The edge of the porphyrin macrocycle breaks through the solvent-contact surface; it is estimated that only four atoms (7.4% of the porphyrin's surface area) are exposed to the solvent.[39] This portion of the porphyrin would be expected to sense directly the motions of the external solvent; indeed, a solvatochromic blue shift and a narrowing of the continuous absorption and fluorescence spectra occur as the proportion of glycerol in the solvent increases. The ns timescale for the solvent-sensitive part of the dynamic Stokes shift, however, makes it clear that the porphyrin does not stick out of the protein far enough to sense water molecules in the bulk.

The majority of the Zn(II) porphyrin in ZnCytc is embedded in the hydrophobic core, which gives rise to the faster part of the solvent response function. The shorter time scale implies that the range of motion covered by relevant polypeptide motions is shorter than those involved in the slower part of the solvent-response function. The observation that a biexponential model describes the results very well is itself a surprise; one might have anticipated that the dynamic Stokes shift would report a range of time scales given the porphyrin's span from the core to the edge of the protein. The exponential character suggests that each relaxation component is associated with a well-defined class of protein motion that is mechanically uncoupled from that of the other component.

4.4.3. Coupling of Polar and Nonpolar Solvation in ZnCytc

The dynamics discussed so far are associated with the *polar* solvation response in ZnCytc to the formation of the Zn(II) porphyrin's excited-state dipole moment. We discussed in the previous chapter how there is also a *nonpolar* solvation response that arises from a ground-to-excited-state change in *size* of the Zn(II) porphyrin owing to a dissociation of the Zn(II) ion's axial ligands.

The time evolution of the vibronic structure in ZnCytc's fluorescence spectrum can be expressed in terms of the intensity ratio for the 0–1 and 0–0 transitions, Q_{01}/Q_{00}. In water and glycerol/water mixtures, the time evolution of Q_{01}/Q_{00} observed from ZnCytc describes a biexponential increasing trend that reports a net dissociation of the two axial ligands. The faster of the two time constants lengthens from 120 ± 50 ps to 400 ± 50 ps in moving from water to 50% (v/v) glycerol; the slower of the two time constants, 7.0 ±1.0 ns is unaffected by the addition of glycerol. The 95% confidence intervals for these two time constants exclude those for the dynamic Stokes shift (see Table 2.). Thus, the time evolution of the vibronic structure and dynamic Stokes shift are apparently uncorrelated in time scale. Further, the effect of solvent on the two parameters occurs on different time scales, with the presence of glycerol slowing the fast component of the vibronic structure change and the slow component of the dynamic Stokes shift. These results show that the nonpolar and polar solvation dynamics of ZnCytc are largely uncoupled.

A consideration of the spectroscopic origins of the nonpolar and polar solvation dynamics in ZnCytc accounts for their uncoupled character. The polar solvation dynamics involve a response of the surrounding protein to the porphyrin's change in dipole moment along the direction of the transition-dipole moment for the Q absorption band, which is polarized in the plane of the porphyrin.[22] The vibronic structure of the Q-band involves a progression in a totally symmetric methine stretching mode that also is polarized in the plane of the porphyrin. The *intensities* of the vibronic transitions change owing to the presence or absence of a Lewis base at the axial ligation position, an interaction that couples some out-of-plane character into the Q-band transition. As the axial ligands attack or withdraw from the Zn(II) ion, the surrounding protein and solvent have to reorganize to accommodate the new positions of the axial ligands. This motion is mostly orthogonal to the types of motion that would be directly coupled to the Q-band transition-dipole moment. Thus, two types of solvation dynamics involve motions that should be at best weakly coupled.

4.4.4. Estimation of the Magnitude of the Internal Solvation Response in ZnCytc

Although the acquired data limit us to a direct consideration of the time-resolved fluorescence spectra obtained from ZnCytc from the 100-ps time point onward, we have some knowledge of the sub-100-ps portion of the solvation response from a consideration of the range of the dynamic Stokes shift that is subsequently observed and the reorganization energy that is obtained from the continuous absorption and fluorescence spectra.[23,24,40] The directly observed range of the dynamic Stokes shift is obtained from

fits to $\nu_{00}(t)$ (see Table 2. and Figures 4.4 and 4.5) at the 100-ps delay and extrapolated to infinite time. The total shift is 125 cm^{-1} on average in the three solvent mixtures. This shift is about 85% of the reorganization energy, l=145 cm^{-1}, that is obtained as half of the difference between the 0–0 transition energies of the absorption and fluorescence dipole strength spectra (see figures 4.2 and 4.3).[24] This quantity is strictly equivalent to the full range of the dynamic Stokes shift, $\nu(0)-\nu(\infty)$, when excitation at the spectral origin (or 0–0 transition energy, where the absorption and fluorescence dipole strength spectra cross) is employed.[41] In comparison, the sum of the amplitudes of the two exponential components, 160 cm^{-1}, is significantly larger than the reorganization energy.

Figure 4.6 shows that the summed amplitudes extrapolate the observed biexponential solvation response to the zero of time. The sub-100-ps portion of the response must connect the total range of the shift, $\nu(0)-\nu(\infty)=\lambda$, with the shift observed at 100 ps; in Figure 4.6, a Gaussian is drawn to suggest one possibility that is consistent with the shape of the response observed in liquids.[42] The point of the exercise is to make it clear that no matter what functional form is chosen, the magnitude of the sub-100 ps solvation response in ZnCytc is much smaller than the magnitude of the observed response from 100 ps onward. It is safe to say that the sub-ps fraction of the solvent-response function that would include inertial motions is restricted in ZnCytc to less than 10% of the reorganization energy. This result strongly contrasts with the previous observations of the sub-ps solvent response function in other protein systems, where the sub-ps fraction accounted for the majority of the response.

The most likely explanation for the present results is that most of the dynamic Stokes shift response observed in ZnCytc arises from a direct sensing of motions of the hydrophobic core of the protein. This region contains very few embedded charges, polar residues, or water molecules that are capable of the free-streaming character of motion that contributes to the polar solvation response on the sub-ps time scale in molecular liquids. In contrast, the protein systems that exhibit large sub-ps solvation responses were probed with intrinsic or extrinsic chromophores that sense motions of polar groups near to or at the surface of the protein. In the case of bacteriorhodopsin, the retinal chromophore is found in a polar channel through which the transmembrane ion-pumping action occurs and mobile protein groups are found. In ZnCytc, the hydrophobic region is apparently densely packed in the native state, and reorganization of the protein inresponse to the formation of the Zn(II) porphyrin's excited-state dipole moment is limited to slow, small-amplitude motions of a relatively large reduced mass. We infer that the Zn(II) porphyrin chromophore largely obtains its sensitivity to the motions of the solvent-sheathed outer parts of the protein indirectly through the polypeptide backbone; but the part of the reorganization energy that must be reserved for a fast solvation response is on the same order of the porphyrin's surface area that breaks through the solvent contact surface. A direct consideration of this hypothesis will have to wait for future experiments on ZnCytc employing femtosecond experiments.

The present results raise the interesting possibility that the motions that a globular protein makes in its hydrophobic core mostly lack the free-streaming or inertial character that dominates the solvation response of water and other small molecular liquids. That the

polypeptide motions in the hydrophobic core and in the polar exterior of a protein are different in time scale and are associated with different types of motion is a novel suggestion that deserves additional attention because of its possible impact on the potentials used in molecular dynamics simulations of folded and partially folded proteins.

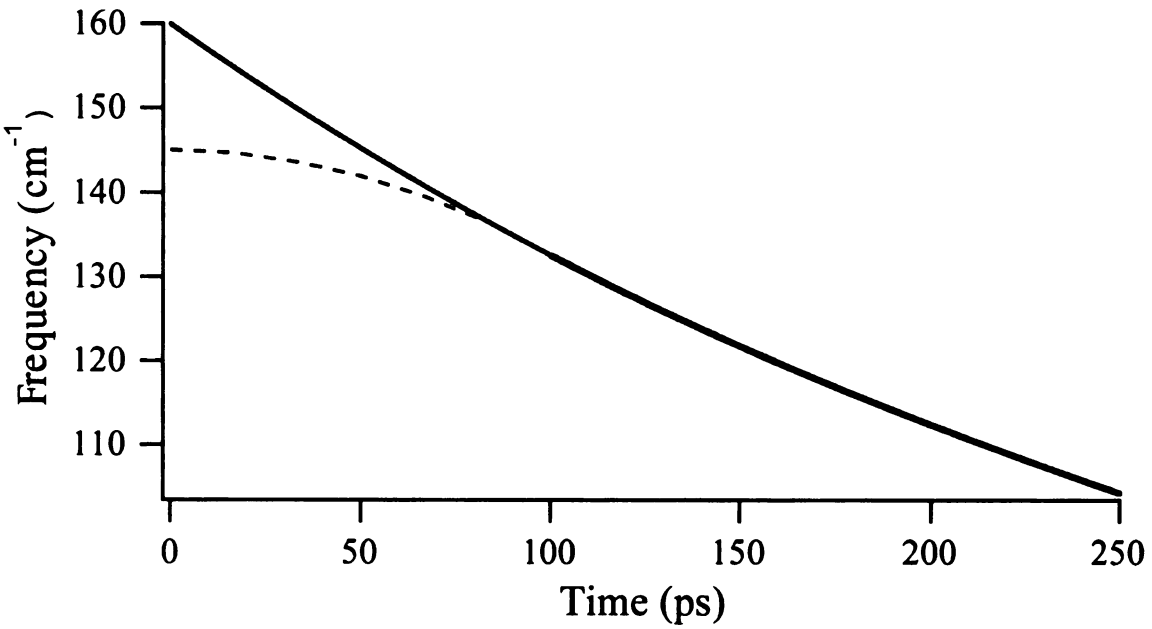

Figure 4.6. Model for the early time evolution ν_{00} for ZnCytc in water. The ordinate corresponds to the remaining Stokes shift at the indicated delay following excitation. The thick solid line shows the fitted trend obtained from Figures 4 and 5 from fits to the time-resolved fluorescence spectra observed over the 100-ps to 12-ns time window. The thin solid line extrapolates the fitted trend to zero time. The dashed line shows a hypothetical Gaussian trend that connects the reorganization energy (see Figures 4.2 and 4.3) with the observed shift of ν_{00} at the 100-ps delay.

4.5. References

(1) Lampa-Pastirk, S.; Beck, W. F. *J. Phys. Chem. B.* **2004**, *108*, 16288.

(2) Frauenfelder, H.; Sligar, S. G.; Wolynes, P. G. *Science* **1991**, *254*, 1598–1603.

(3) Vanderkooi, J. M. *Biochim. Biophys. Acta* **1998**, *1386*, 241–253.

(4) Vanderkooi, J. M.; Adar, F.; Erecìnska, M. *Eur. J. Biochem.* **1976**, *64*, 381.

(5) Leeson, D. T.; Berg, O.; Wiersma, D. A. *J. Phys. Chem.* **1994**, *98*, 3913–3916.

(6) Anni, H.; Vanderkooi, J. M.; Mayne, L. *Biochemistry* **1995**, *34*, 5744–5753.

(7) Quian, C.; Yao, Y.; Tong, Y.; Wang, J.; Tang, W. *J. Biol. Inorg. Chem.* **2003**, *8*, 394–400.

(8) Vanderkooi, J. M.; Erecìnska, M. *Eur. J. Biochem.* **1975**, *60*, 199–207.

(9) Crnogorac, M. M.; Kostìc, N. M. *Inorg. Chem.* **2000**, *39*, 5028–5035.

(10) Kang, T. J.; Yu, J.; Berg, M. *Chem. Phys. Lett.* **1990**, *174*, 476–480.

(11) Saven, J. G.; Skinner, J. L. *J. Chem. Phys.* **1993**, *99*, 4391–4402.

(12) Bagchi, B. *J. Chem. Phys.* **1994**, *100*, 6658–6664.

(13) Fourkas, J. T.; Benigno, A.; Berg, M. *J. Chem. Phys.* **1993**, *99*, 8552–8558.

(14) Ladanyi, B. M.; Stratt, R. M. *J. Phys. Chem.* **1995**, *99*, 2502–2511.

(15) Berg, M. *J. Phys. Chem. A* **1998**, *102*, 17–30.

(16) Berg, M. *J. Chem. Phys.* **1999**, *110*, 8577–8588.

(17) Delano, W. L. *The PyMOL molecular graphics system*; DeLano Scientific: San Carlos, California, 2002.

(18) Bushnell, G. W.; Louie, G. V.; Brayer, G. D. *J. Mol. Biol.* **1990**, *214*, 585–595.

(19) Kantor, C. R.; Schimmel, P. R. Biophysical Chemistry, Part II: Techniques for the study of Biological Structure and Function; Freeman and Co: San Francisco, 1980.

(20) Lakowicz, J. R. *Principles of Fluorescence Spectroscopy*, Second ed.; Kluwer Academic/Plenum Publishers: New York, 1999.

(21) McHale, J. L. *Molecular Spectroscopy*; Prentice Hall: Upper Saddle River, New Jersey, 1999.

(22) Gouterman, M. Optical spectra and electronic structure of porphyrins and related rings. In *The Porphyrins*; Dolphin, D., Ed.; Academic Press: New York, 1978; Vol. 3; pp 1–159.

(23) Kennis, J. T. M.; Larsen, D. S.; Ohta, K.; Facciotti, M. T.; Glaeser, R. M.; Fleming, G. R. *J. Phys. Chem. B* **2002**, *106*, 6067–6080.

(24) Jordanides, X. J.; Lang, M. J.; Song, X.; Fleming, G. R. *J. Phys. Chem. B* **1999**, *103*, 7995–8005.

(25) Lampa-Pastirk, S.; Lafuente, R. C.; Beck, W. F. *J. Phys. Chem. B* **2004**, *108*, 12602–12607.

(26) Siano, D. B.; Metzler, D. E. *J. Chem. Phys.* **1969**, *51*, 1856–1861.

(27) Cohen, B. E.; McAnaney, T. B.; Park, E. S.; Jan, Y. N.; Boxer, S. G.; Jan, L. Y. *Science* **2002**, *296*, 1700–1703.

(28) Homoelle, B. J.; Beck, W. F. *Biochemistry* **1997**, *36*, 12970–12975.

(29) Homoelle, B. J.; Edington, M. D.; Diffey, W. M.; Beck, W. F. *J. Phys. Chem. B* **1998**, *102*, 3044–3052.

(30) Changenet-Barret, P.; Choma, C. T.; Gooding, E. F.; DeGrado, W.; Hochstrasser, R. M. *J. Phys. Chem. B* **2000**, *104*, 9322–9329.

(31) Bashkin, J. S.; McLendon, G.; Mukamel, S.; Marohn, J. *J. Phys. Chem.* **1990**, *94*, 4757–4761.

(32) Pierce, D. W.; Boxer, S. G. *J. Phys. Chem.* **1992**, *96*, 5560.

(33) Rosenthal, S. J.; Xie, X.; Du, M.; Fleming, G. R. *J. Chem. Phys.* **1991**, *95*, 4715–4718.

(34) Maroncelli, M.; Kumar, P. V.; Papazyan, A.; Horng, M. L.; Rosenthal, S. J.; Fleming, G. R. Studies of the inertial component of polar solvation dynamics. In *Ultrafast Reaction Dynamics and Solvent Effects*; Guaduel, Y., Rossky, P. J., Eds.; AIP Press: Woodbury, NY, 1994; pp 310–333.

(35) Nandi, N.; Bagchi, B. *J. Phys. Chem. B* **1997**, *101*, 10954–10961.

(36) Nandi, N.; Bhattacharyya, K.; Bagchi, B. *Chem. Rev.* **2000**, *100*, 2013–2045.

(37) Bizzari, A. R.; Cannistraro, S. *J. Phys. Chem. B* **2002**, *106*, 6617–6633.

(38) Pal, S. K.; Peon, J.; Bagchi, B.; Zewail, A. H. *J. Phys. Chem. B* **2002**, *106*, 12376–12395.

(39) Brayer, G. D.; Murphy, M. E. Structural studies of eukaryotic cytochromes *c*. In *Cytochrome c: a Multidisciplinary Approach*; Scott, R. A., Mauk, A. G., Eds.; University Science Books: Sausalito, California, 1996; pp 103–166.

(40) Fee, R. S.; Maroncelli, M. *Chem. Phys.* **1994**, *183*, 235–247.

(41) Mukamel, S. *Principles of Nonlinear Optical Spectroscopy*; Oxford University Press: New York, 1995.

(42) Stratt, R. M.; Maroncelli, M. *J. Phys. Chem.* **1996,** *100*, 12981–12996.

5. Light-Induced Protein Unfolding of Zn(II)-substituted Cytochrome *c*: Dynamics of Entry and Exit of Water Molecules to and from the Hydrophobic Core During Unfolding and Refolding

5.1. Introduction

The role of misfolded proteins and the mechanism that produces them from correctly folded, native structures are not understood.[1-6] A central problem in this area is that existing methods for studying the kinetics and mechanism of protein folding, unfolding and misfolding reactions involve macroscopic manipulation of the solution conditions or temperature. The most common methods involve stopped-flow or rapid-flow mixing techniques that involve removal or addition of a chemical denaturant to the solution as the means to start the reaction.[7-9] Temperature-jump methods have been used for many years; the most recent versions of this class of experiment have involved laser-induced temperature jumps mediated by the near IR overtone absorption of water molecules in the solution.[10-16] While these methods have yielded a wealth of information that has been used in the shaping of current theories for protein-folding dynamics, none of these methods can be used under the physiological conditions that promote the progress of disease nor can they be used in intact cells or *in vivo*. These methods also usually suffer from the disadvantage of being one-shot in character; the reaction can be initiated only once, and recycling to reform the initial state requires either a long relaxation time to permit the solution temperature to reequilibrate or a chemical

separation of the reactant proteins from the supporting solution. Study of a misfolding mechanisms would be aided tremendously if there were a way to initiate synchronously a reaction in an ensemble of proteins, rendering it possible to detect intermediate structures, but in a range of solution conditions and temperatures under control of the experimentor rather than just as required to initiate folding, unfolding or misfolding reactions.

The approach discussed in this chapter is motivated by the idea that there are many possible folding trajectories between the unfolded and native folded states on the folding potential-energy surface, which has been termed an *energy landscape* (see chapter 1).[17-25] Protein misfolding can be taken as a consequence of the possibility of alternate Gibbs free-energy minima on the energy landscape that act as kinetic sinks or traps. This picture suggests immediately the possibility that the native structure is formed under a combination of kinetic and thermodynamic control.[26] Further, misfolded proteins may arise spontaneously from the native state; folded proteins are only marginally stable.[24] Nevertheless, owing to the topology of the funnel, it is possible that most unfolding trajectories subsequently are steered along refolding paths toward the native structure. The infinitesimal number of trajectories that lead to trapping in alternate minima may be the origin of the misfolded proteins that are active in disease.

It has been long established that the origin of protein stability lies in the hydrophobic effect, the ability of a protein to pack its hydrophobic side chains inside the molecule and away from water.[27] The hydrophobic effect results in a decrease in the free energy of protein and its surrounding solvent. Manipulation of the free energy of the hydrophobic core could be used as a direct means to initiate an unfolding reaction.

We suggest here an approach that uses an electronic chromophore in the hydrophobic core of a folded protein as an optical trigger for unfolding reactions. We call this method the *optical G jump*. With excitation sufficiently above the 0–0 vibronic transition from the ground state to the lowest singlet excited state (S_1), the electronic chromophore injects the Gibbs free energy required to generate the transition state for unfolding through vibrational energy transfer from the chromophore to the protein. The vibrationally equilibrated electronic chromophore's subsequent recovery of the ground state by emission of a photon provides a local solvatochromic probe of the unfolding reaction. We show in this chapter that this approach uniquely provides a means to detect the entry and exit of water molecules into the hydrophobic core that is probably associated with the formation and decay of the folding/unfolding transition state and control of the reaction rate.

5.2. Experimental

5.2.1. Zn(II)-Substituted Cytochrome *c*

The method for preparation of ZnCytc is described in detail in chapter 2. The experiments in this chapter employ ZnCytc samples dissolved in a 50 mM HEPES buffer solution at pH 7.5 or in a 40% (v/v) methanol/HEPES or 50% (v/v) glycerol/HEPES buffer solution mixture. Sample handling is described in detail in chapter 2.

5.2.2. Continuous-Wave Absorption and Fluorescence Instrumentation

Steady-state absorption and fluorescence spectra instrumentation is described in chapter 3. The temperature dependent continuous-wave fluorescence spectra shown in this chapter were acquired with a Hitachi F-4500 fluorescence spectrophotometer employing temperature controlled sample holder. The excitation wavelength was 585 nm. The samples were equilibrated at each temperature for 20 minutes prior to recording the fluorescence emission spectrum.

5.2.3. Picosecond Time-Resolved Fluorescence Spectroscopy

For the experiments discussed in this chapter, the 355-nm third-harmonic of the Antares Nd-YAG laser was used to synchronously pump a cavity dumped dye laser operating with Stilbene 420 laser dye (Exciton). The details of the experimental apparatus are provided in chapter 2. ZnCytc samples were excited with 420-nm light corresponding to the Soret-band region of the spectrum. Fluorescence signals were collected at magic angle, 54.7° with respect to the vertically polarized excitation pulse. The samples were held in 1-cm quartz cuvettes mounted in a home-built temperature controlled mount. During the experiments, the samples were kept at 22 °C with Neslab RTE-7 circulating water bath. The instrument response function was 35 ps fwhm.

5.3. Results

5.3.1. Time-Resolved Fluorescence Spectra

Figure 5.1 shows a series of time-resolved fluorescence spectra obtained at six selected time delays from ZnCytc in water at pH 7.5. The spectra are obtained as slices of a time-wavelength-intensity surface by the method described in detail in chapter 2. The surface was obtained by recording a set of TCSPC fluorescence transients following excitation of the Soret-band at 420 nm. The transients, collected with 5 nm spacing, span most of the fluorescence spectrum.

The time-resolved spectra shown in Figure 5.1 exhibit time evolution of the intensities of the 0–0 and 0–1 vibronic components. At time delays < 150 ps the relative intensity of the Q_{01} vibronic line increases at the expense of Q_{00}. At time delays near 250 ps the time-resolved fluorescence spectra pass through the first turn-around point characterized by equal relative intensities of 0–0 and 0–1 vibronic components. After the first turn-around point the relative intensity of the Q_{00} vibronic line slowly increases at the expense of that of the Q_{01}. Second turn-around point is reached at 5 ns. Beyond this point the very slow increase in intensity of Q_{01} vibronic line is observed.

In chapter 3 we discussed time evolution of the intensities of the 0–0 and 0–1 vibronic components in the time-resolved fluorescence spectra in the native state of ZnCytc following Q-band excitation. The observed response was biexponential with a monotonic increase of the intensity of the 0–1 transition. The time evolution of the

vibrational structure of the Q-band fluorescence spectrum from ZnCytc was rate limited by protein-matrix and solvent reorganization. We attributed this response to the excited-state release of axial ligands from the Zn(II) ion. Figure 1 indicates that the vibronic structure following Soret-band excitation exhibits multiphasic behavior with at least two turn-around points. Increase of the Q_{01} intensity at the initial time delay indicates the possibility for the release of one of the axial ligands, but the overall response is far more complex.

Figure 5.1 depicts that 0–1 vibronic line exhibits additional structure, with a partially resolved shoulder emerging at 16 250 cm^{-1}. The intensity of this structure decays with respect to time, and at ~250 ps completely disappears. The type of spectral changes observed here could result from distortions of the heme caused by perturbations in its near vicinity.[28] The observed response is an indication of the significant structural changes that occur in the protein upon the Soret-band excitation that were not observed in the Q-band experiments described in chapter 3.

The time-resolved spectra at early time delays from 100 to 250 ps exhibit a red shift of the center of the Q_{00} line. At delays beyond 250 ps, the center of the Q_{00} line shifts to the blue. The dashed line on Figure 5.1 depicts this behavior.

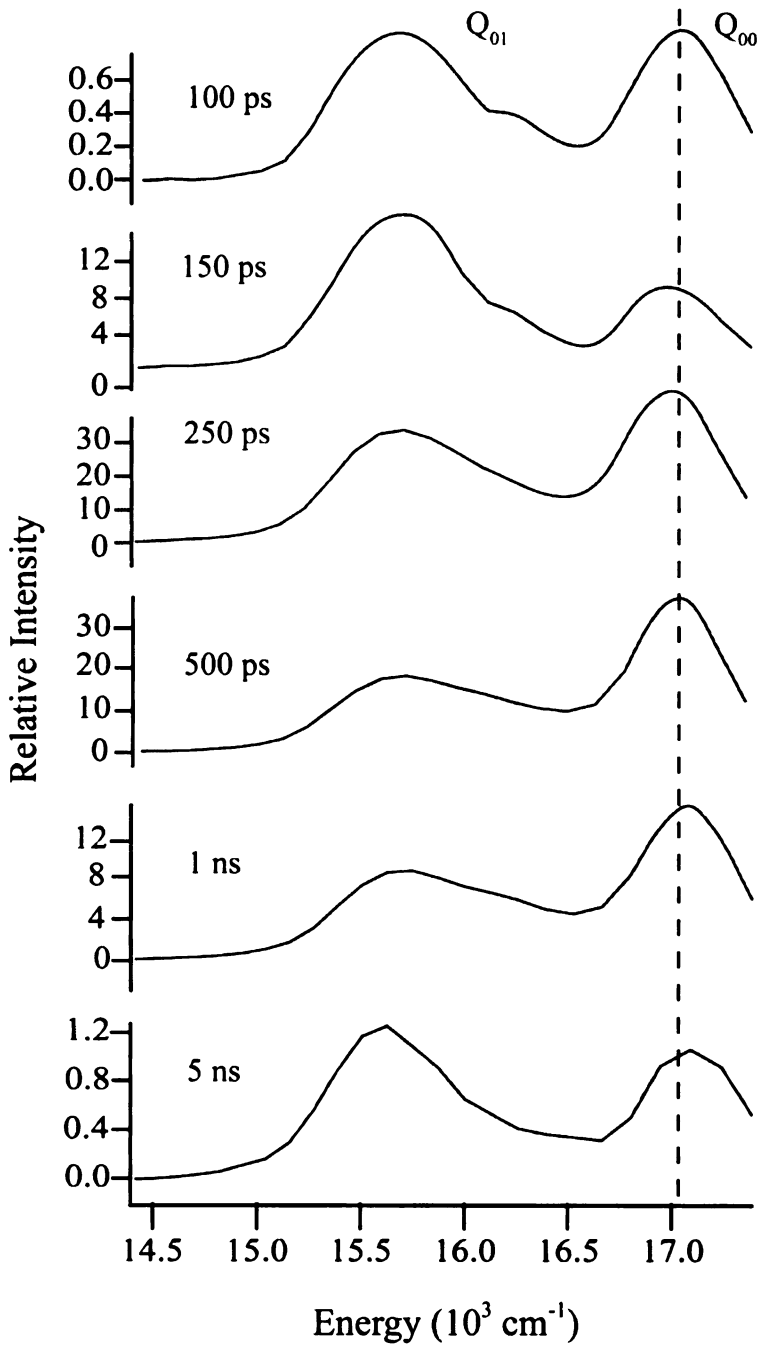

Figure 5.1. Time-resolved fluorescence spectra from ZnCytc in aqueous solution at 22 °C at six delays. The dashed line depicts the initial red shift of the Q_{00} vibronic band of the fluorescence spectrum followed by the blue shift at time-delays longer than 250 ps.

5.3.2. Dynamic Stokes Shift

In order to examine the shift of the spectra in more detail, we obtained the dynamic Stokes shift, a plot of the center of the Q_{00} vibronic line as a function of time, by the method described in detail in chapter 2. Figure 5.2 shows the early time components of the dynamic Stokes shift response observed in ZnCytc with Soret-band excitation.

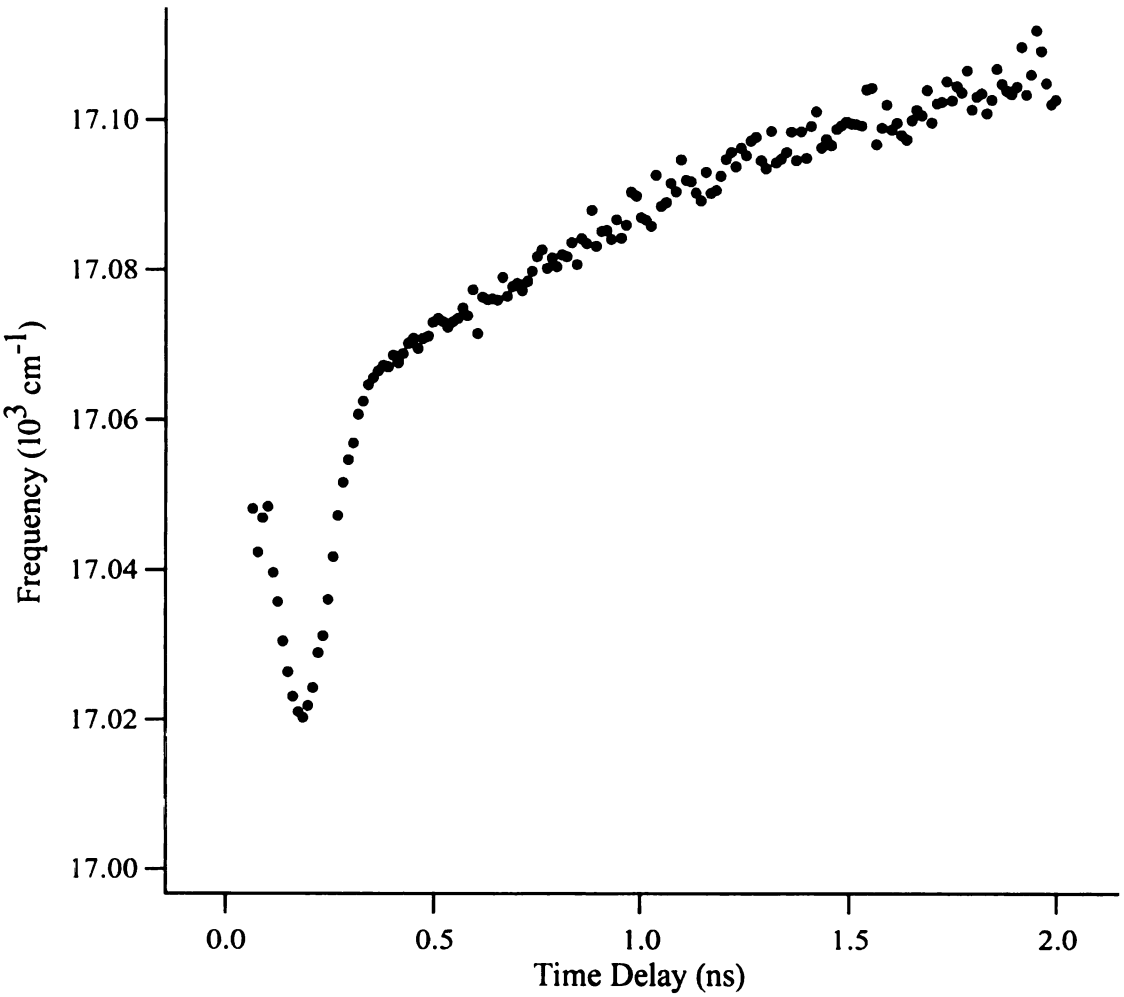

Figure 5.2. Early time response of the frequency of the center of the Q_{00} vibronic line of the fluorescence spectrum from ZnCytc in aqueous solution at 22 °C. The excitation laser was tuned to 420 nm, the peak of the Soret absorption band.

The dynamic Stokes shift response with Soret-band excitation shown in Figure 5.2, exhibits a biphasic character. The initial segment from 100–250 ps is a very fast red shift. The time constant of 125 ps is significantly shorter than of the fast component observed with *Q*-band excitation discussed in chapter 4. At the 200-ps delay point, however, the response turns around and starts a biexponential shift to the blue with time constants of 330 ps and 3.1 ns that continues throughout the observation window permitted by the fluorescence lifetime. Figure 5.3 compares the dynamic Stokes shift responses obtained with Soret-band excitation (top curve) and with Q-band excitation (bottom curve). The response with Q-band excitation is well modeled with a sum of two exponentials (as explained in chapter 4), but the response resulting from Soret-band excitation requires at least three exponentials to be adequately modeled. Note that the final observed position of the fluorescence spectrum with Soret-band excitation is 200 cm^{-1} to the blue of the equilibrium position observed with *Q*-band excitation.

Figure 5.4 compares the dynamic Stokes shift response observed in ZnCytc following Soret-band excitation in water, 50% glycerol and in 40% methanol. The compositions of the glycerol and methanol solutions were chosen to obtain the same, decreased polarity compared to water, but significantly different viscosities. The three responses allow a separate determination of the effects of the external solvent polarity and viscosity on the nature of the response. Note first that the initial red shift is shifted to a shorter time scale in glycerol/water and in methanol/water compared to that in water so that the amplitude of the initial component is very small (glycerol) or even absent (methanol) in the >100-ps observation window available in these results.

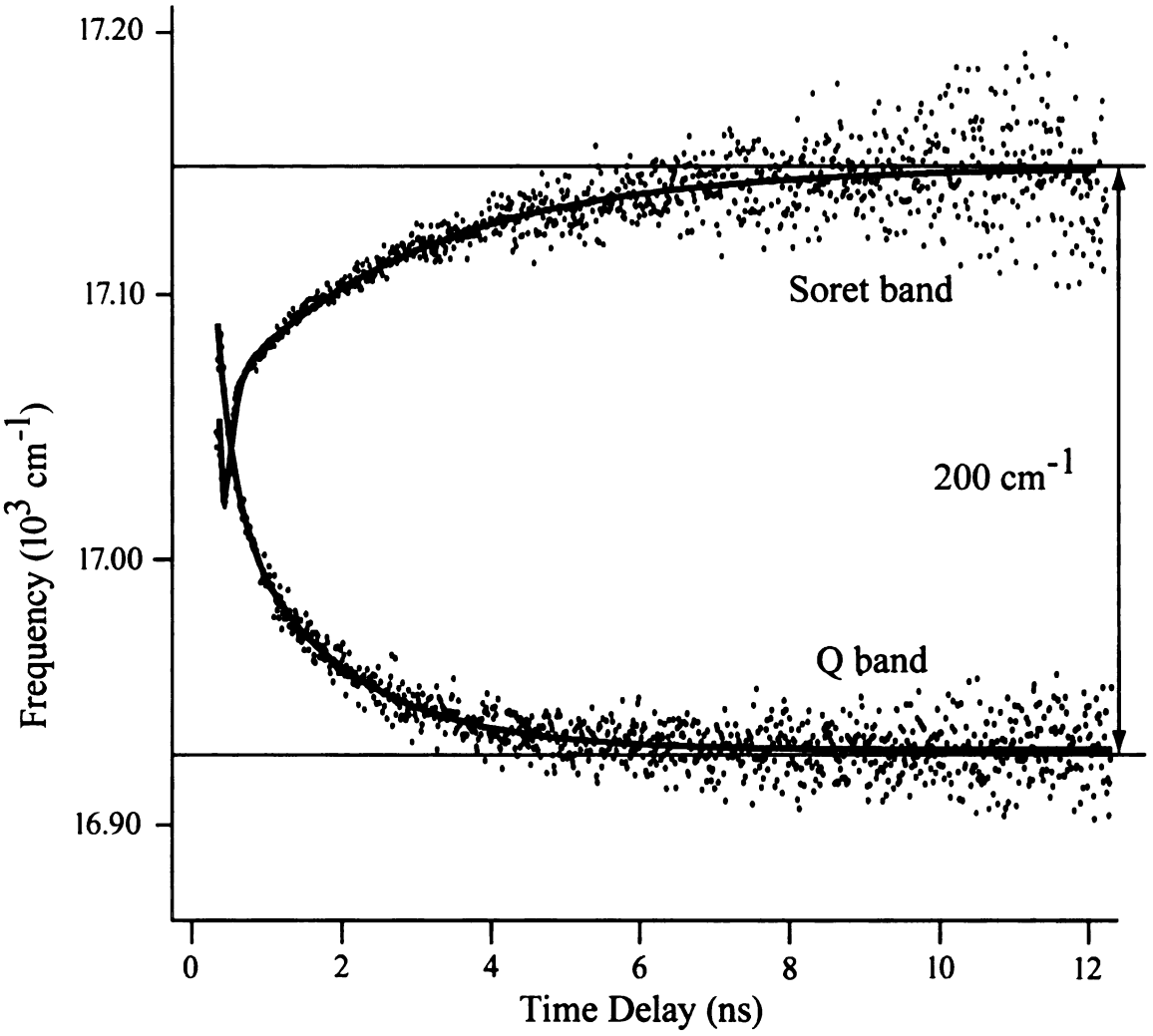

Figure 5.3. Time evolution of the frequency of the Q_{00} intensity maximum of the ZnCytc fluorescence spectrum in aqueous solution at 22 °C. The top curve was obtained with the excitation laser tuned to 420 nm, the peak of the Soret absorption band. The early time portion of this trace is shown on Figure 2. The bottom curve is that obtained with Q-band excitation (chapter 4). Each data trace is superimposed with an exponential fit of the form $y = C + \sum_i A_i e^{-t/\tau_i}$.

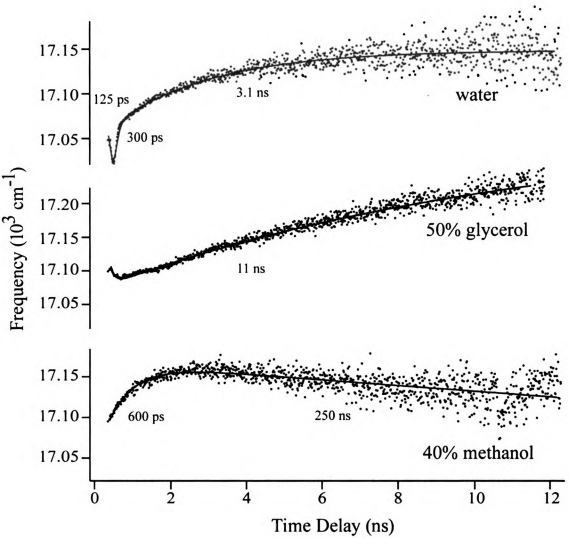

Figure 5.4. Comparison of the time evolution of the frequency of the Q_{00} intensity maximum of the fluorescence spectrum from ZnCytc in three solvent systems at 22 °C. The excitation laser was tuned to 420 nm, the peak of the Soret absorption band. The data is superimposed with exponential fit of the form $y = C + \sum_i A_i e^{-t/\tau_i}$.

Figure 5.5 compares the time evolution of the linewidth of the Q_{00} vibronic line in the fluorescence spectrum from ZnCytc in water, 50% glycerol and in 40% methanol. For the experiments discussed in this chapter we fit the time resolved spectra with the model described with equation 2.2, allowing the linewidth parameter to float. In the Soret-band excitation experiments, the width of the fluorescence Q_{00} line exhibits time dependence that is not observed in Q-band excitation experiments discussed in chapter 4. The linewidth data in Figure 5.5 are modeled as exponentials. Initial narrowing of the line shape is observed in water and to a smaller extent in a glycerol/water mixture. It is followed with slow line broadening in both solvents. The linewidth time dependence observed in methanol/water mixture exhibits only a slow line broadening component in the observation window available in these experiments.

5.4. Discussion

5.4.1. Nature of Dynamical Stokes Shift in ZnCytc with Soret-Band excitation

This chapter presents the Soret-band excitation of ZnCytc that results in optical triggering of protein unfolding reactions. As discussed in chapter 2, the Zn(II)-porphyrin chromophore exhibits two strong absorption bands, the Q band and the Soret (or B) band, which arise from transitions to the S_1 and to the S_n ($n \geq 2$) manifold of states (Figure 5.6).[28,29] The S_1 state has a good fluorescence quantum yield and a long emission lifetime ($\tau_F > 2$ ns).[30,31] With excitation of the Q band, the S_1 state is prepared directly, and a photon is emitted subsequent to vibrational equilibration at the ambient temperature.

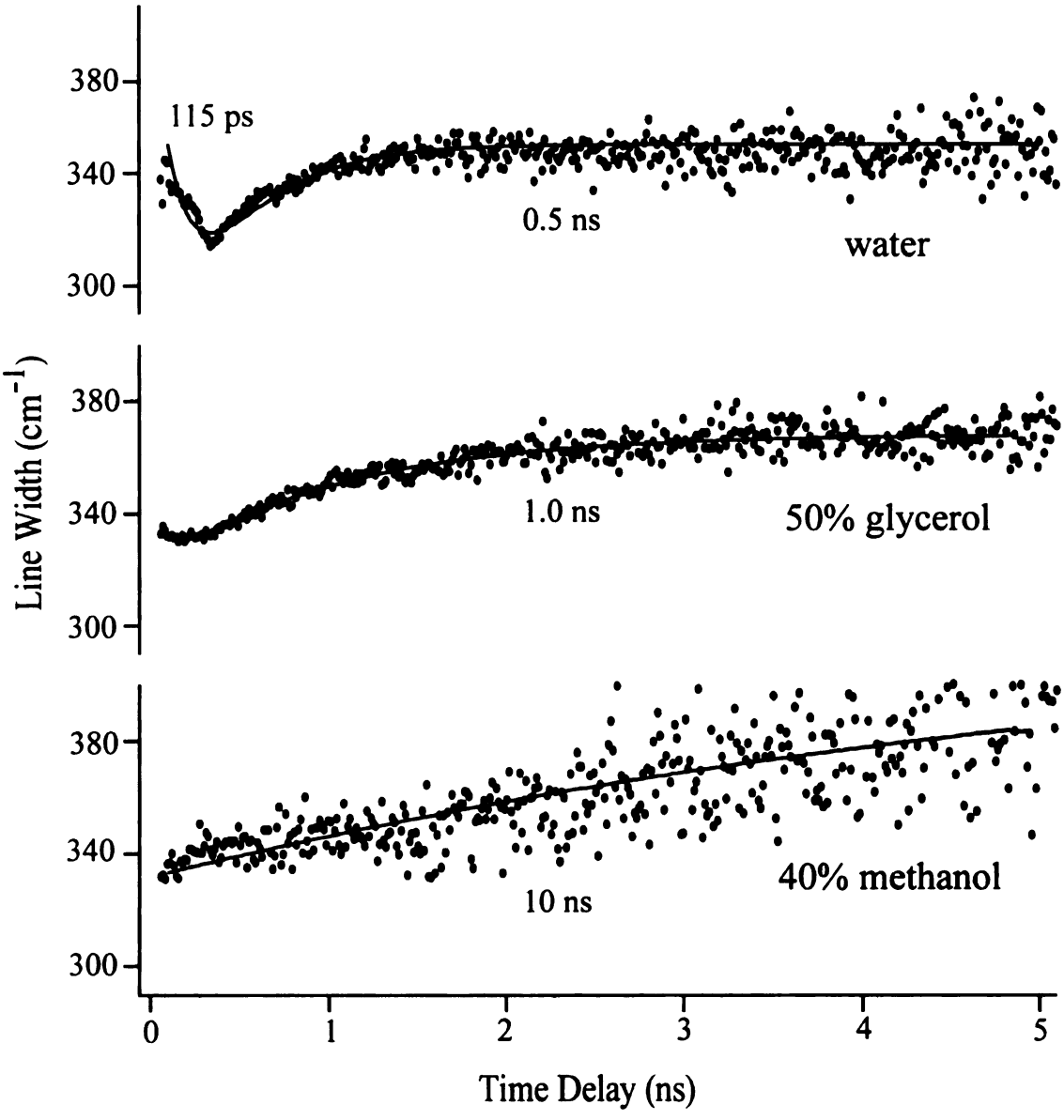

Figure 5.5. Comparison of the time evolution of the linewidth of the Q_{00} vibronic line of the fluorescence spectrum from ZnCytc in three solvent systems at 22 °C. The excitation laser was tuned to 420 nm, the peak of the Soret absorption band. The data is superimposed with exponential fit of the form $y = C + \sum_i A_i e^{-t/\tau_i}$.

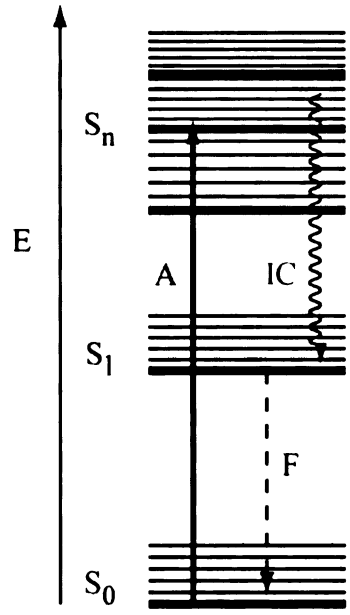

Figure 5.6. Energy level diagram for Zn(II) porphyrins, showing an absorption (A) transition in the Soret band to the S_n manifold of states followed by internal conversion (IC) to the S_1 state and recovery of the ground state S_0 by emission of a fluorescence photon (F).

Intramolecular vibrational redistribution (IVR) occurs on the sub-ps time scale and vibrational relaxation occurs on the < 10-ps time scale.[32,33] With excitation of the Soret band at 420 nm, however, an entirely different response is observed. Here, the initially prepared S_n state rapidly decays *nonradiatively* on the < 5-ps time scale to produce the S_1 state (see Figure 5.7). The hydrophobic core of ZnCytc accordingly obtains a significant vibrational excitation (~6850 cm^{-1}) when the Soret band is excited. The time-resolved fluorescence spectra report that this excitation results in an unfolding event. In the following section, we propose an explanation for the sequence of events that occur following Soret-band excitation and a discussion of the associated Stokes shift response.

We suggest that the initial response of the fluorescence spectrum to the red following Soret-band excitation, accompanies unfolding of the protein and entry of water molecules into the hydrophobic core. This conclusion is warranted by the subsequent shift of the spectrum to the blue that persists over the fluorescence time window. The dumping of energy into the hydrophobic core of the protein that accompanies internal conversion and IVR certainly would be expected to induce a fast red shift of the fluorescence spectrum owing to an accelerated reorganization of the protein. A faster reorganizational response would be similarly expected if the temperature of the surroundings were raised. The following shift of the fluorescence spectrum to the blue, however, is not anticipated if all that happens is an accelerated sampling of the energy landscape. The blue shift reports that the average polarity of the protein/solvent medium that surrounds the Zn(II) porphyrin is *decreasing* with time, and the simplest explanation for this response is a reorganizational response of the protein structure that results in *expulsion* of water molecules from the hydrophobic core. So, the fast initial red shift includes a component that corresponds to the rapid entry of water molecules into the hydrophobic core that accompanies unfolding of the protein.

The results shown in Figures 5.2 and 5.3, then, report a sequence of events that is consistent with an essentially vertical transition of the protein on the energy landscape owing to the internal vibrational excitation of the protein that results from internal conversion and IVR of the energy difference between the excitation laser's energy and the energy of the 0–0 vibronic transition of the S_1 state. Having absorbed the vibrational excitation, the protein begins to move away from the native structure for a short time,

perhaps 200 ps; owing to vibrational energy transfer with the cold bulk solvent water that surrounds the protein, the vibrational excitation does not last indefinitely. The protein is then dropped on the energy landscape at a displaced position and begins to evolve at the ambient temperature. The initial displacement involves unfolding and entry of water molecules into the hydrophobic core. The trajectory subsequently assumed by ZnCytc apparently involves motion towards the native configuration; the refolding trajectory involves a collapse of the unfolded structure and ejection of the water that entered. At the end of the observation window, the protein has not had enough time to recover to the initial state; the fluorescence spectrum remains well shifted to the blue with respect to the equilibrium position indicated by the Q-band response.

Figure 5.4 compares the dynamic Stokes shift response observed in ZnCytc following Soret-band excitation in water with that in 50% glycerol/water and in 40% methanol/water. The three responses allow a separate determination of the effects of the external solvent polarity and viscosity on the nature of the response. Note first that the initial red shift is shifted to a shorter time scale in glycerol/water and in methanol/water compared to that in water so that the amplitude of the initial component is very small (glycerol) or even absent (methanol) in the >100-ps observation window available in these results. These observations suggest that the initial unfolding reaction occurs more rapidly in the presence of glycerol or methanol than in water. We suggest that this result is consistent with a lowering of the activation energy for the unfolding reaction owing to a reduction in the polarity difference between the external bulk solvent and the native (anhydrous) hydrophobic core. Next, observe that the shift back to the blue is

considerably slower in glycerol/water and considerably accelerated in methanol/water; the observed time constants are 11 ns and 600 ps, respectively. These observations show that the initial refolding response that we assign to collapse of the protein is rate limited by the viscosity of the external solvent; the viscosity of the glycerol/water mixture is significantly larger compared to that of water, but the viscosity of the methanol/water mixture is significantly lower compared to water. The blue shift is apparently nearly completed in water by the 12-ns point; in comparison, the blue shift is completed in the methanol/water mixture at the 2-ns point, and we can see the beginning of the shift *back to the red* that must accompany the approach to the native folding state of the protein on a much longer time scale in water.

The dynamic Stokes shift response is accompanied with a change in the width of the Q_{00} vibronic line (see Figure 5.5). The initial line narrowing observed in water corresponds well to the time scale of the initial red shift component of the dynamic Stokes shift response described above. It could be that this line narrowing arises from a motional line narrowing caused by averaging between two or more structures that occur as a consequence of expansion of the protein core due to the unfolding process. The subsequent broadening of the Q_{00} vibronic line relates to the collapse of the protein structure around the porphyrin and concomitant slowing of the dynamics.

5.4.2. The Optical G Jump in ZnCytc: Dynamics of Unfolding and Refolding following Soret-Band excitation

The results discussed in this chapter show that Soret band excitation provides an optical trigger for unfolding and misfolding reactions in ZnCytc. We suggest that the

dynamic Stokes-shift response exhibited by an electronic probe in the hydrophobic core of a target protein can be explained by the sequence of events shown in Figure 5.7.

In the first step, the excess vibrational energy of the chromophore is deposited in the protein by vibrational energy transfer on the < 20-ps time scale. The chromophore is left in a vibrationally relaxed state from which it can recover the ground electronic state by emitting a photon; the fluorescence spectrum emitted by an ensemble of proteins can be used as a zero-background probe of the following protein dynamics. Next, the protein obtains a nearly instantaneous change in enthalpy without suffering a change in structure or solvent structure, which would contribute to an associated entropy change, so the change in enthalpy is equivalent to a change in Gibbs energy (step 2 in Figure 5.7). On the ~100-ps time scale, however, the vibrationally excited protein is "cooled" by the surrounding solvent, so the protein is dropped (vibrationally equilibrates) at a displaced position on the energy landscape after having evolved at the excited energy level for the intervening period of time (step 3). The next event involves initiation of a refolding (step 4a) or a misfolding trajectory (step 4b). If the energy difference between the absorbed and emitted photons is made large enough to overcome the unfolding activation-energy barrier, the optical G jump can launch an unfolding trajectory. It is important to note, however, that this process occurs without causing a significant change in the temperature of the surrounding solvent; in optically dilute solutions, the heat capacity of the solvent is effectively infinite.

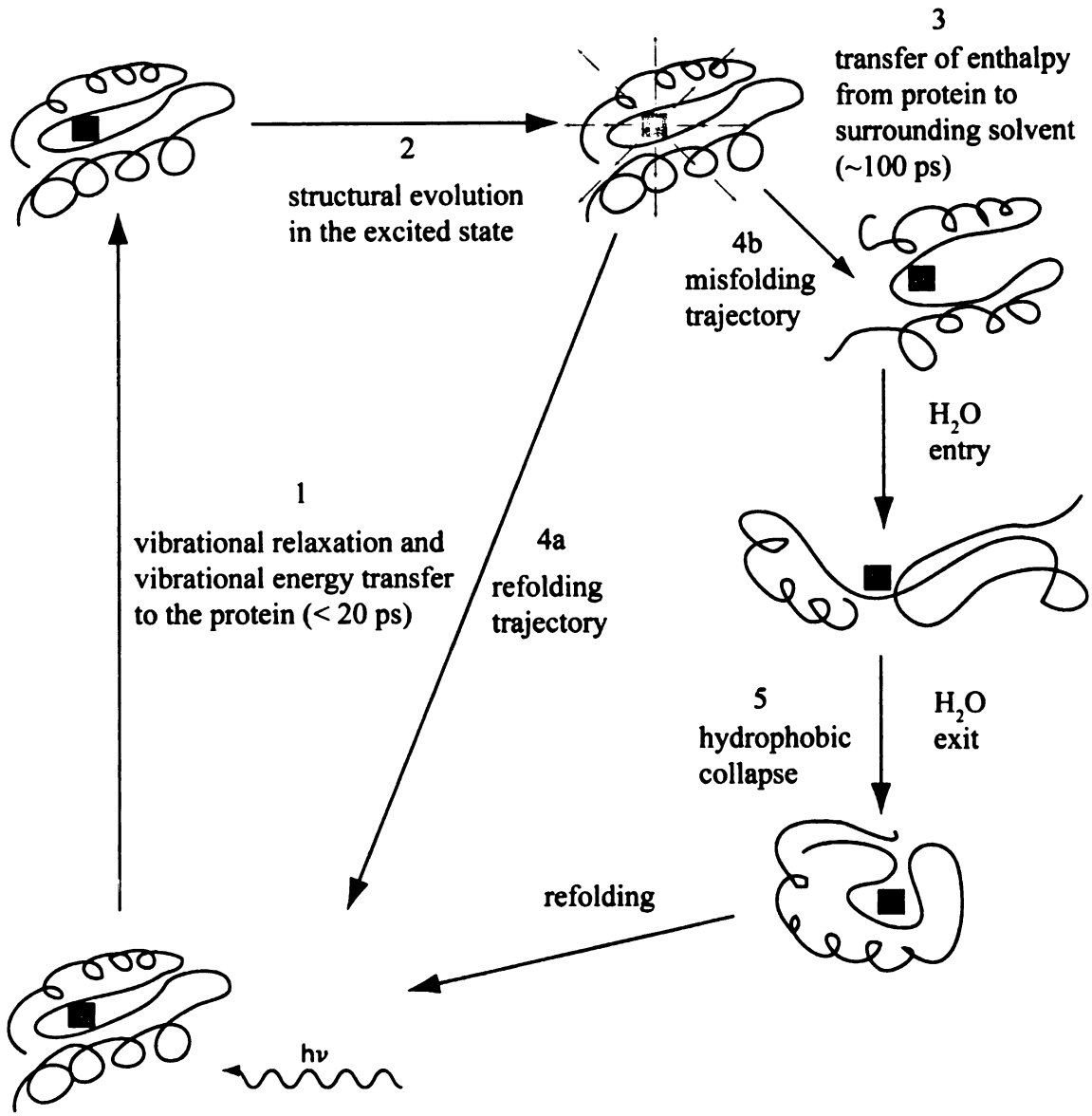

Figure 5.7. Sequence of events following the excitation of the electronic probe in the hydrophobic core of a target protein in the optical G jump experiment: 1. the initial vibrational relaxation of the probe and associated vibrational energy transfer to the protein, 2. structural evolution of the protein at an excited vibrational level, 3. transfer of enthalpy from the protein to the surrounding solvent, and the associated vibrational equilibration of the protein at a displaced position on the energy landscape, 4. initiation of a refolding (4a) or misfolding (4b) trajectory, 5. hydrophobic collapse of the unfolded protein and ejection of water, 6. slow refolding into the final, native state.

These initial four steps accompany the fast initial red shift of the fluorescence spectrum from the probe. The nature of the structural evolution of the protein at an excited vibrational energy level described in step 2, depends on whether the amount of vibrational energy delivered by the probe is large enough to allow the protein to overcome the activation barrier that retained it in the initial folding state under the ambient conditions. If the excitation wavelength is too far to the red, the G jump that will be delivered will be insufficiently large to get the protein over the barrier; the red shift of the fluorescence spectrum will just be a report of the vibrational relaxation of the probe and the sampling of the energy landscape by the surrounding protein in a region near to the initial folding state. If the excitation wavelength is far enough to the blue, however, an unfolding trajectory will be launched, and the red shift will include contributions from the increased polarity of the region around the probe that accompanies unfolding of the protein and solvation of the polypeptide. In that case, once vibrational energy transfer from the protein to the surrounding solvent has occurred and the protein has vibrationally equilibrated, the dynamic Stokes-shift response that follows is determined by the events that occur during the refolding or misfolding trajectory:

The observed turn-around and blue shift of the fluorescence spectrum corresponds to a hydrophobic collapse of the unfolded protein and an ejection of a significant number of water molecules (step 5 in Figure 5.7). It is likely, however, that some water molecules stay behind and hydrate the polypeptide in its core region.[34] The ejection of these residual water molecules is likely to correspond to the rate limitation for the folding into the native fold. This leads to an apparent *metastability* of the state that follows the blue shift,

at least on the fluorescence time scale. This event is followed by the much slower ultimate red shift of the system into the final, native state (step 6). This phase of the dynamics is evidently strongly limited by solvent friction.

The possible role of solvent friction in the final refolding of the protein is suggested by the effect of the solvent viscosity on the time constants for the blue and final red shifts observed in the preliminary work on ZnCytc. Given such an observation, one is prompted to suggest that the fold that a protein assumes could be kinetically controlled by friction with a surrounding surface, such as from a chaperone protein.[35]

The key to the success of the optical G-jump is the dynamical bottleneck that evidently exists in the vibrational energy transfer from the protein to the surrounding solvent. The intramolecular vibrational redistribution (IVR) processes that inject the excess vibrational energy of the chromophore into the protein occur on a much shorter time scale than the formally vibrational energy-transfer processes that dissipate the excitation into the surrounding solvent. This bottleneck provides a short time for the protein to evolve at an excited energy level before equilibrating at the ambient solution temperature. At first glance, it might be considered remarkable that perhaps 100 ps of evolution is sufficient to initiate an unfolding transition that results in entry of a significant number of water molecules into the hydrophobic core. The rate at which the protein diffuses away from the initial structure, however, is much faster at the elevated free energy level provided by the G-jump than it is at the ambient temperature. This argument suggests that it will be of interest to vary the excitation energy provided to the protein *above the unfolding barrier* by tuning the excitation wavelength significantly

above the threshold wavelength at which unfolding occurs in order to vary the displacement from the native structure; larger excitations above the barrier will result in longer periods of accelerated diffusion prior to the clamping of the dynamics by the equilibration with the surrounding solvent.

5.5. References

(1) Sunde, M.; Blake, C. The structure of amyloid fibrils by electron microscopy and X-ray diffraction. In *Adv. Prot. Chem.*, 1997; Vol. 50; pp 123–159.

(2) Prusiner, S. B. *Proc. Natl. Acad. Sci. USA* **1998**, *95*, 13363–13383.

(3) Dobson, C. M. *Trends Biochem.Sci.* **1999**, *24*, 329–332.

(4) Bucciantini, M.; Giannoni, E.; Chiti, F.; Baroni, F.; Formigli, L.; Zurdo, J. S.; Taddei, N.; Ramponi, G.; Dobson, C. M.; Stefani, M. *Nature* **2002**, *416*, 507–511.

(5) Caughey, B.; Lansbury, P. T. *Annu. Rev. Neurosci.* **2003**, *26*, 267–298.

(6) Selkoe, D. J. *Nature* **2003**, *426*, 900–904.

(7) Shastry, M. C. R.; Luck, S. D.; Roder, H. *Biophys. J.* **1998**, *74*, 2714–2721.

(8) Gianni, S.; Travaglini-Allocateli, C.; Cutruzzolla, F.; Brunori, M.; Shastry, M. C. R.; Roder, H. *J. Mol. Biol.* **2003**, *330*, 1145–1152.

(9) Kumar, R.; Bhuyan, A. K. *Biochemistry* **2005**, *44*, 3024–3033.

(10) Callender, R.; Dyer, R. B. *Curr. Opin. Struc. Biol.* **2002**, *12*, 628.

(11) Williams, S.; Causgrove, T. P.; Gilmanshin, R.; Fang, K. S.; Callender, R. H.; Woodruff, W. H.; Dyer, R. B. *Biochemistry* **1996**, *35*, 691–697.

(12) Werner, J. H.; Dyer, R. B.; Fesinmeyer, R. M.; Anderson, N. H. *J. Phys. Chem. B.* **2002**, *106*, 487–494.

(13) Pandit, A.; Ma, H. R.; van Stokkum, I. H. M.; Gruebele, M.; van Grondelle, R. *Biochemistry* **2002**, *41*, 15115–15120.

(14) Vu, D. M.; Peterson, E. S.; Dyer, R. B. *J. Am. Chem. Soc.* **2004**, *126*, 6546.

(15) Snow, C. D.; Nguyen, N.; Pande, V. S.; Gruebele, M. *Nature* **2002**, *420*, 102–106.

(16) Ma, H. R.; Gruebele, M. *Proc. Natl. Acad. Sci. U. S. A.* **2005**, *102*, 2283–2287.

(17) Bryngelson, J. D.; Wolynes, P. G. *Proc. Natl. Acad. Sci. U. S. A.* **1987**, *84*, 7524–7528.

(18) Chan, H. S.; Dill, K. A. *Proteins: Struct. Funct. Genet.* **1998**, *30*, 2–33.

(19) Brooks III, C. L.; Onuchic, J. N.; Wales, D. J. *Science* **2001**, *293*, 612.

(20) Dill, K. A.; Chan, H. S. *Nature Struct. Biol.* **1997**, *4*, 10–19.

(21) Dill, K. A. *Protein Sci.* **1999**, *8*, 1166–1180.

(22) Frauenfelder, H.; Sligar, S. G.; Wolynes, P. G. *Science* **1991**, *254*, 1598–1603.

(23) Leopold, P. E.; Montal, M.; Onuchic, J. N. *Proc. Natl. Acad. Sci. U. S. A.* **1992**, *89*.

(24) Onuchic, J. N.; Luthey-Schulten, Z.; Wolynes, P. G. *Annu. Rev. Phys. Chem.* **1997**, *48*, 545–600.

(25) Shea, J.-E.; Brooks III, C. L. *Annu. Rev. Phys. Chem.* **2001**, *52*, 499–535.

(26) Baker, D.; Agard, D. A. *Biochemistry* **1994**, *33*, 7505–7509.

(27) Kauzmann, W. *Adv. Protein. Chem.* **1959**, *14*, 1–63.

(28) Gouterman, M. Optical spectra and electronic structure of porphyrins and related rings. In *The Porphyrins*; Dolphin, D., Ed.; Academic Press: New York, 1978; Vol. 3; pp 1–159.

(29) Adar, F. Electronic absorption spectra of hemes and hemoproteins. In *The Porphyrins*; Dolphin, D., Ed.; Academic Press: New York, 1978; Vol. 3; pp 167–209.

(30) Leeson, D. T.; Berg, O.; Wiersma, D. A. *J. Phys. Chem.* **1994**, *98*, 3913–3916.

(31) Vanderkooi, J. M.; Adar, F.; Erecìnska, M. *Eur. J. Biochem.* **1976**, *64*, 381.

(32) Miller, R. J. D. *Annu. Rev. Phys. Chem.* **1991**, *42*, 581–614.

(33) Henry, E. R.; Eaton, W. A.; Hochstrasser, R. M. *Proc. Natl. Acad. Sci. USA* **1986**, *83*, 8296–8696.

(34) Cheung, M. S.; Garcia, A. E.; Onuchic, J. N. *Proc. Natl. Acad. Sci. USA* **2002**, *99*, 685–690.

(35) Shtilerman, M.; Lorimer, G. H.; Englander, S. W. *Science* **1999**, *284*, 822–825.

6. Future Directions

The work in this dissertation opens an exciting possibility for the application of the optical G-jump method in studying protein unfolding and misfolding dynamics. The method can be used under controlled solvent and temperature conditions that relate far better to the conditions relevant to disease than are possible using existing temperature-jump and denaturant-mixing experiments. We anticipate that it will be generally possible to use the optical G-jump method with any protein of interest provided that a suitable electronic probe can be engineered into the structure using site-directed mutagenesis or by solid-state peptide synthesis.

The optical G jump experiment can be triggered with a large number of intrinsic or extrinsic probes. The choice of the probe is limited only by the excitation-energy range that is accessible to the optical G-jump which is restricted to the spectral range to the red of the ~320-nm onset of the absorption of tryptophan.[1] Most organic chromophores emit fluorescence solely from the lowest excited singlet electronic state, which is prepared by internal conversion from the higher singlet states S_n.[2] Furthermore, most fluorophores have non-negligible oscillator strengths for absorption transitions to these higher singlet states,[3] so the optical G-jump excitation scheme will work with any fluorescent probe that has a red-shifted absorption compared to the 320 nm cut off.

The work presented in this dissertation suggests that the characterization of the apparent barrier heights for unfolding reactions in the target systems mentioned above

could be carried out through a comparison of dynamic Stokes-shift responses obtained as a function of laser excitation wavelength. Below the barrier for unfolding, the response will resemble the one observed for ZnCytc with *Q*-band excitation described in chapter 4. As the laser wavelength is tuned to the blue, at some point the barrier should be overcome, and an unfolding transition should occur. The barrier crossing could be reported by responses like the ones observed for ZnCytc with its Soret band. The characteristics of this response is fast initial red shift of the fluorescence spectrum, but the key diagnostic observation is the breaking back to the blue as the refolding begins. At excitation wavelengths to the blue of the spectral origin but below the unfolding barrier, the initial red shift could exhibit fast components that arise from vibrational relaxation that are added to the ones that arise from normal sampling of the energy landscape near the native state, but no break to the blue should be observed.

Scanning the excitation wavelength farther to the blue than the wavelength that corresponds to the unfolding threshold may permit longer displacements (in time and in distance along structural coordinates) from the native minimum. A comparison of the dynamic Stokes-shift dynamics at and well above the threshold might reveal the onset of trajectories to alternate minima on the energy landscape that lead to formally misfolded structures.

The barrier-height determination could be repeated for at least two additional experimental variable axes: the sample temperature and the solvent mixture. As has been demonstrated with ZnCytc, addition of alcohols will vary the polarity and viscosity of the surrounding solvents. The variation of polarity provides a direct means to manipulate the

barrier height for the unfolding reaction; this provides a test of the essential ideas of the hydrophobic effect.[4-8]

The determination of the unfolding barrier height at different temperatures takes advantage of a unique feature of the optical G-jump technique, that the temperature at which most of the dynamics take place is that of the ambient, surrounding solvent temperature. This is an important feature because the trajectories that would be accessible to the unfolding/refolding system depend on the sample temperature. At low temperatures, the trajectories would be expected to find the global free-energy minimum on the energy landscape. As the temperature is raised, however, intermediate barriers that steer the protein toward the global minimum may be overcome, allowing the system to find local minima.[9] These local minima may be the kinetic traps that are manifested by the misfolded systems in disease.

6.1. References

(1) Cantor, C. R.; Schimmel, P. R. *Biophysical Chemistry. Part II: Techniques for the Study of Biological Structure and Function*; W. H. Freeman and Company: San Francisco, 1980.

(2) Turro, N. J. *Modern Molecular Photochemistry*; Benjamin/Cummings Publishing Company: Menlo Park, California, 1978.

(3) Lakowicz, J. R. *Principles of Fluorescence Spectroscopy*, Second ed.; Kluwer Academic/Plenum Publishers: New York, 1999.

(4) Lesk, A. M. *Biophys. Chem.* **2003**, *105*, 179–182.

(5) Frank, H. S.; Evans, M. W. *J. Chem. Phys.* **1945**, *13*, 507–532.

(6) Honig, B.; Yang, A. S. *Adv. Prot. Chem.* **1995**, *46*, 27–41.

(7) Privalov, P. L.; Gill, S. J. *Adv. Prot. Chem.* **1988**, *39*, 193–234.

(8) Kauzmann, W. *Adv. Protein. Chem.* **1959**, *14*, 1–63.

(9) Brooks III, C. L.; Onuchic, J. N.; Wales, D. J. *Science* **2001**, *293*, 612.